PERFORMANCE ANALYSIS FOR A MEMBRANE-BASED LIQUID DESICCANT AIR DEHUMIDIFIER: EXPERIMENT AND MODELING

by

Xiaoli Liu

A Thesis

Submitted to the Faculty of Purdue University

In Partial Fulfillment of the Requirements for the degree of

Master of Science in Civil Engineering

Lyles School of Civil Engineering

West Lafayette, Indiana

December 2018

THE PURDUE UNIVERSITY GRADUATE SCHOOL
STATEMENT OF COMMITTEE APPROVAL

Dr. Ming Qu, Chair
Lyles School of Civil Engineering
Dr. Xiaobing Liu
Oak Ridge National Laboratory
Dr. W. Travis Horton
Lyles School of Civil Engineering
Dr. Eckhard Groll
School of Mechanical Engineering

Approved by:

Dr. Dulcy Abraham
Head of the Graduate Program

To my mom and dad

For all their love and support

ACKNOWLEDGMENTS

I would like to thank my advisor Prof. Ming Qu in Purdue University, who gave me valuable opportunities to access the field of academic research with her patience, encouragement, and support; and Dr. Xiaobing Liu, my mentor in Oak Ridge National Lab, for his instruction and assistance in the research. I would also like to thank my collaborator, Joseph Warner, and Linshi Wang, for their efforts in the experiment part. And thank Dr. Zhiming Gao for the help of the modeling part. Moreover, I want to express my gratitude to all my committee members, Dr. Travis Horton, Dr. Ekhard Groll, Dr. Xiaobing Liu, and Dr. Ming Qu. Thank you for all your questions and suggestions, which benefit me a lot. Finally, all our researchers of this project thank the Emerging Technologies Program of the Buildings Technology Office at the US Department of Energy for supporting this research project; and Xergy, a small business technology inventor, for providing the prototype.

TABLE OF CONTENTS

LIST OF TABLES

LIST OF FIGURES

NOMENCLATURE

Symbol	Description	Units
C	Concentration	-
c_p	heat capacity	J/kg·K
D	permeability coefficient	kg/(m^2·Pa·s)
D_{wm}	diffusivity of water in membrane	m^2/s
h	convective heat transfer coefficient	kW/m^2·K
H	operating factor	-
H	Height	m
H_d	heat of dilution	kJ
$\dot{j}$	vapor flux	kg/(m^2·s)
k	thermal conductivity	kW/(m·K)
K	transfer coefficient	kg/(m^2·Pa·s)
L	characteristic length	m
$\dot{m}$	mass flow rate	kg/s
M_v	molar mass of vapor	g/mol
NTU	number of transfer units	-
Nu	Nusselt number	-
P	pressure	Pa
Pr	Prandtl number	-
P'	permeability of the membrane	kg/(m·Pa·s)
$\dot{q}$	heat flux	kW/m^2
R	gas constant	J/(mol·K)
Re	Reynolds number	-
R	transfer resistance	m^2·K/ kW
RH or rh	relative humidity	-
Sh	Sherwood number	-
T	temperature	C or K
U_{total}	overall transfer coefficient	kW/m^2·K

X_{sol}	mass ratio of water to salt	-
x, y, z	coordinates	-
Greek	**Description**	**Units**
ε	Effectiveness / porosity	-
τ	pore tortuosity of the membrane	-
r	pore radius of the membrane	m
δ	thickness of the membrane	m
ω or W	humidity ratio	g/kg or kg/kg
λ_m	membrane thermal conductivity	kW/m·K
β	correction factor	-
ρ	density	kg/m^3
γ	kinetic viscosity	m^2/s
α	thermal diffusivity	m^2/s
μ	dynamic viscosity	Pa·s
Superscripts	**Description**	
*	dimensionless	
Subscripts	**Description**	
a	air flow	
am	air-membrane surface	
i or in	inlet	
lat	latent	
m	mass transfer	
max	maximum	
min	minimum	
mem	membrane	
o or out	outlet	
sen	sensible	
sol	solution flow	
sm	solution-membrane surface	
kd	Knudsen diffusion	
pf	Poiseuille flow / permeate-side fluid	

md	molecular diffusion
p	permeate side
pm	permeate side membrane
f	feed side
cross	cross flow
parallel	parallel flow
counter	counter flow
w	water
s	surface
salt	salt in liquid desiccant
Abbreviations	**Description**
DMPC	dynamic moisture permeation cell
EVP	equilibrium vapor pressure
HVAC	heating, ventilation and air conditioning
ILD	ionic liquid desiccant
LD	liquid desiccant
LDAD	liquid desiccant air dehumidification
MHMX	membrane-based heat and mass exchanger
MLDAD	membrane-based liquid desiccant air dehumidification
OA	outdoor air
ORNL	Oak Ridge National Laboratory
PE	polyethylene
PP	polypropylene
PTFE	polytetrafluoroethylene
PVDF	polyvinylidene fluoride
SA	supply air
VDR	vapor diffusion resistance
SAMR	solution to air flow rate ratio

ABSTRACT

Author: Xiaoli, Liu. MSCE
Institution: Purdue University
Degree Received: December 2018
Title: Performance Analysis for a Membrane-based Liquid Desiccant Air Dehumidifier: Experiment and Modeling.
Committee Chair: Ming Qu

Liquid desiccant air dehumidification (LDAD) is a promising substitute for the conventional dehumidification systems that use mechanical cooling. However, the LDAD system shares a little market because of its high installation cost, carryover problem, and severe corrosion problem caused by the conventional liquid desiccant. The research reported in this thesis aimed to address these challenges by applying membrane technology and ionic liquid desiccants (ILDs) in LDAD. The membrane technology uses semi-permeable materials to separate the air and liquid desiccants, therefore, the solution droplets cannot enter into the air stream to corrode the metal piping and degrade the air quality. The ILDs are synthesized salts in the liquid phase, with a large dehumidification capacity but no corrosion problems. In order to study the applicability and performance of these two technologies, both experimental and modeling investigations were made as follows.

In the study, experimental researches and existing models on the membrane-based LDAD (MLDAD) was extensively reviewed with respects of the characteristics of liquid desiccants and membranes, the module design, the performance assessment and comparison, as well as the modeling methods for MLDAD.

A small-scale prototype of the MLDAD was tested by using ILD in controlled conditions to characterize its performance in Oak Ridge National Lab. The preliminary experimental results indicated that the MLDAD was able to dehumidify the air and the ILD could be regenerated at 40 ºC temperature. However, the latent effectiveness is relatively lower compared with conventional LDAD systems, and the current design was prone to leakage, especially under the conditions of high air and solution flow rates.

To improve the dehumidification performance of our MLDAD prototype, the two-dimensional numerical heat and mass transfer models were developed for both porous and nonporous membranes based on the microstructure of the membrane material. The finite element method was used to solve the equations in MATLAB. The models for porous and nonporous membranes were

validated by the experimental data available from literature and our performance test, respectively. The validated models were able to predict the performance of the MLDAD module and conduct parametric studies to identify the optimal material selection, design, and operation of the MLDAD.

1. INTRODUCTION

1.1 Background

1.1.1 Energy and environmental issues

From 1950 to 2017, the American energy consumption grew from 32 to 97.7 quadrillion British Thermal Units (BTUs) approximately, with a considerable increase as high as 203% [1], and the trend is projected to continue in the future [2]. Among the total energy consumption, about 38% (or about 38 quadrillion BTUs) was consumed by the building sector, where the residential building held 20%, and the commercial building held 18% [1]. Based on the historical data, about 54% and 34% of the energy consumed by residential and commercial buildings, respectively, in the U.S. were for space heating, ventilation and air conditioning (HVAC) [3][4]. It was found that the HVAC system counted nearly 17% of the U.S. total energy used as shown in Figure 1.1. Thus, the building HVAC systems have a high impact on the energy and environment.

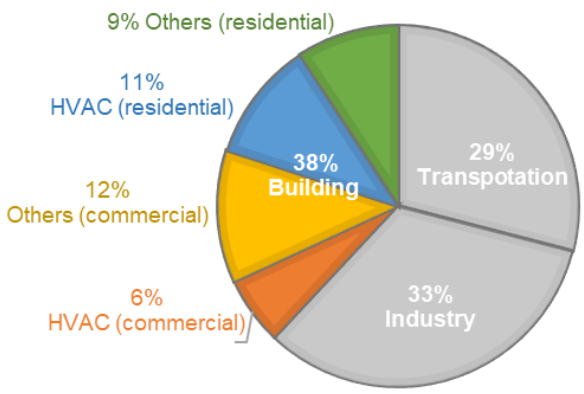

Figure 1.1 Share of total U.S. energy consumption by end-use sectors.

The energy structure in the U.S. is dominated by natural gas and electricity generated by burning fossil fuels [2][4]. Both natural gas and fossil fuels are primary energy and non-renewable. The unlimited use of them is unsustainable and will undoubtedly accelerate the energy crisis. On the other hand, the combustion of fossil fuels produces greenhouse gases emitted to the atmosphere, leading to global warming, sea level rise, acid rain, and other environmental deterioration issues.

However, with the improvement of the society, people's demand for indoor environment comfort will continue to grow [6]. This is in contradiction with the increasing energy shortage and

environmental deterioration. Thus, it is highly needed to develop more energy-efficient, environment-friendly, and more controllable technologies in HVAC systems, which are not only able to alleviate the energy and environment crisis but also to enhance the indoor air quality.

1.1.2 Indoor air environment issues

People spend nearly 90% of their life in enclosed buildings [8], so the indoor air environment (IEQ) has a severe and direct influence on people's productivity and health. The humidity of the indoor space is one of the significant parameters in IEQ. High humidity can inhibit the evaporation of sweat, resulting in discomfort, headache, or even productivity decline [9]. Also, high humidity provides a major breeding ground for the growth of bacteria and fungi in buildings, thus, affecting people's health [10][11]. Therefore, the humidity should be controlled sufficiently. To maintain indoor thermal comfort and to reduce the likelihood for microbial growth, ASHRAE standard 55-2013 and 62.1-2016 require that the HVAC system must be able to keep a humidity ratio below 0.012 and to control the relative humidity between 30-60%, respectively [12][13].

In hot and humid areas like the southern region of the United States, the relative humidity of air usually fluctuates between 60% and 90%. The latent load, which is the energy required to remove the moisture in the air, becomes the main load of buildings, especially in humid summers [14]. Therefore, the air dehumidification would be an important technology to reduce building energy consumption, as well as the occupancy health and productivity.

1.1.3 Current air dehumidification systems

The air dehumidification methods in buildings generally include the moisture condensing method and the desiccant method. Among them, the moisture condensing method is the most commonly used one. During this process, the moisture in the air decreases with the decrease of air temperature [15]. When the outdoor air (OA) is cooled at its dew point temperature as shown in 1a of Figure 1.2, the air gradually loses the ability to hold more water vapor and reaches the saturation point. As the air continues to be cooled, the water vapor in the air condenses, thus, reducing the absolute moisture content in the air, as shown in 1b of Figure 1.2. Then the over-cooled and dry air needs to be reheated to an acceptable temperature to serve as the supply air (SA) as shown in 1c of Figure 1.2. As seen, this approach inevitably causes the problems of the large energy waste

due to overcooling and reheating. Also, the condensed water attaching to the cooling coil can easily lead to the growth of bacteria and mold and the reduction of the air quality [16].

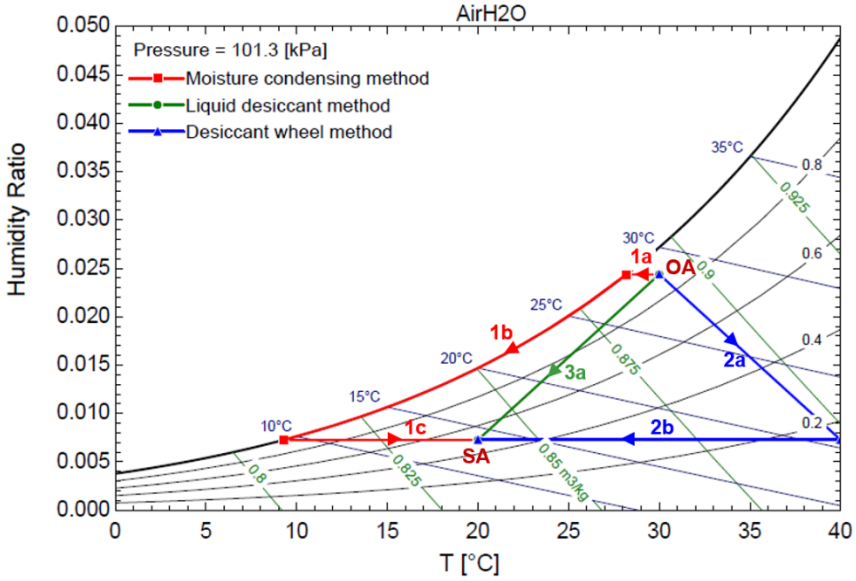

Figure 1.2 Psychometric chart shown dehumidification procedures.

The desiccant dehumidification system uses desiccant materials, which have a high affinity with water, to absorb the moisture in the humid air. These desiccants with an extremely low surface vapor pressure forces the vapor transported from the moist air to desiccants directly. Thus, the desiccant system has some merits over the conventional dehumidification technologies. It enables separated sensible and latent demands so that the sensible cooling efficiency can be improved, and the wasteful reheating can be avoided [17][18]. The reduction of the cooling load is also able to reduce the size of the chiller and the amount of the refrigerant. Thus, it is helpful to reduce the cost of the system and to alleviate the ozone layer depletion caused by refrigerants like chlorofluoro-carbons.

The desiccant dehumidification system includes two types: the desiccant wheel system and the liquid desiccant system. The desiccant wheel method uses solid desiccants, such as silica gels and zeolites, to adsorb water vapor in the air. When the outdoor air passes through the dehumidi-fication section, the water vapor in the air is adsorbed by the desiccant medium. Then the air temperature increases and the humidity decreases as shown in 2a of Figure 1.2. At this point, the temperature of processing air is too high to supply so that additional cooling is needed to lower the air temperature, as shown in 2b of Figure 1.2. After adsorbing enough vapor, the desiccant

tends to be saturated. The desiccant wheel, therefore, needs a regeneration section to keep the system running continuously. So, another stream of air (usually the exhaust air) is needed to pass through the regeneration part of the desiccant wheel to evaporate the moisture inside the desiccant.

The second type, the liquid desiccant system or liquid desiccant air dehumidification (LDAD) uses liquid desiccant, such as glycol and halide salts, to absorb water vapor in the air. This process can be described as the humid air being directly treated from the state point OA to SA, with proper internal cooling, as shown in 3a of Figure 1.2. The LDAD technology has more promising features of dehumidification performance and system flexibility. First, the LDAD system only requires a relatively lower regeneration temperature (40~60°C), allowing the possibility for utilizing low-grade energy (i.e., condensation heat, and waste heat from factories) or renewable energy (i.e., solar energy) [20][22][22]. Second, the LDAD system is much easier to integrate a third heat transfer fluid inside the components in order to provide internal cooling/heating to dehumidify the air or regenerate the solution better.

However, the conventional LDAD system, generally with an open-towel configuration, still shares little market due to the issue of carryover and corrosion. The carryover happens when the airflow directly contacts to the liquid desiccant. Moreover, the relatively high velocities of two streams (the air and solution) flowing across the packing bed make it easier for air to carry small solution droplets into the indoor environment [24]. The carryover not only endangers the health of occupants but also corrodes downstream HVAC pipes and components [25][26]. Additionally, the halide salt aqueous solution is often used as the liquid desiccant so that the corrosion of the pipeline and components in the solution loop is still unavoidable. Thus, new technologies are needed to overcome or mitigate these shortcomings. One of the new technologies is using new non-corrosive liquid desiccant in LDAD. The ionic liquid is the most recent studied non-corrosive liquid as a substitute for a liquid desiccant in LDAD system. ILDs are synthesized salts in the liquid phase. They have extremely low vapor pressure, high thermal stability, high solubility in water, no corrosion to metals, and no crystallization problem [31]. Another new technology is the membrane-based liquid desiccant air dehumidification (MLDAD). The MLDAD uses a semi-permeable membrane to separate the air and liquid desiccant so that the liquid desiccant droplets cannot enter into the air stream to cause the corrosion of HVAC components and the quality deterioration of the supply air. The MLDAD system potentially has a superior performance in energy, economy, and environment [27][28]. Both new technologies now are still in the early stage of research. The

overarching goal of the research is to study the two new technologies, applied separately and integrally through both the experiment and modeling for the design, operation, and performance evaluation.

1.2 Review on membrane-based liquid desiccant air dehumidifier

This section includes the reviews of the characteristics of liquid desiccants and membranes, the design of MLDAD modules, the performance assessment and comparison for MLDAD.

1.2.1 Liquid desiccants

Liquid desiccants are substances in liquid form with a high affinity to water vapor so that they can absorb water vapor in the air. Tri-ethylene glycol (TEG), a mixture of organic liquids, is the earliest liquid desiccant used for air dehumidification. But the high viscosity and high volatility of TEG adversely affect the stability of the dehumidification system and the quality of the air being dehumidified [45][19]. Later, halide salts have been identified to replace TEG because of their better thermodynamic properties and low volatility. The aqueous solutions of halide salts most widely used are Lithium bromide (LiBr), lithium chloride (LiCl) and calcium chloride ($CaCl_2$), and magnesium chloride ($MgCl_2$) [29][19]. The equilibrium vapor pressures (EVP) of saturated LiBr, LiCl, $CaCl_2$ and $MgCl_2$ solutions are equal to that of air at the same temperature with a relative humidity of about 6%, 11%, 30%, and 33%, respectively. Although $MgCl_2$ and $CaCl_2$ solutions have relatively weaker dehumidification capacities and they are easier to crystallize, their prices are much lower than LiBr and LiCl solutions [29][46]. Therefore, mixtures of these halide salts were studied to reduce the cost while maintaining a good dehumidification performance. Al-Farayedhi et al. used a mixture of $CaCl_2$ and LiBr with a mass ratio of 1:1 and found that the mass transfer coefficient of the mixed solution was higher than that of the $CaCl_2$ solution along [47].

However, the conventional halide salt solutions are corrosive to metals. Also, these salt solutions are easy to crystallize when they are saturated. These two drawbacks degrade the reliability and longevity of the system, as well as the dehumidification performance. Therefore, researchers have been looking for the less-corrosive and less-volatile liquid desiccants. The first new type of such liquid desiccants founded is the weak acid including potassium formate (HCO_2K), potassium acetate (CH_3CO_2K), sodium formate (HCO_2Na), or sodium acetate (CH_3CO_2Na) [48][49][50][51]. Compared with the halide salts solutions, these weak acids are less corrosive,

less toxic, and have lower crystallization temperature, lower density and higher solubility [19][45]. Although the dehumidification ability of these weak acids is weaker than LiCl and LiBr solutions, their costs are lower. Another new type of alternative is ionic liquid desiccants (ILDs). ILDs are salts in the liquid phase. They have extremely low vapor pressure, no corrosion to metals, and no crystallization issues [31][52]. Kudasheva et al. hybrid three ILDs, such as [EMIM][ESU], [EMIM][DCA] and [EMIM][BF_4], with porous materials to develop the ionic liquid membrane layers, which shows a good water permeability in experiments [30]. Then, Qu et al. tested 13 different ILDs and identified that [EMIM][OAc] had the maximum adsorption and desorption capabilities among the 13 ILDs [31].

The equilibrium vapor pressures, EVP, is the most critical characteristic of a liquid desiccant because it directly determines the dehumidification effectiveness [29]. EVP of a liquid desiccant equals the partial water vapor pressure of the air above the desiccant surface. It is a dependent of the temperature, concentration, and pressure of the liquid desiccant. A liquid desiccant with higher concentration and lower temperature has a lower EVP so that the more water vapor can transport from air to the liquid desiccant due to a larger vapor pressure difference between the air and the liquid desiccant. EVP values shown in Figure 1.3 are calculated curve-fitted correlations (i.e., the Cisternas-Lam equations [38] and Conde equations [39]), or experimental results [32][33][34] [35][36][37]. The concentrations in the blue region, which indicates the EVP range of 0.5-0.7 kPa, are the generally used concentrations for the various liquid desiccant solutions.

In addition to EVP, other characteristics and properties of liquid desiccants, including the crystallization temperature, specific heat, viscosity, density, and price, should also be accounted for when selecting a liquid desiccant. Firstly, the crystallization of halide salt solution must be avoided in the MLDAD because the salt hydrates can accumulate and eventually block the solution pump, pipe, and other components, as well as contaminate the membrane. Severe crystallization can cause significant maintenance issue and performance deterioration [40]. Therefore, it is desirable to select a liquid desiccant with a suitable concentration and a low crystallization temperature. Secondly, in a dehumidification system, the heat comes from the air, the condensation process and the absorption process. A liquid desiccant with a higher specific heat should be selected for MLDAD to avoid the rapid growth of the liquid temperature, which leads to a sharp

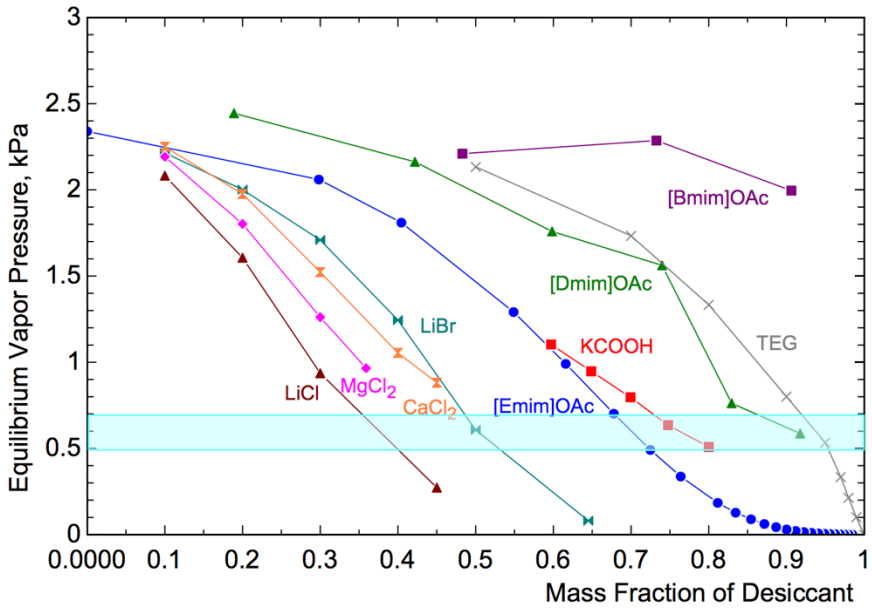

Figure 1.3 Equilibrium vapor pressures of different liquid desiccants at 20°C.

increase in the EVP and degraded dehumidification performance. Thirdly, viscosity and density of the liquid desiccant affect the pumping energy for circulating the liquid desiccants through an MLDAD system. Lower density and viscosity are recommended to save electricity consumption. Besides, the heat of dilution, which is the energy released when the solution absorbs 1kg water (kJ/kg H_2O), contributes to the temperature increase for both air and solution. The heat of dilution of different desiccants depends on the solution concentrations and temperatures.

Table 1.1 shows the saturated concentration and equilibrium relative humidity of the saturated liquid desiccants at 20°C, the cost of anhydrous salts per metric ton, density, viscosity and specific heat, and heat dilution of some commonly used liquid desiccants such as the glycol, halide salt solution, weak acid, and ionic-liquid. Table 1.2 summarized the desiccant solutions used in MLDAD systems in the published researches. As can be seen in this table, the selection of liquid desiccants varies at different experiments. LiCl solution is the most popular liquid desiccant. Its general used concentration ranges from about 35% to 45.8% [53][54][55][56][57][58][60][61]. Another commonly used solution is CaCl2-water brine, whose concentration ranges from 33% to 43% [63][64][65][66].

Table 1.1 Properties for commonly used liquid desiccants at 20°C and saturated concentrations.

Desiccant	Con (-)	RH (%)	Cost (USD/MT)	ρ (kg/m^3)	γ (mPa·s)	c_p (J/kg·K)	H_d (kJ/kg H_2O)	Ref.
TEG	1	~0	1103	1100	49	2150	-	[37]
LiCl	0.45	11.31	7400-8418	1275	9	2700	150- 300 (35-45%)	[44][19]
LiBr	0.63	6.37	3660-3316	1750	18	1750	-	[19]
$CaCl_2$	0.43	~30	284-291	1400	22	2400	-	[19]
$MgCl_2$	0.35	33.07	721	1220	7	2500	-	[44][19]
KCOOH	0.72	23.11	288	1525	20	2400	-	[44]
[EMIM][OAc]	1	~0	814000	1105	90	1900	200 -800 (70-100%)	[31]

Table 1.2 Summary of liquid desiccant used in recent researches.

Research	Solution type	Concentration (%)	Temperature (°C)
Isetti, 1997 [53]	LiCl	42	20, 31
Bergero, 2001 [54]		45.8	29
Bergero, 2011 [55]		36.5	14.6
Moghaddam, 2013 [56]		34.6	24
Huang, 2014 [57]		35.0	25
Zhang, 2014 [58]		29.5	21.6
Abdel-Salam, 2016 [59]		32.5	24.2~25.3
Lin, 2018 [60]		35	25
Bai, 2018 [61]		39	25
Annadurai, 2018 [62]		35	20
			28
Bettahalli, 2016 [63]	$CaCl_2$	43%	35
Chen and Bai, 2016 [64][65]		33%, 36%, 39%	20
Hout, 2017 [66]		38%	16.4
Erb and Ahmadi, 2006~2009 [67][68][69]	$MgCl_2$	31.8%	24
Mahmud, 2009 [70][71]		32.5	27
Fakharnezhad, 2016 [72]	TEG	99.5%	-
Petukhov, 2016 [73]		99.5%	-
Isetti, 1997 [53]	$Ca(NO_3)_2$	56%	28, 38
Meggers, 2017 [74][75]	Alkoxylated siloxane	-	-
Chen, 2018 [76]	KCOOH	36%, 49%, 62%	28~34
Liu, 2018 [77]	[EMIM][OAc]	70%~90%	25

1.2.2 Membranes

The membrane is a selective layer allowing only some specific components of a mixture in one side to pass through but stop others. MLDAD uses a membrane to separate the stream of processing air and the fluid of liquid desiccant. In this process, only water vapor can pass through the membrane. The direction and flux of water vapor are determined by the vapor pressure difference between the two sides of the membrane (Figure 1.4).

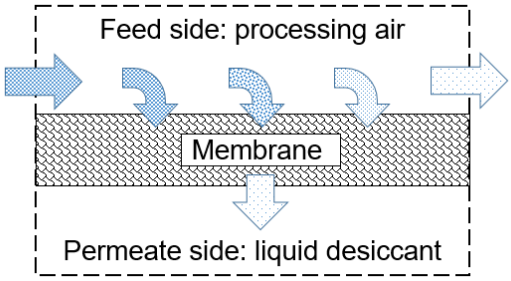

Figure 1.4 A schematic diagram of a membrane-based air dehumidifier

According to the pore size, the mean diameter of pores, membranes can be classified as the dense membrane (or non-porous membrane) with the pore size less than 0.1 nm, and the porous membrane with the pore size at about 0.1 μm [24]. Porous membranes are hydrophobic, and they are mainly used in the air-to-liquid system. In contrast, dense membranes are hydrophilic, and they are more often applied in the air-to-air systems [7].

For porous materials, pore size, porosity (ε) and tortuosity (τ) are the key characteristics determining how much vapor passes cross the membrane. Porosity is the ratio of the pore volume to the total membrane volume [78]. A higher porosity value leads to a better permeate performance. The porosity of the membrane used in MLDAD generally ranges from 0.35 to 0.65, but there is an exception using a membrane with a porosity of 0.7~0.85. Tortuosity (τ) is the degree of deviation between pore shape and cylindrical shape. A higher tortuosity value leads to a lower the permeate flux. The tortuosity also correlates with porosity [79].

Selectivity and Permeability are two of the most important properties of the membrane. Selectivity is the ratio of the amount of water vapor to that of the other components in the humid air passing through the membrane. Larger pore sizes lead to a smaller selectivity so that the purity of permeate is reduced [7]. The water selectivity in recently used membranes for air dehumidification ranges from 178~16300 [24]. In the liquid-to-air application, high water selectivity is preferred to prevent leakage and carryover of liquid desiccants.

The amount of water vapor permeated through the membrane depends on different conditions of temperature and humidity at each side of the membrane. Permeance is the water vapor transmission induced by the vapor pressure difference between two sides of the membrane. The measured data of the vapor-to-vapor permeance of the semi-permeable membrane ranges from 1E-7 to 1E-5 [87][88][89] [90]. The product of permeance and the thickness of the membrane is called permeability. A membrane with high vapor permeability can make water vapor permeate faster,

thus reducing the mass transfer area. The permeability can be measured via wet/dry cup method according to ASTM E96 standard [86]. Vapor diffusion resistance (VDR) is the resistance of vapor diffusion through membranes. VDR is essentially the reciprocal of membrane permeability, so the membrane permeability decreases with the increase of VDR. The VDR can be tested by the dynamic moisture permeation cell (DMPC) method [91].

The membrane materials can be classified as organic (polymeric), inorganic (mental/ceramic/zeolite), mixed matrix membrane (hybrid), and liquid membranes in air dehumidification. The polymer membranes, such as polyvinylidene fluoride (PVDF), polytetrafluoroethylene (PTFE), polypropylene (PP), and polyethylene (PE) films, are widely used in vapor seperation due to their low cost, no defects, repeatability and good physical stability [24]. The zeolite membranes with thermal and chemical stability are produced from a growth solution and porous support sheet using in-situ and seeded methods. The mixed matrix membrane has better reproducibility, better transmission performance and higher stability, as well as simpler manufacture and lower cost, by mixing polymer and zeolite membranes [92][93][94][95]. The support liquid membrane is designed to fix the solution in the porous support membrane by capillary force, so as to improve the vapor transmission rate and selectivity [96][97][98][99][100][101][102][103]. Table 1.3 summarizes the membrane material, thickness, pore size, porosity, VDR and thermal conductivity for membranes used in MLDAD.

Table 1.3 Properties for membrane used in liquid-to-air membrane contactor.

Research	Membrane Material	Thickness (μm)	Pore size (μm)	Porosity (-)	VDR (s/m)	Conductivity (W/mK)
Bergero 2001 [54]	PP	200	0.4	0.4-0.45	-	0.334
Hemingson 2005		-	2-15	0.45	215-329	
Erb 2006~2009 [55][68][69]		500	< 1	-	345[b]	
Mahmud 2009 [70][71]		224	< 1	-	158	
Fakharnezhad 2016 [72]		50	0.2	-	-	
Petukhov 2017[73]		35	0.2	0.45	-	
Bergero 2011 [55]	PP + PTFE	100+70	-	-	-	-
Huang 2014 [57]	PVDF + silica gel	150	0.24[b]	0.35~0.4[b]	-	-
Zhang 2011 [104]	PVDF + PVAL[c]	150	0.15	0.65	-	0.36
Zhang 2012 [105]	PVDF	100	0.15[b]	0.65[b]	-	0.17
Zhang 2014 [58]	PVDF + PVAL	200	0.15[b]	0.65[b]	-	-
Bettahalli 2016 [63]	PVDF	-	0.39	-	-	-
Fakharnezhad 2016 [72]	Hydrophilic PVDF	300	0.1	-	-	-
Hout 2017 [66]	PVDF	110	-	0.8	-	0.0608
Lin 2018 [60]	PVDF + silica gel	100	-	-	-	-

Annadurai 2018 [62]	PVDF	220	0.2	-	-	-
Isetti 1997 [53]	PE	170	16	39[a]	-	0.04
Moghaddam 2013 [56]	GE ePTFE	265	-	-	56	0.065
Abdel-Salam 2016 [59]	GE membrane	300	-	-	38	-
Meggers 2017 [74][75]	Highly selective Pebax 1074 nonporous membrane					
Chen 2018 [76]	-	100	0.2	0.6	-	0.17
Liu 2018 [77]	Nafion ionomer	25	-	-	-	-

[a] Tortuosity/porosity=39
[b] Guess value
[c] dense polyvinyl alcohol

1.2.3 MLDAD module – heat and mass exchanger

Module configuration: The MLDAD is a membrane-based heat and mass exchanger (MHMX). MHMXs include two types of modules according to the existing studies and products: flat-plate module and hollow-fiber module. Similar to the flat plate heat exchanger, flat-plate MHMX uses semi-permeable membranes instead of metals to separate process air and liquid desiccant solution as shown in Figure 1.5 [5]. The flat-plate MHMX is used in most existing MILAD studies because it has a simple structure, easy sealing, cleaning and replacing [110]. However, due to the pressure of the solution side is significantly higher than that of the air side, structural support (e.g., a plastic grid) for the membranes would be needed to reduce deformation of membranes under large differential pressure across the membrane [5].

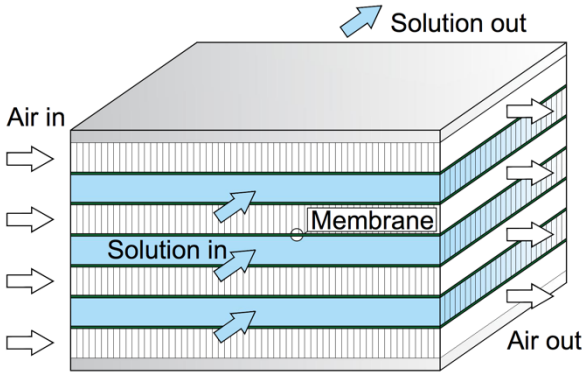

Figure 1.5 A schematic of a flat-plate MLDAD.

The hollow-fiber MHMX is similar to the shell-tube heat exchanger but replacing the metal tubes with membrane tubes as shown in Figure 1.6 [5]. It separates the air and the liquid desiccant by tube-shaped semi-permeable membranes. Either stream flows inside the membrane tubes while the other stream flows in the annulus between the outside of the membrane tubes and the inside of

the shell. The number of membrane tubes can vary from 200 [114] to 12,000 [115] in one module [5]. The hollow-fiber module does not require any additional supporting grid because the membrane tubes have more strength than the membrane plates. Also, the hollow-fiber module has a higher packing density than a flat-plate module, which is the total surface area per unit volume of the module. A typical hollow-fiber module can have a packing density of 30,000 m^2/m^3 [113]. The higher the packing density is, the better the heat and mass transfer performance will be [28], and the smaller the equipment size can be made [111][112]. However, one drawback of the hollow-fiber module is that the liquid desiccant is unevenly distributed among the membrane tubes. This uneven distribution will reduce the heat and mass transfer performance. The small diameter membrane tubes could be blocked by particulates in the air and liquid desiccant. Also, the complexity of installing internal-cooling system assemblies have limited the industrial application of hollow fiber modules [111][112].

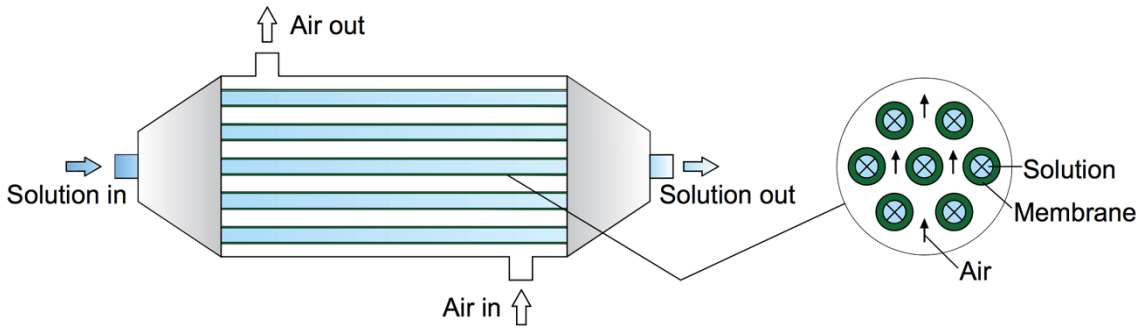

Figure 1.6 A schematic of a hollow-fiber MLDAD (reproduced by referring to [140]).

A new triple-bore hollow-fiber membrane contactor was designed by Bettahalli [63] to dehumidify the indoor air. The dehumidifier was made of a single hollow fiber with three holes inside. The solution flowed into three internal channels of the fiber. This design had a relatively higher heat transfer area, and high mechanical stability compared with single-bore hollow fibers.

Meggers et al. developed another type of hollow fiber module [74][75]. The membrane used is high water-permeability nonporous Pebax® membrane so that cross infection can be completely eliminated. The air flows inside the plastic shell, and its flow direction is opposite to the solution. Their experimental result indicated that 10 cm is the optimal length for the tube because the absorption speed is five times faster in the first 10 centimeters of contact length.

Module flow pattern: There are several different flow patterns for a two-fluid exchanger, including co-current, counter-flow, cross-flow, and counter-cross flow, as shown in Figure 1.7. It

is well known that the heat and mass exchange efficiency of counter-flow is better than that of cross flow, and the co-current is the worst type. However, counter-flow is not easy to apply due to the difficulties in separating and sealing the two streams of fluids at the entrance and exit. Counter-cross flow is usually used in MHMXs, in which one stream enters from the upper right corner of the exchanger and leave from the lower left corner, forming an 'S' shaped track line; and the other stream flows left to the right horizontally. It is because the heat transfer and mass transfer co-occur between the air and the solution in the energy exchanger, and coupled with each other. Thus, due to the existence of heat of phase change and heat of solution dilution, the higher heat exchange may lead to a worse mass exchange. Therefore, after considering the coupling of heat and mass, the best flow form for MLDAD deserves attention.

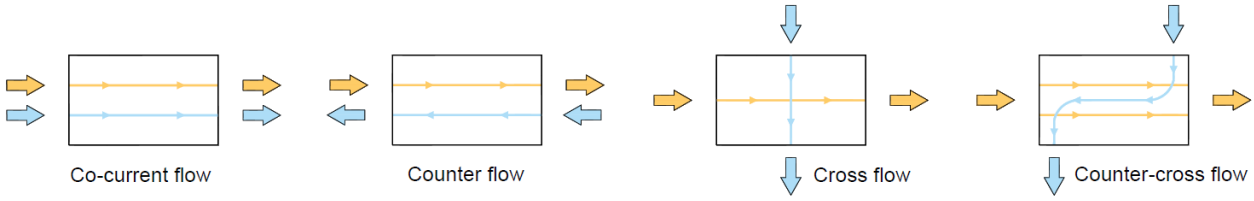

Figure 1.7 A schematic of flow patterns for air and solution in a heat and mass exchanger.

Internal cooling: In the process of liquid desiccant air dehumidification, the temperature difference and the vapor pressure difference between air and liquid desiccant are the drives for the heat and mass transfer. When the desiccant absorbs water vapor, the heat of condensation and absorption will increase the temperature of the liquid desiccant. As the liquid desiccant temperature becomes higher, its EVP increases, resulting in the deterioration of the dehumidification performance. To enlarge the water absorption capacity of the liquid desiccant, the internal cooling is necessary to keep liquid desiccant at a nearly constant temperature during the dehumidification process.

Abdel-Salam designed a three-fluid fluid internally-cooled MLDAD module, which includes a cooling water loop, a desiccant loop, and an air stream [59]. Seven cooling water tubes made of Titanium were placed inside the solution channel to decrease the solution temperature. The solution and air flowed in a counter-cross pattern, while the solution and cooling water were in a counter-flow configuration. Annadurai et al. then designed an adjacent internally-cooled MLDAD module [62]. Different from Abdel-Salam's setting, the cooling water channel in this experiment was placed parallel to the adjacent side of the solution layer. Huang studied a four-

fluid adjacent internally-cooled MLDAD [119]. This module consisted of a processing air channel, a solution channel, a falling water film, and a sweep air channel. The falling water film and the sweep air flowed in a plastic-plate channel next to the cooling channels. The heat was carried away by the sweep air and was cooled by evaporation of the falling water. Compared with the three-fluid internally-cooled MLDAD module [120], which has cooling water tubes inside the solution channel, this adjacent internally-cooled MLDAD had a smaller pressure drop of the cooling water. Thus, it led to less pumping energy consumption.

Summary and comparison of the MLDAD modules: The characteristics of the dehumidification modules used MLDAD systems are summarized in Table 1.4. Accordingly, in the flat-plate module, the length of the air channel is at the range of 200~400 mm, except for a few cases, where the length is smaller than 100 or larger than 1000 mm. It is also very common to make the length of the solution channel to 1/2 of the length of the air channel. Moreover, the numbers of both the air channels and solution channels usually range from 10 to 15 approximately. The heights (or the thickness) of a single solution channel and air channel are commonly less than 2 and 5 mm, respectively. The length and thickness of the air channel are larger than that of the solution channel. For the hollow-fiber module, the length of fibers usually ranges within 300~600 mm. The number of fibers is from 200 to 5000 in different cases. Most of the packing density is around 500~800 m^2/m^3. The packing density can be as high as 2000~3000 m^2/m^3. The length of the fibers is around 300~600 mm. For the longer fibers, the membrane deflection and fix are considered. The diameter of the fiber is around 1 mm in most designs of membrane tubes.

Table 1.4 Summary of configurations of existing MLDAD modules.

Research	Module	Flow Pattern	Channels		Remark
			At the solution side	At the air side	
Isetti 1997 [53]	Flat-plate	Co-current	Number [a]: 1 Length[b]: 300 mm Width: 50 mm Height: 5 mm	A blower forces an air stream over the LD channel.	-
Erb, 2006~2009 [55][68][69]		Cross	Number: 10 Length: 300 mm Height: 1.7 mm	Number: 10 Length: 600 mm Height: 4.9 mm	Metal screen + Fiberglass screen
Bergero 2011 [55]			Number: 15 Length: 340 mm Height: 1.2 mm	Number: 16 Length: 174 mm Height: 2.5 mm	-
Chen & Bai 2016 [64][65]			Number: 21 Length: 230 mm Height: 4.3 mm	Number: 21 Length: 410 mm Height: 7.73 mm	Air channel barrier: PE sheet
Lin			Number: 1	Number: 1	-

2018 [60]			Length: 1000 mm Width: 1000 mm Height: 2 mm	Length: 1000 mm Width: 1000 mm Height: 2 mm	
Bai 2018 [61]			Number: 22 Length: 230 mm Height: 4.3 mm	Number: 23 Length: 410 mm Height: 7.7 mm	-
Mahmud 2009 [70][71]		Counter-cross	Number: 11 Length: 1800 mm Height: 1.5 mm Width: 280 mm	Number: 10 Length: 1800 mm Height: 3.18 mm Width: 280 mm	Solution: bottom to top.
Moghaddam 2013 [56]			Number: 2 Length: 490 mm Height: 0.8 mm	Number: 1 Length: 490 mm Height: 5 mm	Channel inlet width: 0.54 cm
Huang 2014 [57]			Number: 1 Length: 200 mm Height: 2 mm Width: 100 mm	Number: 1 Length: 200 mm Height: 2 mm Width: 100 mm	Channel inlet width: 4 cm
Abdel-Salam 2016 [59]			Number: 1 Length: 470 mm Height: 4.2 mm Width: 100 mm	Number: 2 Length: 470 mm Height: 5 mm Width: 100 mm	Internally-cooled. Water tube: L x D=660 mm x 2.362 mm
Huang 2018 [119]			Number: 1 Length: 100 mm Height: 1 mm Width: 100 mm	Number: 1 Length: 100 mm Height: 2 mm Width: 100 mm	Internally-cooled. Water channel: L x W x H: 100 mm x 100 mm x 2 mm
Annadurai 2018 [62]			Number: 1 Length: 1100 mm Height: 5 mm Width: 550 mm	Number: 1 Length: 1100 mm Height: 5 mm Width: 550 mm	Internally-cooled. Metal screws were used to avoid membrane deflection.
Hout 2017 [66]		Open air system	Number: 1 Length: 1000 mm Width: 200 mm Height: 10 mm	Ambient air	Liquid desiccant membrane ceiling
Fakharnezha 2016 [72]	Hollow fiber	Co-current	Number: 200 Length: 320 mm Diameter: 0.8 mm	Number: 1 Length: 320 mm Diameter: 50 mm	-
			Number: 1200 Length: 360 mm Diameter: 0.275 mm	Number: 1 Length: 360 mm Diameter: 25 mm	-
Bergero 2001 [54]		Cross	Number: 800 Length: 450 mm Diameter: 0.6 mm	A blower forces an air stream over the LD channel.	Packing density =593 m^2/m^3.
Zhang 2012 [105]			Number: 2900 Length: 350 mm Diameter: 1.3 mm	Number: 1 Length: 350 mm Width: 90 mm Height: 200 mm	Packing density =759 m^2/m^3.
Zhang 2014 [58]			Number: - Length: 380 mm Diameter: 1.1 mm	Number: 1 Length: 380 mm	-
Chen 2018 [76]			Number: 5000 Height: 500 mm Diameter: 1.4 mm	Number: 1 Length: 200 mm	Packing density =832 m^2/m^3.
Zhang 2011 [104]		Counter	Number: 200 Length: 300 mm Diameter: 1.2 mm	Number: 1 Length: 300 mm Diameter: 40 mm	Packing density=750 m^2/m^3.

Petukhov 2017 [73]			Number: 1200 Length: 500 mm Diameter: 0.24 mm	Number: 1 Length: 500 mm	-
Bettahalli 2016 [63]		Open air system	Number: 3 Length: 580 mm Diameter: 3 mm	Ambient air	-
Meggers 2017 [74][75]			Number: Diameter: 1.4 mm	Number: 1 Diameter: 3.5 mm	-

[a] Number of channels
[b] Length refers to the distance along the direction of fluid flow

1.2.4 MLDAD performance

Table 1.5 summarizes the measured performance of the reviewed MLDAD systems, including the operating conditions, NTU values, MRR, air-side effectiveness. The operating inlet temperature of air and solution are around 30~35 ºC and 20~25 ºC for dehumidification and cooling mode, respectively. The humidity ratio of inlet air ranges from 9 to 18g/kg. The flow rates of air and solution in different tests are not the same. The most frequently used NTU value to performance testing is about 3~4, and the Cr* (solution to air heat capacity ratio) can be taken from 1 to 12. The latent effectiveness of dehumidifiers generally ranges from 0.3 to 0.95 depending on different operating conditions, module designs, and types and concentrations of liquid desiccants.

Table 1.5 Dehumidification performances of MLDADs

Research	Flow pattern	Operating condition		Performance		
		Air side	Liquid side	NTU/Cr*	MMR (g/h)	Latent effectiveness
Isetti, 1997, [53]	Co-current	T: 20 ºC w: 5.2 g/kg v: 2.7 m/s	T: 20 ºC C: 42% LiCl v: 3.42 kg/h	-	51	-
Bergero, 2001, [55]	Cross	T: 25 ºC w: 10.5 g/kg v: 30~80 m^3/h	T: 29 ºC C: 42% LiCl v: 25, 41 kg/h	-	180~380	0.52~0.65
Moghaddm, 2013, [56]	Counter-cross	T: 35 ºC w: 17.3 g/kg	T: 24 ºC C: 34.6% LiCl	NTU=3 Cr*=1~7	-	0.54~0.84
			T: 24 ºC C: 25% LiCl		-	0.23~0.75
			T: 24 ºC C: 30% LiCl		-	0.37~0.78
			T: 24 ºC C: 35.8% $MgCl_2$		-	0.5~0.86
Bettahalli, 2017, [63]	-	T: 30 ºC rh: 70% fan/chiller off	C: 43% $CaCl_2$ v: 1~5 ml/min	-	0.06 g/m^2hPa	-
		T: 30 ºC rh: 70% fan off/chiller on	C: 43% $CaCl_2$ v: 5 ml/min	-	0.22 g/m^2hPa	-

		T: 30 ºC rh: 70% fan/chiller on	C: 43% $CaCl_2$ v: 5 ml/min	-	0.25 g/m^{2}hPa	-
Huang, 2014, [57]	Counter-cross	T: 30 ºC w: 19 g/kg v: 0.4~1.2 kg/h	T: 25 ºC C: 35% LiCl v: 3~6 kg/h	-	5~8.6	0.4~0.8
Chen&Bai, 2016, [64][65]	Cross-flow	T: 30 ºC w: 18 g/kg	T: 20 ºC C: 39% $CaCl_2$ v: 36~108 kg/h	NTU=4~12 Cr*=1.55	-	0.3~0.45
				NTU=4~12 Cr*=3.1	-	0.4~0.65
				NTU=6 Cr*=1.6~10.9	-	0.31~0.44
Bai, 2018 [61]	Cross-flow	T: 30 ºC rh: 70% v: 438 kg/h	T: 20 ºC C: 39% LiCl v: 438~1750 kg/h	NTU=2 Cr*=3~12.5	-	0.46~0.51
				NTU=4 Cr*=3~12.5	-	0.65~0.75
				NTU=8 Cr*=3~12.5	-	0.82~0.93
Annadurai, 2018, [62]	Counter-cross	T: 36 ºC w: 25 g/kg v: 5 kg/h	T: 20 ºC C: 35% LiCl v: 5 kg/h	-	18000	0.2
			T: 28 ºC C: 35% LiCl v: 5 kg/h cooling water: T: 15 ºC v: 15 kg/h	-	32400	0.32
Chen, 2018, [76]	Cross-flow	T: 35~40 ºC Rh: 60~70% v: 0.65~0.7 m/s	T: 29 ºC C: 62% KCO_2H v: 3 L/h	-	745~1390	0.4~0.43
		T: 35 ºC Rh: 60% v: 0.65 m/s	T: 28.5 ºC C: 49% KCO_2H v: 3 L/h	-	691	0.387
		T: 35 ºC Rh: 60% v: 0.65 m/s	T: 28.1 ºC C: 36% KCO_2H v: 3 L/h	-	651	0.356
Huang, 2014, [57]	Cross-flow	Fresh air: T: 35 ºC Rh: 65% v: 240 kg/h	T: 28 ºC C: 40% LiCl v: 250 L/h T: 25 ºC water	-	1320	0.335
Fakharnezhad, 2016, [72]	Cross-flow	v: 6 l/h	C: 98~99.9% TEG v: 0.54 l/h	-	-	Module 1: 0.7~0.8 Module 2: 0.8~0.95
Abdel-Salam, 2016, [59]	Counter-cross	T: 34.9~35.3 ºC w: 17~18.7 g/k	T: 24.2~25.3 ºC C: 32.5% LiCl cooling water: T: 10~24.6 ºC	NTU=1.8 Cr*=1.8	30~20	0.66~0.45

1.2.5 Heat and Mass Transfer Model for MLDAD

The modeling methods for MLDAD process can be roughly divided into two types: effectiveness NTU (e-NTU) method and the finite element method. E-NTU approach is an analytical

way to calculate the effectiveness of a component. The effectiveness is generally related to NTU value, mass flow rate ratio, and capacity ratio. NTU is the calculated number of transfer units for either heat or mass transfer, and it is related to the transfer resistance, transfer area, and fluid heat capacity. The analytical solution of the sensible and latent effectiveness for a flat-plate membrane module with all flow patterns have been developed in [56][125][126]. These correlations for the heat transfer are based on the pure analogy for a flat-plate heat exchanger, and the mass transfer is based on the analogy of the heat and mass transfer. Later, Zhang developed other correlations of the sensible and latent effectiveness for both flat-plate and hollow-fiber membrane-based enthalpy exchangers [127]. These solutions can be used for both air-to-air modules and air-to-liquid modules. However, the e-NTU method regards the module as a whole black box, so it can only solve the problem of approximate effectiveness without studying the detailed profiles of temperature and humidity inside the module. Thus, it is easy, time-saving, but inaccurate relatively.

The most popular numerical modeling for MLDAD module is the finite element method. It discretizes the domain into finite segments and analyzes the heat and mass transport process for each segment. Through multiple iterations, the unknown conditions of the entire domain can be solved. The smaller the segments are, the more accurate the numerical results will be obtained. In the finite element method, the governing equations of the heat or mass transfer depends on the conservation of energy, that is, for every minimal control volume, the heat and mass difference between the inlet and outlet of the fluid (either the air or the solution) is equal to the energy of heat and mass absorbed from or transferred to the outside.

The heat and mass transfer coefficients are two major parameters during the energy transport process. Generally, there are three ways to calculate them. The first one is using heat/mass transfer coefficient equations, such as the typical Nusselt number and Sherwood number, calculating the approximate coefficients. The second one uses directly measured overall heat and mass transfer coefficients to calculate the NTU value. Another method uses the principle of mass, momentum and heat conservation to calculate the values of Nu and Sh numbers under different temperature and humidity conditions, thus, obtaining the transient heat and mass transfer coefficients of each control volume [129]. The last method is called microstructure-level analysis, uses the physical properties of materials, driving forces, and membrane microstructural parameters at to model the mass transfer. It combines Knudsen diffusion, molecular diffusion, and Poiseuille flow to explain mass transport through the membrane [130][131]. The heat transfer coefficients

are obtained from equations. To a conclusion, the finite difference method is more complicated but accurate. It can provide detailed information about the temperature and humidity at different locations inside the module. Table 1.6 summarizes commonly used governing equations for membrane-based energy exchangers from the related literature.

1.3 Research objectives

The Heat and mass transfer model is the core component for the development of new technology. It assists in the module design, operation simulation, and performance evaluation. A good model can save a lot of time and investments in the experimental studies while specifying a clear and accurate direction for the product design and development. Therefore, the thesis focuses on the development of numerical models for the membrane-based liquid desiccant air dehumidifier for both porous and nonporous membranes by using a microstructure-level analysis with the finite element method. The developed model needs to be validated by the experimental data. Then the validated model will be able to offer the guidance for optimizing the dimensions of the MLDAD module, the materials, and characteristics of the membrane, the proper operating conditions under various ambient conditions, through a series of parametric studies.

1.4 Chapter overview

In order to realize and explain the above objectives clearly, the thesis follows the organization as shown below:

In Chapter 1, the background information along with an introduction and a state-of-the-art literature review on both experimental and modeling researches for the MLDAD components are presented. The objective of this research and the chapter overview of this thesis are summarized.

In Chapter 2, the research significance and the key contributions for the thesis are highlighted. The research method is discussed to provide the general procedures of the research.

In Chapter 3, the system performance of an initial MLDAD prototype using ionic liquid desiccant tested in the Oak Ridge National Laboratory is presented. The prototype design and experimental setup, followed by the experimental data analysis and discussions are covered.

In Chapter 4, two-dimensional heat and mass transfer models for both porous and non-porous MLDAD module are presented. The finite-element method is applied in the MATLAB-based program to solve the governing equations and the whole algorithm.

In Chapter 5, the heat and mass transfer models for porous and nonporous membranes are validated. A comparison between the modeling results and the published experimental data from the literature is used to validate the porous membrane-based model. Moreover, the performance data from the MLDAD prototype in ORNL is for the validation of the nonporous membrane-based model.

In Chapter 6, a performance analysis and parametric studies using the validated numerical model are presented. The comparison studies include material selection including liquid desiccants and membranes, the module design including module dimensions, membrane characteristics and flow patterns, and the operating conditions including the temperature, humidity, and flow rate.

In Chapter 7, the major conclusions of this research are summarized, along with suggested improvements and recommendations for future work.

Table 1.6 Summarizes of governing equations for commonly used modeling methods.

Method	Module	Heat Transfer	Mass Transfer
e-NTU [125][126]	Flat-plate MLDAD	Cross-flow $\varepsilon_{sen,cross} = 1 - exp\left[\frac{exp(-NTU^{0.78}R_1) - 1}{NTU^{-0.22}R_1}\right]$ (1.1) Counter-flow $\varepsilon_{sen,counter} = \frac{1 - exp[-NTU(1 - R_1)]}{1 - R_1 exp[-NTU(1 - R_1)]}$ (1.2) Parallel-flow $\varepsilon_{sen,parallel} = \frac{1 - exp[-NTU(1 + R_1)]}{1 + R_1}$ (1.3) $R_1 = \frac{(\dot{m}_a C_{p,a})_{min}}{(\dot{m}_a C_{p,a})_{max}}$ (1.4)	Cross-flow $\varepsilon_{lat,cross} = 1 - exp\left[\frac{exp(-NTU_{lat}^{0.78}R_2) - 1}{NTU_{lat}^{-0.22}R_2}\right]$ (1.5) Counter-flow $\varepsilon_{lat,counter} = \frac{1 - exp[-NTU_{lat}(1 - R_2)]}{1 - R_2 exp[-NTU_{lat}(1 - R_2)]}$ (1.6) Parallel-flow $\varepsilon_{lat,parallel} = \frac{1 - exp[-NTU_{lat}(1 + R_2)]}{1 + R_2}$ (1.7) $R_2 = \frac{\dot{m}_{min}}{\dot{m}_{max}}$ (1.8)
e-NTU [127][128]	Hollow-fiber MLDAD	$\varepsilon_{sen} = 1 - C_1 e^{\lambda_1} - C_2 e^{\lambda_2}$ (1.9)	$\varepsilon_{lat} = 1 - K_1 C_1 e^{\lambda_1} - K_2 C_2 e^{\lambda_2}$ (1.10)
Finite difference method + NTU [129]	Flat-plate MLDAD	Solution side $\frac{dT_p^*}{dx^*} - NTU_m \cdot H^* \cdot R_1(\omega_f^* - \omega_{pf}^*) - NTU \cdot R_1(T_f^* - T_{pm}^*) = 0$ (1.11) Air side $\frac{dT_f^*}{dx^*} + 2NTU(T_f^* - T_p^*) = 0$ (1.12) Membrane side $NTU(T_f^* - T_p^*) + NTU_m H^*(\omega_f^* - \omega_{pf}^*) = NTU_p(T_{pm}^* - T_p^*)$ (1.13)	Solution side $\frac{dX_{sol}}{dx^*} - (\omega_{p,i} - \omega_{f,i})NTU_m \cdot R_2(1 + X_{sol})(\omega_f^* - \omega_{pm}^*) = 0$ (1.14) Air side $\frac{d\omega_f^*}{dx^*} + 2NTU_m(\omega_f^* - \omega_{pm}^*) = 0$ (1.15) Membrane side $(\omega_{p,i} - \omega_{f,i})NTU_m(\omega_f^* - \omega_{pm}^*) = NTU_{m,p}(C_{salt} - C_{salt,mem})$ (1.16)
Finite difference method + transfer coefficients [132]	ERV	Feed $\dot{m}_1 c_{pi} \frac{\partial T_{f,i}}{\partial x} + \frac{2h_{f,i}}{H_f}(T_{f,i} - T_{s,i}) = 0$ (1.17) Sweep $\dot{m}_2 c_{po} \frac{\partial T_{f,o}}{\partial y} + \frac{2h_{p,i}}{H_p}(T_{f,o} - T_{s,o}) = 0$ (1.18) Membrane $\dot{m}_w c_{pw} \frac{\partial T_m}{\partial z} - \lambda_m \frac{\partial^2 T_m}{\partial x^2} - \lambda_m \frac{\partial^2 T_m}{\partial y^2} - \lambda_m \frac{\partial^2 T_m}{\partial z^2} = 0$ (1.19)	Feed $\dot{m}_1 \frac{\partial \omega_1}{\partial x} + \frac{2k_1}{H_1}(\rho_{w1} - \rho_{s1}) = 0$ (1.20) Sweep $\dot{m}_2 \frac{\partial \omega_2}{\partial y} + \frac{2k_2}{H_2}(\rho_{w2} - \rho_{s2}) = 0$ (1.21) Membrane $\dot{m}_w = -D_{wm} \frac{\partial C}{\partial z} = D_{wm} \frac{C_{1s} - C_{2s}}{\delta}$ (1.22)

2. RESEARCH SIGNIFICANCE AND METHOD

2.1 Research significance

Table 2.1 compared the previous researches in the literature. Accordingly, MLDAD has been studied for more than 15 years since the first research on MLDAD. Till now the MLDAD still stays at the early stage of research. The technology did not develop much in the first decade due to the limitations of the characteristics such as easy-deformation and low permeability of the selected membranes. The thin and flexible membranes made the systems leak and make the lifespan of the system short. In recent years, the new membranes such as PVDF developed with engineered microstructure offer much more robust modules for MLDAD.

Additionally, almost all of the existing research on the MLDAD used traditional halide salt solutions. Although the use of the membrane can reduce the carryover and corrosion problem, the corrosion to the supply and return solution piping and modules is still the big challenge for the development of the MLDAD. No research can be found by using an ionic liquid as a liquid desiccant in MLDAD. With respect to the heat and mass transfer modeling from the existing literature, few researchers use the microstructure-based model to describe the mechanism of heat and mass transfer occurring through the membrane in MLDAD. This is very important for the membrane materials, namely porous material.

Therefore, it is highly needed to address these challenges. Our ultimate goal of this research is to design a cost-effective, energy-efficient, and environmentally friendly MLDAD system using an ionic liquid desiccant to overcome the challenges. The ionic liquid as a liquid desiccant and the membrane have been studied separately and integrally through both experiments and modeling method for design, operation, and performance evaluation. In the study, we have developed an MLDAD module with high dehumidification effectiveness theoretically. We then carried out the design and performance test of the MLDAD prototype by using ionic liquid. The heat and mass transfer models for both porous and nonporous membranes have developed to analyze and predict the performance of the moisture removals of the system. The thesis focuses on the development and validation of the models. Both the experimental data and the data from the existing literature were used to validate the models. The models now enable to assist in the design, operation, and prediction of the MLDAD system by using various liquid materials including both the traditional

and synthesized ionic liquid. The guidelines of the system design and operation are given according to the results of the parametric studies and sensitivity study by using the developed models. Finally, the thesis offers the conclusion of the performance analysis and model developments, as well as the outlook for the MLDAD technology in the future.

Compared with these researches in the past, as shown in Table 2.1, the unique significances of our study are shown as follows:

1. The experimental investigation on a flat-plate MLDAD prototype integrated the membrane technology with the ionic liquid desiccant [EMIM][OAc] to eliminate the carryover and corrosion issues.
2. Two types of membranes were studied: the porous membrane and the nonporous membrane. We measured the vapor permeance of different membranes, including nonporous ionomer, porous PP and PTFE membranes, under different operating conditions according to ASTM E-96 standard. The various cup methods were used to explore the applicability of different types of membranes in MLDAD and the actual water vapor transfer. Also, the scanning electron microscope (SEM) images are obtained to study the microstructure of porous membranes.
3. The heat and mass transfer models developed are two-dimensional microstructure-based. The model can not only study the impacts of the module dimensions, flow patterns, operating conditions on dehumidification performance but also analyze the effect of membrane types and physical properties on the dehumidification performance. The results can guide the development of membrane materials used in MLDAD in future.
4. The heat and mass transfer models were used to compare the performance of the MLDAD module using conventional liquid desiccant LiCl solution and the [EMIM][OAc] solution. An interactive interface based on the graphical user interface (GUI) in MATLAB environment developed can provide a clear and intuitive, convenient and accurate performance prediction and analysis for the MLDAD module.

Table 2.1 Summary of works of existing MLDAD researches.

Research	Experiment			Model development				
	LDs	Membrane		H&M model		Method for H&M coefficients		
		Po-rous	Non-porous	e-NTU	FEM	Calculated /measured NTU Method	Conjugate method	Micro-structure method
Bergero, 2001 [54]	LiCl	√	×	×	√	√	×	×
Zhang, 2002&11 [127][128]	-	×	×	√	×	×	×	×
Zhang, 2006 [131]	NaCl	√	×	×	×	×	×	√
Erb, 2006~2009 [55][68][69]	$MgCl_2$	√	×	×	√	√	×	×
Mahmud, 2009 [70][71]	$MgCl_2$	√	×	×	×	×	×	×
Huang, et al. 2012 [129]	LiCl	√	×	×	√	×	√	×
Moghaddam, 2013 [56]	LiCl	√	×	√	√	√	×	×
Huang, 2014 [57]	LiCl	√	×	×	√	×	√	×
Zhang, 2014 [58]	LiCl	√	×	×	√	√	×	×
Chen & Bai, 2016 [64][65]	$CaCl_2$	√	×	√	×	×	×	×
Abdel-Salam, 2016 [59]	LiCl	√	×	×	√	√	×	×
Fakharnezha, 2016 [72]	TEG	√	×	×	×	×	×	×
Bettahalli, 2016 [63]	$CaCl_2$	√	×	×	×	×	×	×
Petukhov, 2017 [73]	TEG	√	×	×	×	×	×	×
Meggers,2017 [74][75]	Alkoxylated siloxane	×	√	×	×	×	×	×
Lin, 2018 [60]	LiCl	√	×	×	√	√	×	×
Bai, 2018 [61]	LiCl	√	×	×	√	√	×	×
Huang, 2018 [119]	LiCl	√	×	×	√	√	×	×
Annadurai, 2018 [62]	LiCl	√	×	×	√	×	×	×
Chen, 2018 [76]	KCOOH	√	×	×	√	×	×	×
Xiaoli Liu, 2018	ILD: [Emim][OAc]	√	√	×	√	√	×	√

2.2 Research method

The research method is illustrated as follows. The design and performance testing of the first MLDAD prototype were carried out by the researchers of Dr. Xiaobing Liu and Joseph Warner, our research partners in Oak Ridge National Laboratory (ORNL). In this experiment, the nonporous ionomer provided by Xergy and [EMIM][OAc] aqueous solution was selected as the membrane material and liquid desiccant, respectively.

Then, in order to guide the improvement of the dehumidification performance of the prototype, two-dimensional heat and mass transfer models were developed. The models integrated the microstructures of the membrane materials, the flow patterns of air and solution streams, the module dimensions, and the operating conditions of air and solution. According to the types of the membrane used in the MLDAD module, different mechanisms of water vapor transfer were employed: the pore-flow diffusion for porous membranes, and the solution-diffusion for nonporous membranes. The water vapor transfer coefficient for the porous membrane was calculated by Knudson diffusion mechanism, molecular diffusion mechanism, and poises flow mechanism. The water vapor transfer coefficient for the nonporous membrane was obtained by the direct measurement conducted in ORNL by the author, Dr. Xiaobing Liu, and Lishi Wang. The test was followed by the instructions from ASTM E-96 standard, using the wet-cup method, dry-cup method, inversed wet-cup method, and the liquid-desiccant-cup method. In order to further observe the difference of microstructures of different membranes, SEM images were obtained in ORNL.

After the models were developed, the experimental data given in the literature was used to validate the model using porous membranes. The experimental data from our first preliminary test was used to validate the model using nonporous membranes. The validated model can be used to analyze the heat and mass transfer effectiveness of different flow patterns, different kinds of membrane materials, different liquid desiccant materials under different operating conditions and module specifications. It provides guidance and suggestions for the improvement of the MLDAD.

3. EXPERIMENTAL PERFORMANCE ANALYSIS OF A MLDAD MODULE

This section provides detailed information for the performance testing of an initial MLDAD prototype in the Oak Ridge National Laboratory (ORNL). The mass transfer coefficient, the permeance of the membranes studied were measured in indoor chambers in ORNL (shown in Appendix B). The following sections cover on the experiment setup and the experimental data analysis and discussions of the MLDAD prototype using ionic liquid desiccant.

3.1 Experiment setup

An experimental apparatus was set up in an artificial climate chamber in ORNL to characterize the performance of a small-scale MLDAD prototype by using ionic liquid. The MLDAD module is made of four layers of air plates and three layers of ILD plates. The ILD plates and air plates are separated by the membrane in a sandwich configuration, as illustrated in Figure 3.1.

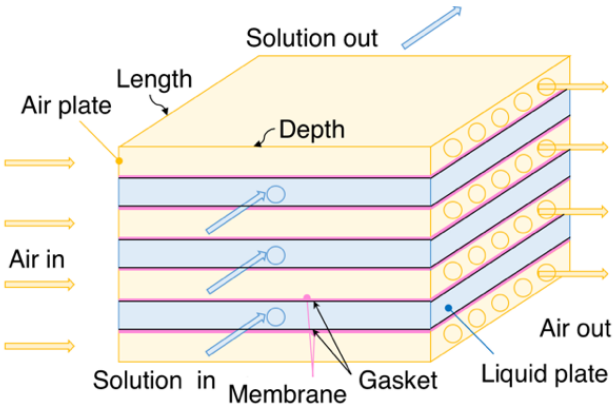

Figure 3.1 The structure of the small-scale MLDAD Prototype.

The module is a crossflow exchanger, so the direction of the air stream and the ILD flow are perpendicular. The height, length, and depth of the module are 3.75 in, 6 in, and 7.25 in, respectively. The membrane used in the module has a specific surface area of 261 in^2 and a thickness of 0.001 in. In this study, the aqueous solution of an ionic liquid – [EMIM][OAc] – is used as the liquid desiccant. It has high thermal stability and low or no corrosion to metals [31]. Moreover, it does not have a crystallization problem. The membrane used in the prototype is a variant similar to Nafion® PFSA.

Figure 3.2 shows the testing apparatus for the MLDAD prototype. An Omega WT4401-D wind tunnel was connected to the air plates to provide the processing air for the air dehumidifier. The air pressure, temperature, and relative humidity at the inlet and outlet of the MLDAD were measured. A data acquisition system was used to collect and save data from all sensors during each test. The measurement devices and corresponding accuracies are shown in Table 3.1.

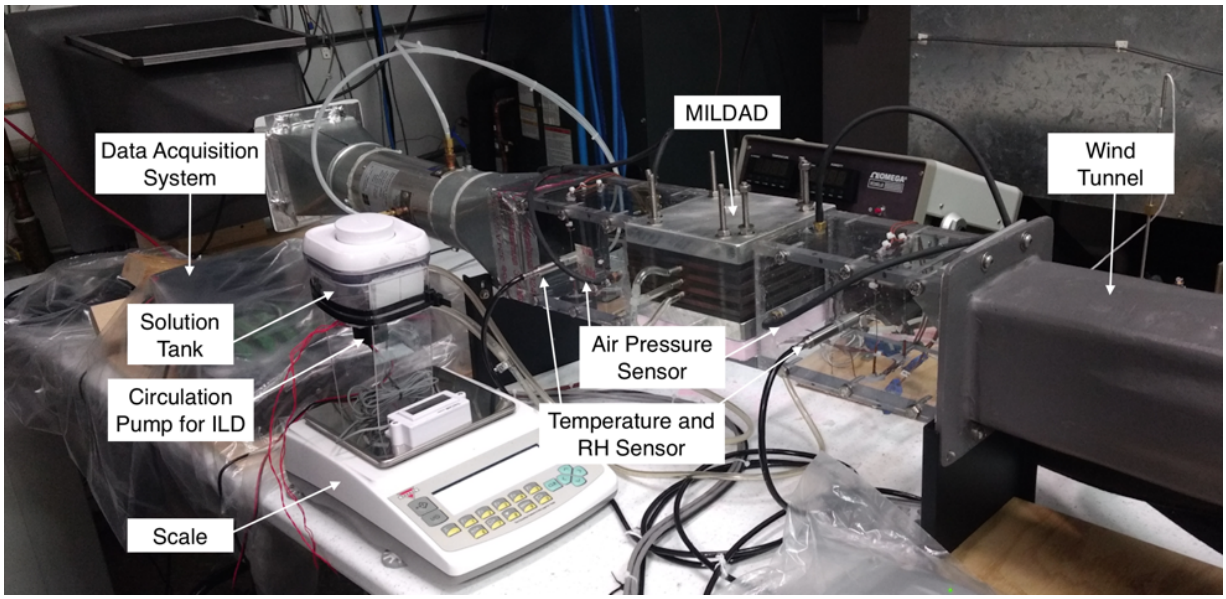

Figure 3.2 The experimental apparatus for testing a small-scale MLDAD prototype [77].

Table 3.1 The measurement devices and corresponding accuracies.

Target parameters	Measurement devices	Corresponding accuracies	Range
Temperature	Vaisala HMT330	± 0.45 F	-4~ +104 F
Relative humidity	Vaisala HMT330	± (1.0 + 0.008 X reading) %	0 – 95%
Differential air pressure	Omega PX02K1-16A5T	0.25%	0 – 32 in. Hg
Scale	Torbal AG4000	0.01 gram	4,000 grams

Three groups of tests under different operating conditions are conducted, including two dehumidification tests and one regeneration test. Table 3.2 summarizes the operating conditions of the tests. For each test, the temperature and relative humidity of the air was maintained at a pre-defined condition by adjusting the temperature and relative humidity setpoint of the climate chamber. The air flow rate can be adjusted by regulating the wind tunnel's variable speed fan. The ILD was circulated through the prototype at a fixed flow rate. A solution tank and a circulation pump were used to circulate ILD through the prototype. An electric heater was installed in the solution tank to control the temperature of the ILD solution. The actual ILD flow rate was reduced to about

0.3 L/min, and the air flow rate was kept below about 3 CFM to prevent leakage from the membrane to the air stream. To determine the air flow rate at a low fan speed, a flow rate measurement was first taken at a sufficiently high flow rate. The affinity law was then used to determine the flow rate at lower speeds based on the measured pressure difference. For the dehumidification test, the initial temperature of the ILD was at the ambient temperature; but the ILD was warmed up to a prescribed temperature before the regeneration test. Once the prescribed test conditions were reached, the system was allowed to run while the temperature and relative humidity of the inlet and outlet air were measured. The weight of the solution tank was measured throught each test to determine the change in the weight of the ILD solution during the test. A sample of the ILD solution was also taken before and after each test and was measured to determine the concentration using a correlation between the concentration and density of the ILD solution. This correlation was derived from the measured densities of the aqueous solution of [EMIM][OAc] at various mass fractions.

Table 3.2. Operating conditions of MLDAD prototype

Mode	$T_{air,in}$ [°C]	$rh_{air,in}$ [%]	$\dot{m}_{air,in}$ [CFM]	$T_{sol,in}$ [°C]	$C_{sol,in}$ [%]	$\dot{m}_{sol,in}$ [L/min]
Dehumidification	28±0.5	53±1	3	25	90	0.3
	28±0.5	80±3	1.5	25	90	0.3
Regeneration	35±0.5	14~19	1.5~3	40	70	0.3

3.2 Performance indicators

According to the related literature, the most frequently used indicators for evaluating the performance of a dehumidifier include latent, sensible and total effectiveness, which are expressed with Equations 3.1-3.3, respectively. Latent effectiveness (ε_{lan}) is the ratio between the actual and maximum possible mass transfer rates in mass exchangers. Sensible effectiveness (ε_{sen}) is the ratio between the actual and maximum possible heat transfer rates in heat exchangers. Moreover, the total effectiveness (ε_{tot}) is the ratio between the actual and maximum possible energy (enthalpy) transfer rates in energy exchangers. For a dehumidifier, the change of air conditions is worthier of note compared with the change of solution conditions. Therefore, the air side effectiveness has been widely used in evaluate the performance of dehumidifiers.

$$\varepsilon_{lat} = \frac{w_{air,in} - w_{air,out}}{w_{air,in} - w_{sol,in}} \tag{3.1}$$

$$\varepsilon_{sen} = \frac{T_{air,in} - T_{air,out}}{T_{air,in} - T_{sol,in}} \tag{3.2}$$

$$\varepsilon_{tot} = \frac{\varepsilon_{sen} + \varepsilon_{lat} H^*}{1 + H^*} \tag{3.3}$$

where, T is the temperature and w is the humidity ratio referring to the moisture content in the air (i.e., kg of water vapor in each kg of dry air). For the liquid desiccant, w_{sol} represents the equilibrium humidity ratio of the solution, which can be calculated by air pressure (P_{air}) and solution equilibrium vapor pressure ($P_{v,sol}$) as shown in Equation 3.4. H^* is the ratio of the enthalpy difference to the sensible heat difference between the inlet air and the inlet liquid desiccant.

$$W_{sol,in} = \frac{0.622 \cdot P_{v,sol}}{P_{air} - P_{v,sol}} \tag{3.4}$$

Except for the effectiveness, the absolute moisture removal and the rate of dehumidification are also two crucial performance indicators and need to consider. The absolute moisture removal (MR) can be evaluated by the humidity difference between the inlet and outlet air. The moisture removal rate (MRR) then is defined as the absolute moisture removal times the mass flow rate (m_{air}). So, MRR represents the weight of water vapor removed in the air per second (kg/s), as shown in Equation 3.5.

$$MRR = m_{air}\left(w_{air,in} - w_{air,out}\right) \tag{3.5}$$

3.3 Experimental results

3.3.1 Dehumidification

The initial dehumidification test was run with an average air flow rate of 3 CFM. The indoor air condition of the climate chamber was maintained at 28±0.5 ºC air temperature and 53±1% relative humidity. An aqueous solution of [EMIM][OAc] with a concentration of approximately 90% was used for this test. Figure 3.3 shows the relative humidity of the air at the inlet and outlet of the prototype MLDAD during the test. As shown in this figure, the relative humidity at the outlet of the MLDAD (downstream RH) was reduced by 2~3 percentage points compared with that at the inlet of the MLDAD (upstream RH). This indicates that air was dehumidified by the

MLDAD. It is noted that the RH values varied slightly but continuously during the test, which was resulted from the humidity control of the climate chamber. Surprisingly, the response of the down-stream RH was a few minutes ahead of the upstream RH. It is thought to be due to the location of the air supply of the climate chamber, which is closer to the outlet of the MLDAD. Figure 3.4 shows the calculated latent effectiveness of the MLDAD prototype. The average value of the latent effectiveness of the MLDAD is 0.02 approximately.

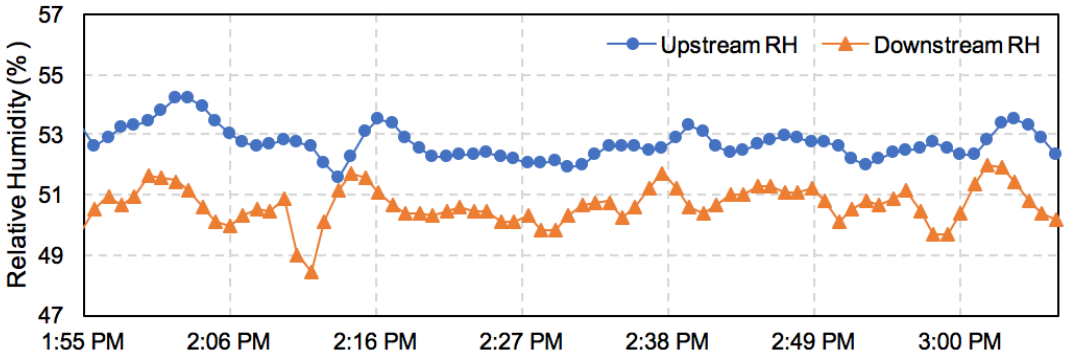

Figure 3.3 Relative humidity of the inlet and outlet air as well as the difference in humidity ratio during the first dehumidification test [77].

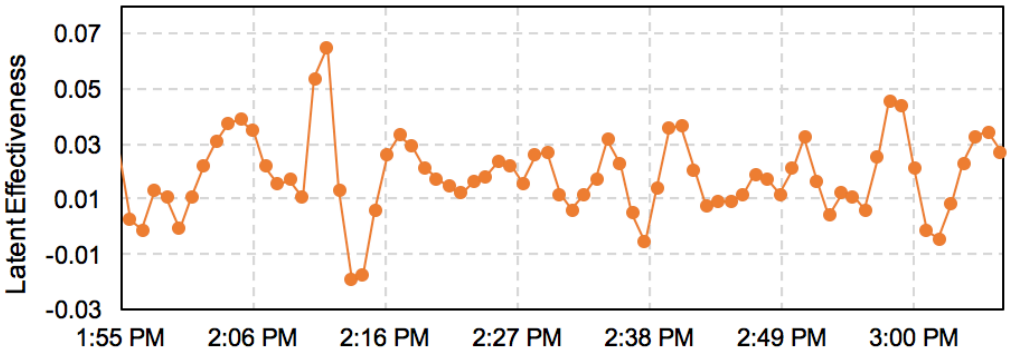

Figure 3.4 Latent effectiveness and mass transfer coefficient during the first dehumidification test [77].

During the test, the average value of the calculated mass transfer coefficient of the MLDAD module, which is the vapor transmission rate per unit membrane area, per unit drive force, is about 2.1E-14 [s]. The average rate of dehumidification is 3.14E-05 lb/min (0.85 g/hr). In terms of moisture removal rate per unit membrane area, this is equivalent to 2.88E-6 lb/min·ft^2 (or 0.84 g/hr·m^2). These values indicate that a large surface area is needed to remove a significant amount of moisture from the air flow. The high concentration (90%) of the ILD created a large potential between the equilibrium water vapor of the ILD and the partial water vapor of the air stream. However, the low

mass transfer flux from air to the ILD indicates that the water vapor transfer resistance from air to ILD through the membrane is high.

3.3.2 Regeneration

A regeneration test was performed in which the indoor air temperature in the chamber was maintained constant at 35±0.5 °C, and the relative humidity of the air was not controlled, varying between 14~19% during the test. The air flow rate was adjusted in four step changes between 1.5 and 3 CFM. The ILD was heated to 40 °C and kept at this temperature during the regeneration test.

Figures 3.5 and 3.6 show the testing conditions and the resulting latent effectiveness, respectively. The latent effectiveness is pretty much constant when the air flow rate is constant. The RH of the inlet air varied between 14~19 % and there were a couple of sudden changes of inlet air RH, which was due to short time openings of the door of the climate chamber. It appears that the variation of the indoor conditions, especially the sudden changes in RH, resulted in variations the latent effectiveness. The step changes of air flow rate also varied these performance metrics. Reducing air flow rate increased latent effectiveness and vice versa. The average latent effectiveness for the regeneration tests was 0.2 with 1.5 CFM, and it decreased to 0.075 with 3 CFM air flow. During this test, the calculated mass transfer coefficient decreased from 1.0E-13 to 2.0E-13, which is about 34% reduction, when the air flow rate was increased from 1.5 to 3 CFM. These numbers are much higher than that of the dehumidification test. It indicates that the water vapor transfer resistance from ILD to air through the membrane is much lower than that in the opposite direction.

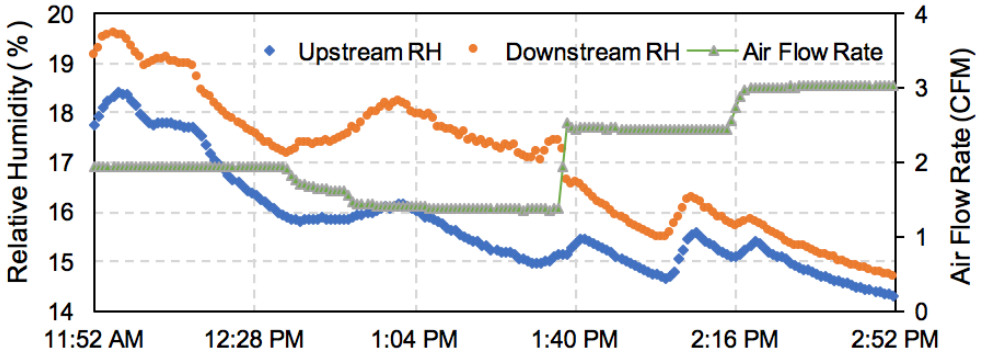

Figure 3.5 Relative humidity and flow rate of air during the regeneration test [77].

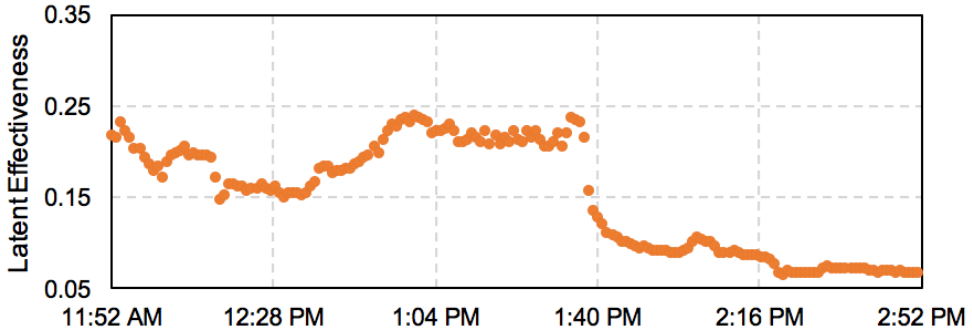

Figure 3.6 Mass transfer coefficient and latent effectiveness during the regeneration test [77].

3.4 Experiment conclusions

For this initial prototype MLDAD, the latent effectiveness and mass transfer coefficient are shown to be functions of inlet air conditions and air flow rate. For an increase in inlet air flow rate, both the latent effectiveness and the mass transfer coefficient decrease. The average latent effectiveness was 0.02 for the dehumidification test and approximately 0.14 for the regeneration tests. The average mass transfer coefficient was 2.1E-14 for the dehumidification test, and approximately 1.5E-13 for the regeneration tests. This indicates that the resistance of mass transfer is greater for the dehumidification test than for the regeneration test. It may be due to different mass transfer characteristics of the membrane for air-to-membrane moisture transfer and for membrane-to-air moisture transfer. The small dehumidification/regeneration rate (on the order of 1E-05/E-4 lb/min) indicates that this initial prototype design has limited capacity. An increased mass transfer coefficient, and increased membrane-air surface area can increase the latent effectiveness. Besides, better structure design of the MLDAD is needed to withstand pressure from the ILD and air flow so that higher air and ILD flow rates can be used without any leakage.

4. HEAT AND MASS TRANSFER MODELS

This chapter covers the heat and mass transfer models developed. The heat and mass field of each fluid channel, and the heat and mass transport in the vertical direction across the membrane were carefully analyzed. Control volume method was used to establish two-dimensional differential governing equations. In these equations, the heat transfer resistance and temperature difference are used to calculate the amount of heat transfer flux. Moreover, the vapor permeability and vapor pressure difference are used to calculate the mass transfer flux across the membrane. Therefore, the inlet temperature and humidity/concentration of air and solution were taken as input parameters, and the Gauss elimination method was used to solve the governing equations so that the outlet temperature and humidity/concentration of air and solution can be obtained. The above thermo-mass analysis was repeated for each control volume, and the temperature and humidity profiles of the whole mass transfer plane are obtained by the finite element method and continuous iterations. Finally, two heat and mass transfer models of MLDAD modules have been developed for the uses of porous and dense membranes, respectively.

4.1 Control volume and assumptions

Figure 4.1 shows a schematic diagram of a cross-flow flat-MLDAD module for the model development. In this module, flat-shaped semi-permeable membranes are used to separate air and solution so that they do not contact directly. The air layer is parallel to the solution layer. The flow pattern of air and solution can be parallel, cross, and counterflow.

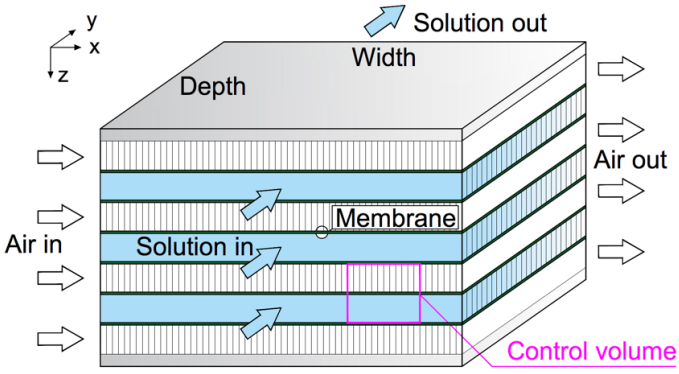

Figure 4.1 A schematic diagram of a membrane-based liquid desiccant air dehumidifier.

To help develop the governing equations for this heat and mass exchanger, the control volume of an MLDAD module is selected on the basis of the coordinates system as shown in Figure 4.2. It consists of segments of the air channel, membrane, and the solution channel. In this control volume, the processing humid air enters into the air channel from left to right in the x-axis direction. Meanwhile, the high-concentrated liquid desiccant enters into the solution channel from front to back in the y-axis direction. In the dehumidification process, the water vapor in the air permeates through the membrane into the solution side, and then be absorbed by the solution in the membrane-solution interface. Then the energy of vapor condensation and the dilution of the solution will be released. This mass transfer happened in the z-axis direction.

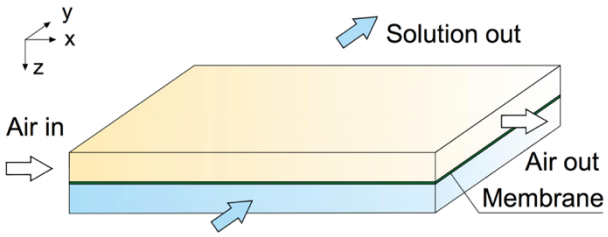

Figure 4.2 A schematic diagram of a membrane-based liquid desiccant air dehumidifier

To assist the model setup, several assumptions are made:

- The humid air is an ideal gas containing water vapor and dry air;
- Heat and mass transfer processes are steady and isothermal, and no moisture accumulates inside the membrane.
- Heat conduction and vapor mass diffusion variations along the flow directions are ignored;
- Air and solution flows are distributed uniformly in each channel respectively;
- Water vapor diffusion through the membrane is in equilibrium with the adsorption and de-sorption rates on air and solution sides, respectively; the rate of water vapor transfer through a membrane is proportional to the vapor partial pressure difference between two sides of the membrane;
- Membrane deflection adjusts effective membrane surface for heat and mass transfer.

4.2 Principles for heat and mass transfer

4.2.1 Principles for heat transfer

In the process of heat transfer, temperature difference becomes the driving force. Assume the air temperature is relatively higher than the solution temperature, then the temperature difference between the air and solution leads to the heat to transfer through the membrane from air to solution. Figure 4.3 illustrates the temperature gradient of this process and its electric analog for heat transfer. It shows that the total amount of heat transfer depends not only on the temperature gradient but also on the overall heat transfer resistance. In this control volume, the heat flux (q) across these resistances is able to be modeled with Equation 4.1, which is the combination of heat transfer coefficient calculated in Equation 4.2 and the temperature difference. The overall heat transfer resistance (R_{total}) is the sum of resistances of the air boundary layer, membrane and solution boundary layer. The heat resistance of the boundary layer is the reciprocal of the heat transfer coefficient (h_i) for each surface (Equation 4.3). And the heat resistance of the membrane is the reciprocal of the membrane conductivity (k_{mem}) (Equation 4.4).

$$\dot{q} = U_{total} dT_{LM} \tag{4.1}$$

$$U_{total} = \frac{1}{R_{total}} = \frac{1}{R_{air} + R_{mem} + R_{sol}} \tag{4.2}$$

$$R_{fluid} = \frac{1}{h_{fluid}} \tag{4.3}$$

$$R_{mem} = \frac{\delta_{mem}}{\lambda_{mem}} \tag{4.4}$$

where: $\dot{q}$ - heat flux [kW/m^2];

U_{total} - overall heat transfer coefficient [kW/m^{2}K];

T - temperature [K];

R - heat transfer resistance [m^{2}K/ kW];

h - convective heat transfer coefficient [kW/m^{2}K];

δ_{mem} - thickness of the membrane [m];

k_{mem} - conductivity of the membrane [kW/mK].

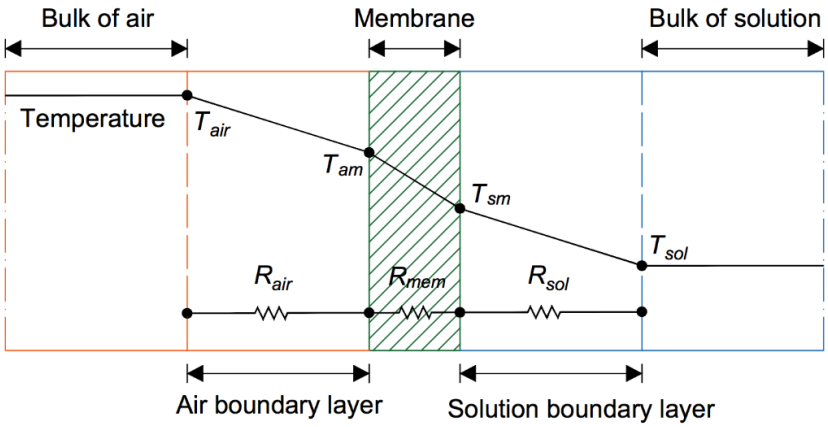

Figure 4.3 A schematic diagram of the heat transfer in a control volume

4.2.2 Principles for mass transfer

The mass transfer from the air side to the solution side occurred in the MLDAD module contains three parts: transport of water vapor through a gas phase (air side boundary layer), transport of water vapor through the membrane, and transport of water vapor through a liquid phase (solution side boundary layer). The driven force gradient and the electric analog for mass transfer in each porous membrane layer are shown in Figure 4.4.

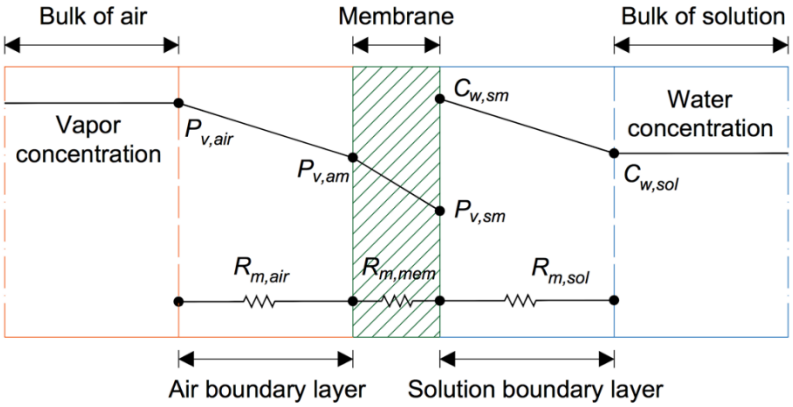

Figure 4.4 A schematic diagram of the mass transfer in a control volume for porous membranes.

Vapor transport in the air film: In the air side, the motion of water vapor molecule is described as a random walk or Brownian motion. The driven force for the movement is the concentration difference of water vapor (or vapor pressure difference). The transport of molecules from the bulk of air with a high concentration of water vapor to the membrane-air surface with a relatively lower concentration follows the Fick's first law of diffusion as shown in Equation 4.5.

$$\dot{J}_{v,air} = D_{v,air} \frac{dC_v}{dx} \tag{4.5}$$

where: $\dot{J}_{v,air}$ - water vapor transfer flux in the air [mol/(m^{2}s)];

$D_{v,air}$ - diffusion coefficient of water vapor [m^2/s];

C_v - concentration of water vapor [mol/m^3];

x - length of water vapor movement [m].

To simplify Equation 4.5, we converted the concentration of water vapor to the partial vapor pressure in the air. Then the water vapor flux in the air side can be calculated by Equation 4.6 [130].

$$\dot{J}_{v,air} = k_{v,air}\left(P_{v,air} - P_{v,am}\right) \tag{4.6}$$

where: $k_{v,air}$ - vapor transfer coefficient in the air [kg/(m^{2}Pa·s)];

$P_{v,air}$ - partial vapor pressure in the bulk of air [Pa];

$P_{v,am}$ - partial vapor pressure in the membrane-air surface [Pa].

Vapor transport through the membrane: In a membrane which only allows water transfer in the vapor phase, the vapor flux in the z-direction is also governed by the gradient of the partial pressure of the water vapor as shown in Equation 4.7. The vapor transfer through the membrane is the mass transfer coefficient times the vapor pressure difference at two sides of the membrane surfaces.

$$\dot{J}_{v,mem} = k_{v,mem}\left(P_{v,am} - P_{v,sm}\right) \tag{4.7}$$

where: $\dot{J}_{v,mem}$ - water vapor transfer flux across the membrane [kg/(m^{2}s)];

$k_{v,mem}$ - vapor transfer coefficient of the membrane [kg/(m^{2}Pa·s)];

$P_{v,am}$ - partial vapor pressure in the bulk of air [Pa];

$P_{v,sm}$ - partial vapor pressure in the membrane-air surface [Pa].

The vapor transfer coefficient of the membrane ($k_{v,mem}$) is a function of permeability and thickness of the membrane as shown in Equation 4.8. The thickness of the membrane used in

MLDAD generally ranges from 25 microns to 500 microns. The permeability of the membrane is discussed in Section 4.3.

$$k_{v,mem} = \frac{P'}{\delta_{mem}} \tag{4.8}$$

where: P' - permeability of the membrane [kg/(m·Pa·s)];

δ_{mem} - thicthe kness of the membrane [m].

Water vapor transport in the liquid film: In the case of physical absorption, the amount of vapor taken up by the solvent is estimated by Henry's law. The movement of water in the solution is driven by the concentration difference of water. Then the water flux through the solution boundary layer can be defined as Equation 4.9. The concentration of water in the membrane-solution surface is the combined impact of absorption and desorption.

$$\dot{J}_{w,sol} = M_w k_{w,sol}\left(C_{w,sm} - C_{w,sol}\right) \tag{4.9}$$

where: $\dot{J}_{w,sol}$ - water transfer flux in liquid phase [kg/(m^{2}s)];

M_w - molar mass of water [kg/kmol];

$k_{w,sol}$ - water transfer coefficient in liquid phase [m/s];

$C_{w,sm}$ - water concentration in membrane-solution surface [kmol/m^3];

$C_{w,sol}$ - water concentration in the bulk of solution [kmol/m^3].

To keep the driving force consistent as the vapor pressure, we can convert the water concentration as the equilibrium vapor pressure. Thus, Equation 4.9 can be re-written as:

$$J_{w,sol} = k'_{w,sol}\left(P_{v,sm} - P_{eq,sol}\right) \tag{4.10}$$

where: $k'_{w,sol}$ - water transfer coefficient in liquid phase [kg/(m^{2}Pa·s)];

$P_{eq,sol}$ - equilibrium vapor pressure of the bulk solution [Pa].

Therefore, the water vapor flux through the air boundary layer, membrane, and solution boundary layer are all defined in Equation 4.6, 4.7 and 4.10. Combine these three equations; then we can get the Equation 4.11. Because of the conservation of mass, the vapor/water flux through

the air boundary layer, membrane, and solution boundary layer are equal to each other (Equation 4.12). Then Equation 4.11 could be simplified as Equation 4.13.

$$\frac{\dot{J}_{v,air}}{k_{v,air}} + \frac{\dot{J}_{v,mem}}{k_{v,mem}} + \frac{\dot{J}_{w,sol}}{k'_{w,sol}} = \left(P_{v,air} - P_{v,am}\right) + \left(P_{v,am} - P_{v,sm}\right) + \left(P_{v,sm} - P_{eq,sol}\right) \quad (4.11)$$

$$\dot{J}_{v,air} = \dot{J}_{v,mem} = \dot{J}_{w,sol} \quad (4.12)$$

$$\dot{J}_v = \frac{\left(P_{v,air} - P_{eq,sol}\right)}{\frac{1}{k_{v,air}} + \frac{1}{k_{v,mem}} + \frac{1}{k'_{w,sol}}} \quad (4.13)$$

Similar to the overall heat transfer coefficient, the overall mass transfer coefficient ($U_{m,total}$) and mass transfer resistance ($R_{m,total}$) are defined as follows. In the control volume, the overall mass transfer resistance is the sum of resistances of the air boundary layer ($R_{m,air}$), membrane ($R_{m,mem}$) and solution boundary layer ($R_{m,sol}$) [137], as shown in Figure 4.4. Then the vapor flux transferring from the air side to the solution side can be calculated by Equation (4.19). It is a function of water vapor pressure and overall mass transfer coefficient.

$$R_{m,air} = \frac{1}{k_{v,air}} \quad (4.14)$$

$$R_{m,mem} = \frac{1}{k_{v,mem}} \quad (4.15)$$

$$R_{m,sol} = \frac{1}{k'_{w,sol}} \quad (4.16)$$

$$R_{m,total} = R_{m,air} + R_{m,mem} + R_{m,sol} \quad (4.17)$$

$$U_{m,total} = \frac{1}{R_{m,total}} = \frac{1}{\frac{1}{k_{v,air}} + \frac{1}{k_{v,mem}} + \frac{1}{k'_{w,sol}}} \quad (4.18)$$

$$J_v = U_{m,total}\left(P_{v,air} - P_{eq,sol}\right) \quad (4.19)$$

where: R_m - mass transfer resistance [(m^2Pa·s)/kg];

$U_{m,total}$ - overall mass transfer coefficient [kg/(m^{2}Pa·s)];

J_v - water vapor flux [kg/(m^2·s)].

4.2.3 Calculation for coefficients

The heat transfer coefficient for the air or the solution is determined by Nusselt number (Nu), th thermal conductivity of the fluid, and dimensions of the fluid channel [67][139]. It can be calculated by Equation 4.20.

$$h_i = \frac{Nu_i k_i}{L_i} \tag{4.20}$$

where: Nu_i - Nusselt number for each boundary layer [-];

L_i - characteristic length for each stream [m];

k_i - thermal conductivity for each stream [kW/(m·K)].

For laminar flow, the local Nusselt number is constant in the fully developed region. It can be obtained from the Re number and Pr number [135]. For force convection on a flat plate, the Nusselt number for laminar flow can be calculated by Equation 4.21. The generally used Nu number for MLDAD module in the literature ranges from 5 to 8.24.

$$Nu_x = 0.322 Re_x^{\frac{1}{2}} Pr^{\frac{1}{3}} \tag{4.21}$$

$$Pr = \frac{\nu}{\alpha} \tag{4.22}$$

where: Re_x - Reynolds number [-];

Pr - Prandtl number, ratio of the momentum and thermal diffusivities [-];

ν - kinematic viscosity [m^2/s];

α - thermal diffusivity [m^2/s].

The mass transfer coefficient for the air or the solution is determined by Sherwood number (Sh), mass diffusivity, and dimensions of the fluid channel [67]. It can be calculated by Equation 4.23.

$$h_{m,i} = \frac{Sh_i D_{v,i}}{L_i} \tag{4.23}$$

where: Sh_i - Sherwood number for each boundary layer [-];

$D_{v,i}$ - vapor diffusivity in the stilled stream [m^2/s].

The Sherwood number can be obtained from the Chilton-Coburn analog which is a certain relation between the Sherwood number and Reynolds number in Equation 4.24.

$$Sh = Nu\left(\frac{Sc}{Pr}\right)^{\frac{1}{3}} \tag{4.24}$$

$$Sc = \frac{\nu}{D_v} \tag{4.25}$$

where: Sc - Schmidt number, ratio of momentum and mass diffusivities [-].

To sum up, the heat and mass transfer coefficients of the air and the solution can be obtained by experimental or analytical Nusselt and Sherwood numbers. Moreover, the heat transfer coefficient of the membrane which is the conductivity does not play an important role and can be ignored. Thus, how to determine the mass transfer coefficient of the membrane becomes a major problem. The mainstream approach is using the dynamic moisture permeation cell to obtain the water vapor diffusion resistance of the membrane. This method highly depends on the complex experiment. In the following section, we are going to use the physical characteristics of the membrane to calculate the water vapor diffusion resistance of the membrane.

4.3 Microscopic mechanism of mass transfer through a membrane

According to the sizes of pores, membranes can be classified as the dense membrane with the pore size at around 0.1 nm, and the porous membrane with the pore size at about 0.1 μm. Thus, the mass transfer mechanisms in the membrane of the air dehumidification system can be grouped into two broad categories: pore-flow type for porous membranes and solution-diffusion type for dense membranes. According to the summary from Woods, porous membranes are mainly used in air to the liquid system while dense membranes are more often applied in the air to air system. Due to the different gas separation mechanism, the mass transport through a porous membrane or a

dense membrane is different. For a porous membrane, the permeability can be calculated through an analytical model by using membrane physical parameters. However, for a dense membrane, the experimental method is the only way to determine its permeability.

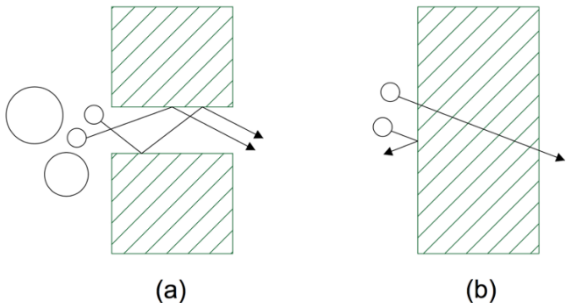

Figure 4.5 Two mass transfer mechanisms: a) pore-flow filtration, b) solution-diffusion [136][144].

4.3.1 Mass transport in the porous membrane

The mass transfer process of porous membranes is a complex process at macro and micro scales [24]. In pore-flow filtration, the vapor molecules in humid air are small enough to flow through some pores in the membrane to the solution side, while most other gases larger than the pores are filtered and remain in the air side. Membrane materials are hydrophobic so that water molecules attract each other more than solid materials. Therefore, mass transfer can be simply divided into four kinds of mechanics, including Knudsen diffusion, molecular diffusion, Poiseuille flow and molecular sieving, as shown in the following figure [137][138].

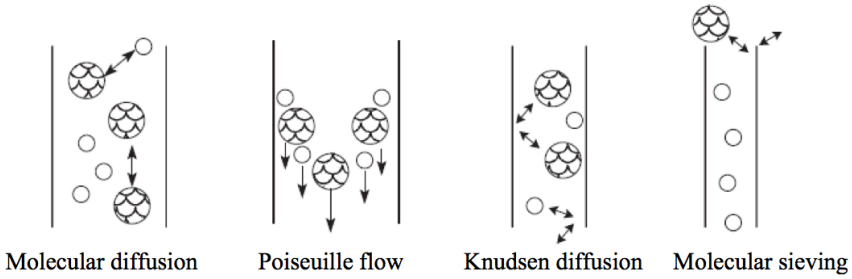

Figure 4.6 Transport mechanism for pore-flow filtration [138].

Knudsen diffusion occurs when the pore size is reduced below 10 μm or with a decrease in gas pressure as shown in Figure 4.6. In this case, the mean free path of molecules exceeds the pore radius, and a collision between molecules is less frequent than between molecules and membrane walls. The separation between different gases with Knudsen flow is possible if they have

molecules with sizes differing by order of magnitude (separation depends on the ratio of the square root of the gasses' corresponding molecular weight). The water vapor permeability due to Knudsen diffusion can be obtained by Equation 4.26 [131][138]. It is considered as a function of membrane pore radius (r), porosity (ε), tortuosity (τ), and membrane temperature (T_m).

$$D_{Kd} = \frac{2}{3}\frac{r\varepsilon}{\tau}\left(\frac{8M_v}{\pi R T_m}\right)^{0.5} \tag{4.26}$$

where: D_{Kd} - Permeability coefficient of a membrane due to Knudsen diffusion [kg/(m^{2}Pa·s)];

r - membrane pore radius [m];

ε - membrane porosity [-];

τ - membrane tortuosity [-];

M_v - molar mass of water vapor, 18 [g/mol];

R - gas constant, 8.314 [J/(mol·K)];

T_m - mean temperature of methe mbrane [K].

Molecular-diffusion dominates in larger pores where the pore radius exceeds the mean free path of molecules so that molecule-molecule collisions dominate over molecule-wall collisions. The rate of the movement is related to the temperature, the viscosity of the fluid and the mass of the particles [131][138]. The permeability due to Molecular diffusion (D_{Md}) is related to

$$D_{Md} = \frac{\varepsilon}{\tau}\frac{10^{-3}\cdot T^{1.75}}{P_m\left(v_v^{\frac{1}{3}} + v_a^{\frac{1}{3}}\right)^2}\sqrt{\frac{1}{M_v}+\frac{1}{M_a}} \tag{4.27}$$

where: D_{Md} - permeability coefficient of a membrane due to Molecular diffusion [kg/(m^{2}Pa·s)];

v_a - molecular diffusion volume of air [m^3/mol];

v_v - molecular diffusion volume of vapor [m^3/mol];

M_a - Molecular weight of air [kg/mol];

Poiseuille flow is typically used to account for a phenomenon, in which the gas behaves as a continuous fluid driven by an absolute pressure gradient between two sides of the membrane as shown in Equation (4.29) [138].

$$D_{Pf} = \frac{1}{8}\frac{r^2\varepsilon}{\tau}\left(\frac{M_v P_v}{\mu R T_m}\right) \tag{4.29}$$

where: D_{Pf} - Permeability coefficient of a membrane due to Poiseuille flow [kg/(m^{2}Pa·s)];

μ - Viscosity [Pa·s].

Molecular sieving occurs when the permeating species exhibits a strong affinity for the membrane surface and absorb along the pore walls. In this case, separation occurs due to the difference in the amount of adsorption of the permeating species based on molecular shape, molecular size, and pore size. The pore size, in this case, is comparable with the molecular size. The water vapor permeability due to molecular sieving can be obtained by Equation (4.28) [130]. It is considered as a function of membrane porosity (ε), tortuosity (τ), water vapor diffusivity (D_v^c) and membrane temperature (Tm).

$$D_{Ms} = D_v^c \frac{\varepsilon}{\tau}\left(\frac{M_v}{R T_m}\right) \tag{4.28}$$

where: D_{MS} - Permeability coefficient of a membrane due to molecular sieving [kg/(m^{2}Pa·s)];

D_v^c - water diffusivity [m^2/s].

For a membrane-base liquid desiccant module, the driving force moving vapor is the difference of vapor pressure or absolute pressure across the membrane. Thus, the vapor flux permeated through a membrane for each mechanism, $\dot{J}_v$ (kg/(m^2·s)), can be calculated from Equations. 4.30~4.33. $\dot{J}_v$ has a linear correlation with the permeability coefficient and pressure difference, as well as an inverse proportional relationship with membrane thickness.

Since the mean free path of water vapor is comparable to the typical pore size used in typical membranes employed in MLDAD, multiple mechanisms may exist in a single membrane simultaneously. In the study, a microstructure model which combines Knudsen diffusion, molecular diffusion, and Poiseuille flow is adopted to account for mass transport through the membrane. For a combination of effects for Knudsen diffusion and molecular diffusion, the effective permeability can be calculated from Equation 4.34 [24][130][138]. Moreover, the overall vapor flux through these three mechanisms can be obtained from Equation 4.36 [24][130][138].

Table 4.1 The vapor permeability and flux for various mass transfer mechanisms

Transport mechanism	Transport coefficient		Vapor flux	
Knudsen diffusion	D_{Kd}	(4.26)	$j_{v,Kd} = D_{Kd}\frac{dP_v}{dx}$	(4.30)
Molecular diffusion	D_{Md}	(4.27)	$j_{v,Md} = D_{Md}\frac{dP_v}{dx}$	(4.31)
Molecular sieving	D_{Ms}	(4.28)	$j_{v,Ms} = D_{Ms}\frac{dP_v}{dx}$	(4.32)
Poiseuille flow	D_{Pf}	(4.29)	$j_{v,Pf} = D_{Pf}\frac{dP}{dx}$	(4.33)
Knudsen- Molecular diffusion	$D_{v,eff} = \frac{1}{\frac{1}{D_{v,Kd}} + \frac{1}{D_{v,Md}}}$	(4.34)	$j_{v,eff} = D_{v,eff}\frac{dP_v}{dx}$	(4.35)
Knudsen-Molecular-Poiseuille diffusion	-		$j_{v,total} = j_{v,eff} + j_{v,Pf}$	(4.36)

4.3.2 Water vapor flux for the nonporous membrane

The gas separation mechanism for nonporous membranes is different from porous membranes. In nonporous membranes, molecular transport is possible only if a molecule dissolves in the membrane (solubility). Therefore, in this process, a molecule will be adsorbed onto the membrane surface, diffuse through the membrane due to a vapor pressure gradient, and then desorb at another surface of the membrane. This gas transport mechanism through nonporous membranes can be described by the solution-diffusion model. The flux of vapor could also be identified by using the difference of the vapor partial pressure and the membrane permeability. However, for a nonporous membrane, the permeability is hard to calculate due to complex chemical reactions. Generally speaking, the permeability is the combination of solubility and diffusivity of water vapor, as shown Equation 4.37 [137].

$$P = S \cdot D \tag{4.37}$$

Solubility is a thermodynamic parameter that reflects a measure of the amount of penetrant absorbed by the membrane under equilibrium conditions with a given pressure of the gas and given temperature. Diffusivity is a kinetic parameter that indicates how fast a penetrant is transported through the membrane in the absence of obstructive sorption. For inorganic fluids in polymer membranes both solubility and diffusivity could be assumed independent of concentration, as well as time and place (relaxation phenomena). A combination of Henry's law and Fick's law integrated across the membrane leads to the definition of permeability coefficient:

$$J_v = S \cdot D \frac{dP_v}{dx} \tag{4.38}$$

To sum up, the difference between the models for porous and dense membranes is the method to calculate the vapor flux across the membrane. The vapor flux is the combination of the mass transfer coefficient and the vapor pressure difference. For the model using porous membranes, the mass transfer coefficient can be calculated through several mass transfer mechanisms in Knudsen diffusion, molecular diffusion, Poiseuille flow, and molecular sieving. The vapor flux through these mechanisms relates to the pore size, porosity, tortuosity, and thickness of the porous material. However, for the nonporous membrane, the mass transfer coefficient can only be obtained by the measurement instead of calculating by equations. Several methods guide the measurement of water vapor transfer coefficient. In our model, we directly used the vapor permeability of the material, tested by the instruction of the ASTM E96 standard. The detailed experiment setup, results, and discussions on the permeability test are shown in Appendix B.

4.4 Governing equations

4.4.1 Heat and mass transfer in the air side

As shown in Figure 4.7, an infinitesimal control volume is cut out in the air layer of the energy exchanger, and the heat and mass transfer equation can be derived assuming that there is no heat and mass diffusion in the X and Y directions (only in the Z direction).

In Figure 4.7, the heat/mass input and output are depicted via yellow arrows. The air flow comes in from the right entrance to the left exit. In this process, the heat exchange mainly due to two parts: heat change caused by forced convection with the membrane, and the heat carried by the diffusion of water vapor. Therefore, from the principle of mass conservation, the governing equation for mass transfer in the air side can be written as Equation 4.39. From the principle of energy conservation, the governing equation for heat transfer in air side can be written as Equation 4.40.

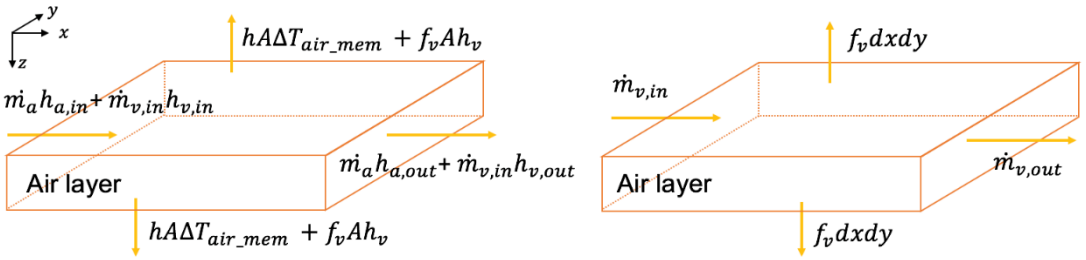

Figure 4.7 Heat and mass transport in the air layer.

$$\left(\dot{m}_{v,in} - \dot{m}_{v,out}\right) + 2f_v \beta dxdy = 0 \tag{4.39}$$

where: $\dot{m}_v$ - the mass flow rate of water vapor in the humid air [kg/s];

f_v - diffusion water vapor flux [kg/m^{2}s];

β - membrane deflection coefficient [-].

$$\begin{aligned}&\dot{m}_{air} h_{air,in} + \dot{m}_{v,in} h_{v,in} - \dot{m}_{air} h_{air,out} - \dot{m}_{v,out} h_{v,out} \\ &-2U_{air}(T_{air} - T_{airmem})\beta dxdy - 2f_v h_v \beta dxdy = 0\end{aligned} \tag{4.40}$$

where: $\dot{m}_{air}$ - mass flow rate of dry air [kg/s];

h_{air} - enthalpy of dry air [kJ/kg];

h_v - enthalpy of water vapor in the humid air [kJ/kg];

U_{air} - heat transfer coefficient between air and membrane [kW/m^{2}K];

T_{air} - mean temperature of air in the control volume [K];

T_{airmem} - mean temperature of the air-membrane interface in the control volume [K].

Assume the specific heat capacity is a constant number in the control volume, and the temperature of the air is the same as the temperature of water vapor in the air. Then the Equation 4.40 could be rewritten as Equation 4.40.

$$\begin{aligned}&\dot{m}_{air} c_{p,air,in}\left(T_{air,in} - T_{air,out}\right) + \dot{m}_{v,in} c_{p,v,in} T_{air,in} - \left(\dot{m}_{v,in} - 2f_v \beta dxdy\right) c_{p,v,in} T_{air,out} \\ &-2U_{air}(T_{air} - T_{airmem})\beta dxdy - f_v c_{p,v,mem}\left(T_{airmem,in} + T_{airmem,out}\right)\beta dxdy = 0\end{aligned} \tag{4.40}$$

4.4.2 Heat and mass transfer in the solution side

As shown in Figure 4.8, an infinitesimal control volume is cut out in the solution layer of the energy exchanger, and the heat and mass transfer equation can be derived assuming that there is no heat and mass diffusion in the X and Y directions (only in the Z direction).

In Figure 4.8, the heat/mass input and output are depicted via blue arrows. The solution flow comes in from the front entrance to the back exit. In this process, the heat exchange mainly due to three parts: the heat change caused by forced convection with the membrane, the heat carried by the diffusion of water vapor, and the heat due to absorption (condensing heat and dilution heat).

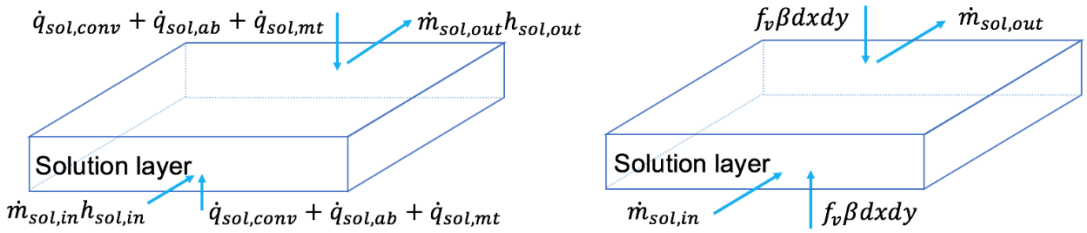

Figure 4.8 (a) Heat transport and (b) mass transport in the solution layer.

Therefore, from the principle of mass conservation, the governing equation for mass transfer in solution side can be written as Equation 4.42. From the principle of energy conservation, the governing equation for heat transfer in air side can be written as Equation 4.43.

$$\left(\dot{m}_{w,in} - \dot{m}_{w,out}\right) - 2f_v\beta dxdy = 0 \tag{4.42}$$

where: $\dot{m}_w$ - mass flow rate of water in the solution [kg/s].

$$\begin{aligned} &\dot{m}_{sol,in}h_{sol,in} - \dot{m}_{sol,out}h_{sol,out} \\ &+2U_{sol}(T_{solmem} - T_{sol})\beta dxdy + 2f_v h_v \beta dxdy + 2f_v h_{ab}\beta dxdy = 0 \end{aligned} \tag{4.43}$$

where: $\dot{m}_{air}$ - mass flow rate of dry air [kg/s];

h_{air} - enthalpy of dry air [kJ/kg];

h_v - enthalpy of water vapor in the humid air [kJ/kg];

U_{air} - heat transfer coefficient between air and membrane [kW/m^{2}K];

T_{air} - mean temperature of air in the control volume [K];

T_{airmem} - mean temperature of the air-mem brane interface in the control volume [K].

Assume the specific heat capacity is a constant number in the control volume. Then the Equation (4.43) could be rewritten as Equation (4.44).

$$\dot{m}_{sol,in}c_{p,sol,in}T_{sol,in} - \left(\dot{m}_{sol,in} + 2f_v\beta dxdy\right)c_{p,sol,in}T_{sol,out} + 2U_{sol}(T_{solmem} - T_{sol})\beta dxdy + 2f_v c_{p,v}T_{solmem}\beta dxdy + 2f_v h_{ab}\beta dxdy = 0 \quad (4.44)$$

4.4.3 Heat transfer across the control volume

The interfacial heat transfer between the membrane and either feed-side or permeate-side flows can be divided into three regions which are visualized by drawing the electrical analog in Figure 4.9.

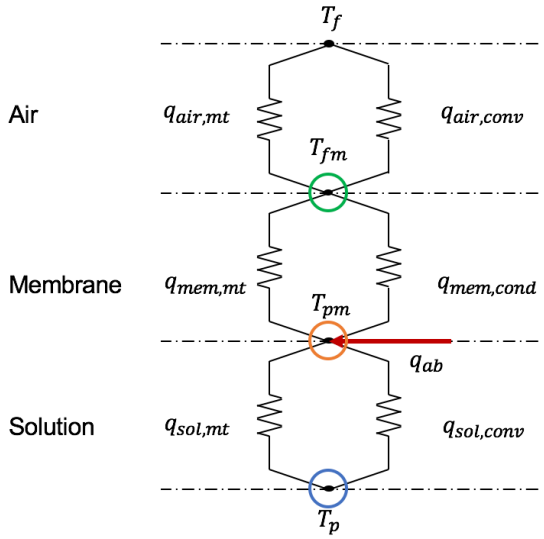

Figure 4.9 Electrical analog of heat transfer in an MLDAD control volume.

For each point at the interface, the heat flux import is the same as the heat flux export. Thus, for the air-membrane surface, the sum of convective heat ($q_{air,conv}$) and heat due to mass transport ($q_{air,mt}$) in the air layer equals the sum of conductive heat ($q_{mem,cond}$) and heat due to mass transport ($q_{mem,mt}$) in the membrane layer. The principle could be written as Equation 4.45.

$$q_{air,conv} + q_{air,mt} = q_{mem,cond} + q_{mem,mt} \quad (4.45)$$

Also, for the solution-membrane surface, the sum of conductive heat ($q_{mem,cond}$) and heat due to mass transport ($q_{mem,mt}$) in the membrane layer, and the heat of absorption (q_{ab}) equals the sum of convective heat ($q_{sol,conv}$) and heat due to mass transport ($q_{sol,mt}$) in the solution layer. The principle could be written as Equation 4.46. The heat of absorption (q_{ab}) is the combination

of heat of dilution and heat of vapor liquefaction. Finally, the equations for heat transfer at two membrane surfaces than can be carried out in Equations 4.47 and 4.48.

$$q_{sol,conv} + q_{sol,mt} = q_{mem,cond} + q_{mem,mt} + q_{ab} \tag{4.46}$$

$$h_{air}(T_{air} - T_{airmem}) - \lambda_{mem}\frac{dT_{mem}}{dz} + f_v(h_{air,v} - h_{airmem,v}) = 0 \tag{4.47}$$

$$h_{sol}(T_{sol} - T_{solmem}) + \lambda_{mem}\frac{dT_{mem}}{dz} + f_v(h_{airmem,v} - h_{solmem,v} + h_{ab}) = 0 \tag{4.48}$$

4.5 Boundary conditions, solution method, and MATLAB realization

4.5.1 Cross-flow MLDAD module

Four governing equations for heat transfer and two equations for mass transfer have been developed which could be used to calculate four temperatures of air, feed-side membrane surface, permeate-side membrane surface, and solution, as well as the vapor flux at both air and solution outlets, respectively. The boundary conditions are given, respectively:

When y=0:

$$T_{air} = T_{air,in} \tag{4.49}$$

$$\dot{m}_{air,v} = \dot{m}_{air,in}\, w_{air,in}/\left(1 + w_{air,in}\right) \tag{4.50}$$

when x=0:

$$T_{sol} = T_{sol,in} \tag{4.51}$$

$$\dot{m}_{sol,w} = \dot{m}_{sol,in} C_{sol,in} \tag{4.52}$$

The finite element method was used to solve these governing equations. The idea of this method is to divide the plane of domain area into many small segments which are regarded as control volumes, and then the heat and mass transfer is analyzed for every control volume. Governing differential equations can be solved in each small volume.

For a cross-flow MLDAD module, the x-y coordinate plane is separated as M·N meshes as shown in Figure 4.10. The outlet status of air/solution in the previous segment (output value) will

become the import of the latter segment (input value). For air side, the output parameters of mesh (1,1) become the input parameters of mesh (1,2). And for solution side, the output parameters of mesh (1,1) becomes the input parameters of mesh (2,1). Through continuous iteration, the final heat and mass exchange of the whole dehumidifier in the horizontal plane and the final exit status of air and solution could be obtained.

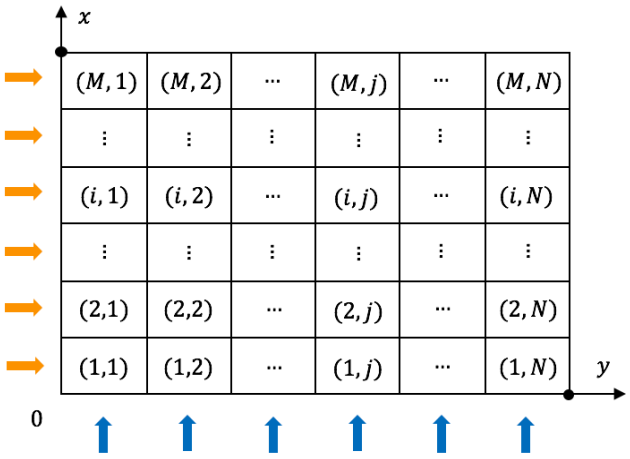

Figure 4.10 Meshes of the heat and mass transfer area in a cross-flow module.

The configuration of the MATLAB program is shown in Figure 4.11. The input of this program is membrane properties including pore radius, porosity, tortuosity, thickness, and thermal conductivity, and geometry of the MLDAD module, and the initial operating conditions. Then the dynamic properties like specific heat capacity, pressure, the permeability of the membrane, and vapor flux through control volume could be calculated. Those data are employed into four heat equations and two mass equations. Later, the output temperature, humidity (or concentration) and mass flow rate are obtained after the governing equations are solved. Update the output data as the input data for the next control volume. Run the loop section in the program until all the control volumes are analyzed. Finally, the whole profiles of temperature and humidity (or concentration) are achieved. The detailed MATLAB algorithm can be seen in Appendix C.

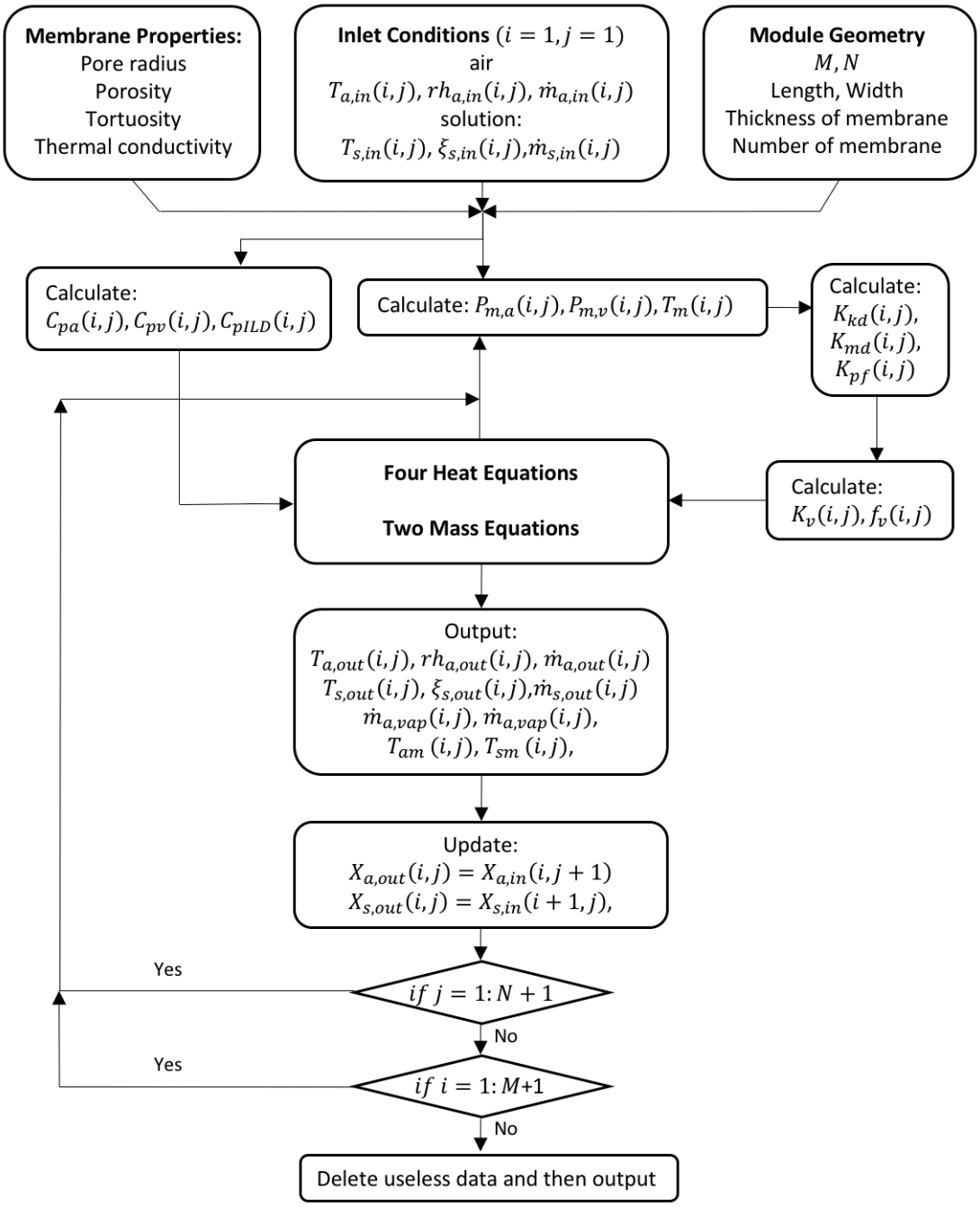

Figure 4.11 The configuration of MATLAB program.

4.5.2 Counter-flow MLDAD module

The boundary conditions for a counter-flow MLDAD module are given, respectively:

When y=0:

$$T_{air} = T_{air,in} \tag{4.53}$$

$$\dot{m}_{air,v} = \dot{m}_{air,in}\, w_{air,in} / \left(1 + w_{air,in}\right) \tag{4.54}$$

when y=length:

$$T_{sol} = T_{sol,in} \tag{4.55}$$

$$\dot{m}_{sol,w} = \dot{m}_{sol,in} C_{sol,in} \tag{4.56}$$

For a counter-flow MLDAD module, the x-y coordinate plane is separated as N meshes as shown in Figure 4.12. For mesh (1,2), the output of mesh (1,1) at air side becomes the input of mesh (1,2) at air aide, and the output of mesh (1,3) at solution side becomes the input of mesh (1,2) at solution side. Due to the special configuration of the counter flow, the boundary conditions for air and solution layers are in different direction. Thus, it is hard to solve the governing equations for each control volume unless several guess values are set.

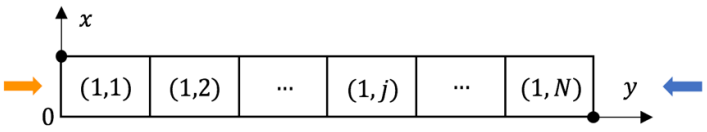

Figure 4.12 Meshes of the heat and mass transfer area in a counter-flow module.

The configuration of the MATLAB program for counterflow is shown in Figure 4.13. First, we guess the air output conditions as one of the inlet conditions for one segment. Then do solve the governing equations using the air-side guess value and the solution side initial conditions. After the whole loop is finished, compare the output value at the air side (which is the estimated air inlet conditions) with the actual inlet conditions. If the difference is larger than the tolerance, change the guess value. If not, the guess values are used as the air outlet conditions. The detailed MATLAB algorithm can be seen in Appendix C.

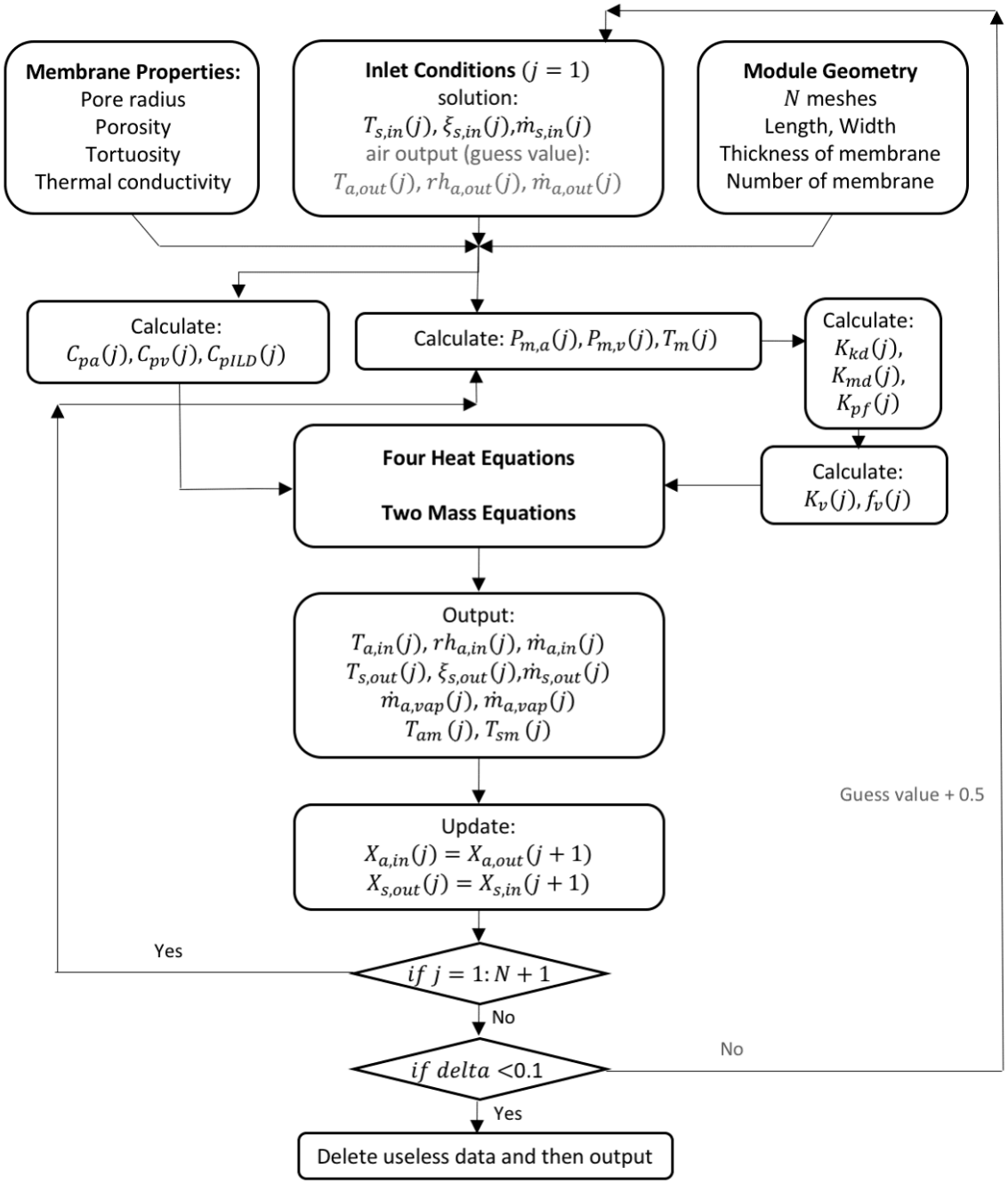

Figure 4.13 The configuration of MATLAB program.

5. MODEL VALIDATION

Two heat and mass transfer models were developed for porous and nonporous (or dense) membranes, respectively. To validate the model using porous membranes, experimental data published in 2014 by Huang's group were used. For the model with nonporous (or dense) membranes, the data were collected from the experiments conducted in ORNL. One of the experiments is the performance testing of the MLDAD prototype using ionic liquid desiccant. The inlet and outlet conditions of air and solutions in the MLDAD were used to validate the model for nonporous membranes. Another is the permeability testing for the nonporous membrane using liquid desiccant-cup method. This data was directly used as the mass transfer coefficient in the model. The follows at first provide the detailed validations for the porous membrane, showing the test setup, inlet and conditions, and the comparison of experimental and numerical outlet conditions. Then the detailed validation for the nonporous membrane is presented, with the comparison of experimental and numerical data of the dehumidification performance.

5.1 The validation of the MLDAD module using porous membranes

5.1.1 Data used for the validation of the MLDAD module using porous membranes

To validate the numerical model for porous membrane-based LDAD modules, the data from the experiment from Huang's group (Huang et al. 2014 [57]) was used. In Huang's research, a membrane-based quasi-cross flow liquid desiccant (LiCl) air dehumidifier was developed. The dehumidifier in the test-bed has a dimension of 100 mm (L) x 200 mm (W) x 4 mm (H) with only one membrane layer, one air channel and one solution channel. The schematic of the MLDAD module in Huang's experiment is shown in Figure 5.1. The air flew from the left to the right, and the solution flew from the right-bottom corner to the left-up corner. The inlet temperatures of air and solutions were 30 °C and 25 °C respectively. The inlet air humidity ratio and mass concentration of LiCl were 19 g/kg and 35%, respectively. A porous PVDF membrane was used. Its microstructure properties such as pore size were collected from commercially available PVDF membranes. Membrane physical properties, fluid transport properties, and operating conditions are listed in Table 5.1.

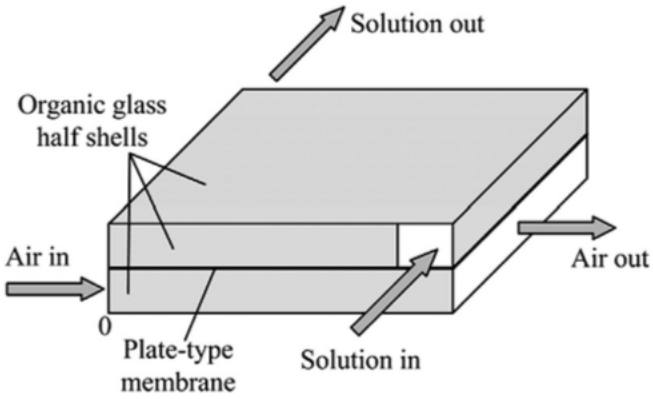

Figure 5.1 The schematic of MLDAD module in Huang's experiment [57].

Table 5.1 Experimental conditions and material properties of the porous MLDAD module.

Parameter	Unit	Value	Parameter	Unit	Value
Liquid desiccant	-	LiCl	Membrane pore size	μm	0.24
Membrane type	-	Porous	Membrane porosity	%	35
Flow pattern	-	Quasi-cross	Membrane thickness	μm	150
Air channel width	m	0.1	Air inlet temperature	°C	30
Solution channel width	m	0.2	Solution inlet temperature	°C	25
Air channel Height	mm	4	Air humidity ratio	g/kg	19
Solution channel Height	mm	4	Solution concentration	%	35
Membrane layer	-	1	Air flow rate	kg/h	0.4~1.2
Membrane conductivity	w/m·k	0.065	Solution flow rate	kg/h	3~6

5.1.2 Data comparison

Eight groups of the experimental data under different operating conditions were used to verify the numerical results. Under each group of operating conditions, the numerical calculation and experimental results of air and solution outlet temperature, air outlet humidity ratio, and latent effectiveness (ε_{lat}) were compared. The sensible performance is shown in Table 5.2, and the latent performance is shown in Table 5.3. It can be seen that the outlet conditions, including temperature, humidity, and effectiveness, from our numerical modeling agreed well with experimental data. The maximum discrepancies between numerical results and experimental data for $T_{air,out}$, $T_{sol,out}$, $w_{air,out}$ and ε_{lat} are 3%, 4%, 5%, and 6%, respectively. The discrepancy of the latent effectiveness ranges from -6% to 5%. Therefore, our microstructure-based H&M model is able to estimate the outlet conditions and latent effectiveness in a MLDAD module using porous membranes accurately.

Table 5.2 Sensible heat comparisons between the experimental data and numerical model.

$T_{air,in}$	$\dot{m}_{air}$	$rh_{air,in}$	$T_{sol,in}$	$C_{sol,in}$	$\dot{m}_{sol}$	$T_{air,out,e}$	$T_{air,out,m}$	e	$T_{sol,out,e}$	$T_{sol,out,m}$	e
°C	(kg/h)	-	°C	-	(kg/h)	°C	°C	(%)	°C	°C	(%)
30	1.01	0.7	25	0.35	6.00	26.4	25.8	-2	26.7	26.2	-2
30	0.79	0.7	25	0.35	6.00	25.9	25.6	-1	26.1	26.1	0
30	0.60	0.7	25	0.35	5.99	25.7	25.4	-1	25.7	25.9	1
30	0.41	0.7	25	0.35	5.99	25	25.2	1	25.2	25.7	2
30	1.20	0.7	25	0.35	6.01	26.5	26.0	-2	27.0	26.3	-3
30	1.21	0.7	25	0.35	5.01	27	26.1	-3	27.3	26.6	-3
30	1.20	0.7	25	0.35	4.02	27.2	26.3	-3	27.8	26.9	-3
30	1.20	0.7	25	0.35	3.01	27.4	26.5	-3	28.5	27.5	-4

Table 5.3 Latent heat comparisons between the experimental data and numerical model.

$T_{air,in}$	$\dot{m}_{air}$	$rh_{air,in}$	$T_{sol,in}$	$C_{sol,in}$	$\dot{m}_{sol}$	$w_{air,out,e}$	$w_{air,out,m}$	e	$\varepsilon_{lat,e}$	$\varepsilon_{lat,m}$	e
°C	(kg/h)	-	°C	-	(kg/h)	(g/kg)	(g/kg)	(%)	(%)	(%)	(%)
30	1.01	0.7	25	0.35	6.00	10.50	11.0	5	62.5	58.8	-6
30	0.79	0.7	25	0.35	6.00	9.98	9.8	-2	66.3	67.6	2
30	0.60	0.7	25	0.35	5.99	8.75	8.4	-4	75.4	77.9	3
30	0.41	0.7	25	0.35	5.99	6.71	6.9	3	90.4	89.0	-2
30	1.20	0.7	25	0.35	6.01	11.83	11.8	0	52.7	52.9	0
30	1.21	0.7	25	0.35	5.01	11.99	11.9	-1	51.5	52.2	1
30	1.20	0.7	25	0.35	4.02	12.10	11.9	-2	50.7	52.2	3
30	1.20	0.7	25	0.35	3.01	12.32	12.0	-3	49.1	51.5	5

5.2 The validation of the MLDAD module using nonporous membranes

5.2.1 Data for the validation of the MLDAD module using nonporous membranes

The data of the preliminary performance test for the MLDAD prototype in ORNL was used to validate the numerical model using nonporous membranes. This is because the first MLDAD prototype employs the hydrophilic nonporous material as the membrane and [EMIM][OAc] as the liquid desiccant. The experimental setup is provided in Chapter 3. The performance test can be separated into two parts: one for the dehumidification mode and another for the regeneration mode. In the dehumidification mode, the air inlet temperature, humidity, and flow rate were 28 °C, 80%, and 1~1.6 CFM, respectively. The solution inlet temperature, concentration, and flow rate were about 25~28°C, 40~70%, and 0.3L/min, respectively. In the regeneration mode, the air inlet temperature, humidity, and flow rate were 35°C, 14~19%, and 1.5~2 CFM, respectively. The solution inlet temperature, concentration, and flow rate were about 40 °C, 70~90%, and 0.3L/min, respectively. After measuring, the membrane permeance is selected as 2.3E-8 kg/m^{2}spa. All these parameters, as well as the module dimensions, are summarized in Table 5.4.

Table 5.4 Experimental conditions and material properties of the nonporous MLDAD module.

Parameter	Unit	Value	Parameter	Unit	Value
Liquid desiccant	-	[EMIM][OAc]	Membrane conductivity	w/m·k	0.065
Membrane type	-	Nonporous	Membrane permeance	kg/m^{2}sPa	2.3E-8
Flow pattern	-	Cross	Air inlet temperature	°C	28/35
Air channel width	m	0.1524	Solution inlet temperature	°C	25~28/40
Solution channel width	m	0.1842	Air relative humidity	%	80/14~19
Air channel Height	m	0.0136	Solution concentration	%	40~70
Solution channel Height	m	0.0136	Air flow rate	CFM	1~2
Membrane layer	-	6	Solution flow rate	L/min	0.3

5.2.2 Data comparison

Four groups of the experimental data under different operating conditions were used to validate the numerical results. Under each group of operating conditions, the numerical calculation and experimental results of humidity difference between the air inlet and outlet conditions were compared. Table 5.5 shows that the discrepancy of the humidity difference ranges from 0% to 6%. The numerical results agreed well with the measured data. Thus, the heat and mass transfer model is able to estimate the latent performance in an MLDAD module using nonporous membranes approximately.

Table 5.5 Performance comparisons between the experimental data and numerical model in both dehumidification and regeneration modes.

$T_{air,in}$	$rh_{air,in}$	$w_{air,in}$	$\dot{m}_{air,in}$	$T_{sol,in}$	$C_{sol,in}$	$\dot{m}_{sol,in}$	$w_{diff,out}$	$w_{diff,m}$	e
°C	%	g/kg	CFM	°C	%	L/min	g/kg	g/kg	%
28	80	19.2	1.6	28	46	0.3	0.31	0.30	3
28	80	19.2	1	28	46	0.3	0.46	0.46	0
35	18	5.2	1.5	35	70	0.3	-0.78	-0.78	0
35	19	6.7	2	35	70	0.3	-0.52	-0.52	6

6. PERFORMANCE SENSITIVITY ANALYSIS AND PARAMETRIC STUDY

Chapter 6 is the parametric study and sensitivity analysis. Firstly, the performance of the baseline, including the temperature, humidity and concentration fields, are presented and discussed. The latter sections analyze the sensible and latent effectiveness, and moisture removal rate (MRR) under the control of various types of liquid desiccants and membranes, flow patterns, module dimensions, and operating conditions. Finally, the optimal design and operation of the MLDAD module are shown. The optimized module can increase the effectiveness and MRR.

6.1 Performance for MLDAD module of baseline cases

The module geometry of the baseline case is the initial MLDAD prototype we used in the laboratory with only a single porous membrane layer. According to the experimental investigation, the dehumidification performance of a porous layer is better than the nonporous one. Therefore, we would like to replace the nonporous membrane with the most commonly used PVDF membrane. The default conditions for the baseline case are listed in Table 6.1 when the MLDAD works as a dehumidifier in the cooling mode. The air has an inlet temperature of 30°C, the humidity of 18.9 g/kg (or the relative humidity of 70%), and the mass flow rate of 1 kg/h. The solution, [EMIM][OAc], has a temperature of 25°C, the mass concentration of 69.7%, and the mass flow rate of 6 kg/h. The air and solution flow in a cross configuration in their parallel channels. The length of the air and solution channels are 0.1842 m and 0.1524 m, respectively. The thicknesses of the air and solution channels are both 13.6 mm. The module uses one porous PVDF membrane with a pore size of 0.24 μm, a porosity of 0.35, a tortuosity of 5, and a thickness of 150 μm. The fields of air and solution states based on the numerical model are plotted in Figure 6.1-6.4.

Table 6.1 Operating conditions of the baseline case

Parameter	Unit	Baseline	Parameter	Unit	Baseline
Liquid desiccant	-	69.7% ILD	Membrane pore size	μm	0.24
Membrane type	-	Porous	Membrane porosity	%	35
Flow pattern	-	Crossflow	Membrane thickness	μm	150
Air channel length	m	0.1842	Air inlet temperature	°C	30
Solution channel length	m	0.1524	Solution inlet temperature	°C	25
Air channel Height	mm	13.6	Air relative humidity	%	70
Solution channel Height	mm	13.6	Air flow rate	kg/h	1

Membrane layer	-	1	Solution flow rate	kg/h	6

Figure 6.1 shows the 3D temperature profile of the air layer in a cross-flow MLDAD module. The air enters the air channel from the length side, which is the length-direction axis, with an inlet temperature of 303.1 K (30.0°C), and it is cooled along the diagonal lines of the membrane surface. The air outlet temperatures at the exit are not the same number but increase along the length direction. Thus, the calculated air outlet temperature is a mean average of outlet temperatures of all control volumes. The outlet air temperature is 300.7 K (27.51°C) in the baseline. Figure 6.2 shows the 3D temperature profile of the solution layer in a cross-flow MLDAD module. The solution enters the solution channel from the depth side, with an inlet temperature of 298.1 K (25.0°C), and it is heated along the diagonal lines. The outlet solution temperature is 301.6 K (28.5°C) in the baseline. It is also found that the solution-membrane interface always has the highest temperature, 30.6°C for this case, when the system reaches to steady state. This is because the heat of absorption released in the solution surface highly raised its temperature. Finally, the sensible effectiveness for the heat transfer from the air layer to the solution layer is reduced to about 49.7%.

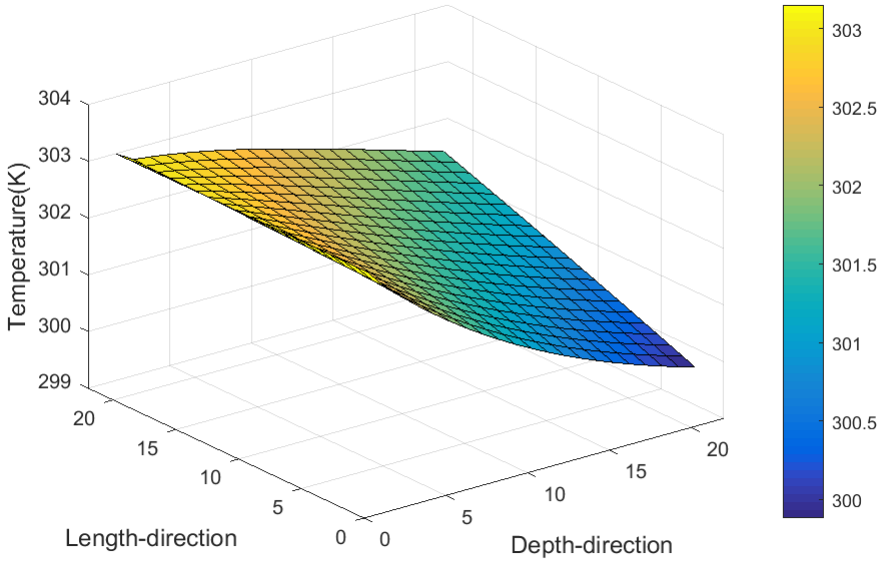

Figure 6.1 Temperature field of the air layer.

Figure 6.3 shows the 3D humidity profile of the air layer in a cross-flow MLDAD module. The air enters the air channel from the length side, with an inlet humidity of air is 18.9 g/kg, and it is dehumidified almost along the diagonal lines of the membrane surface. The air outlet humidity is about 8.8 g/kg. The moisture removal rate is about 2.8E-6 kg/s (10.0 g/h). Figure 6.4 shows the

3D concentration profile of the solution layer in a cross-flow MLDAD module. The solution flows into the solution channel from the depth side, with an inlet concentration of 69.7%, and it is diluted along the diagonal lines. The solution outlet concentrations are about 69.6%. Finally, the latent effectiveness for the baseline is 74.9%.

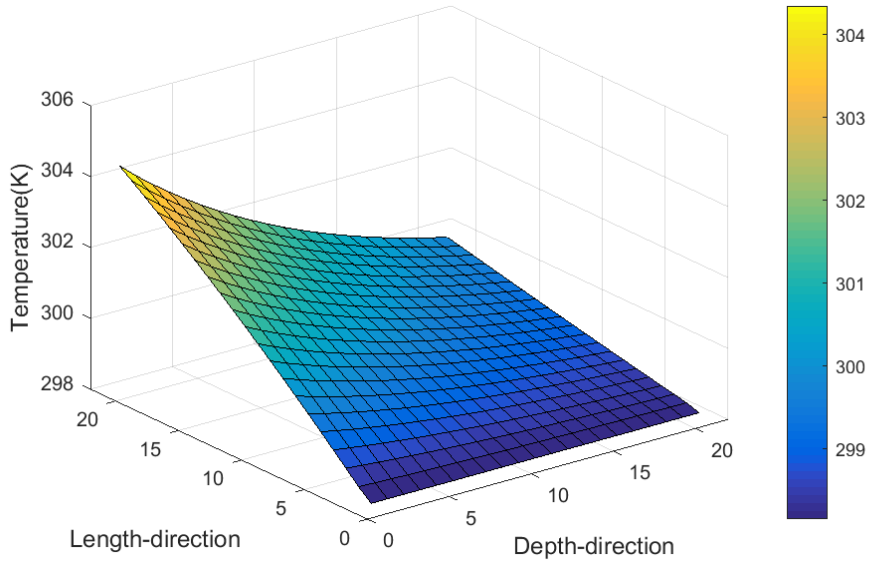

Figure 6.2 Temperature field of the solution layer.

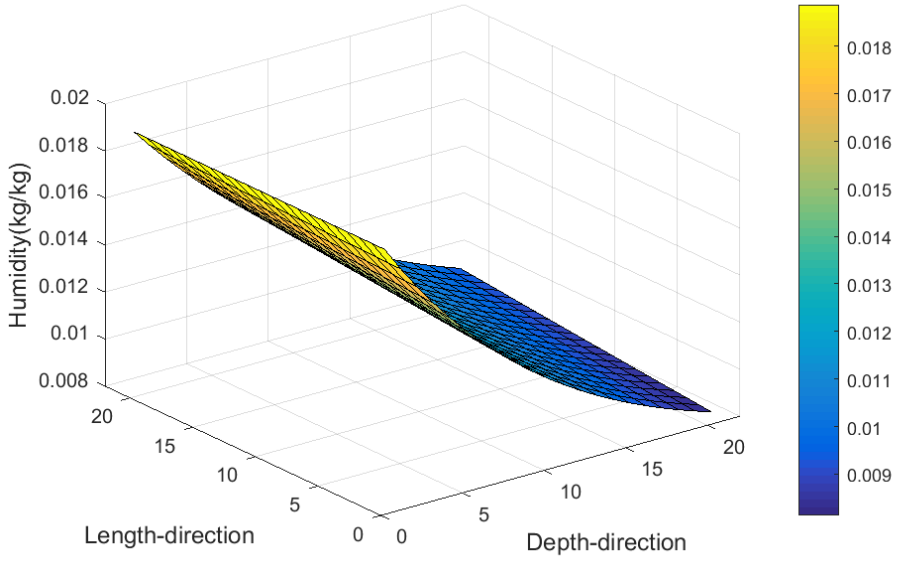

Figure 6.3 Humidity field of the air layer.

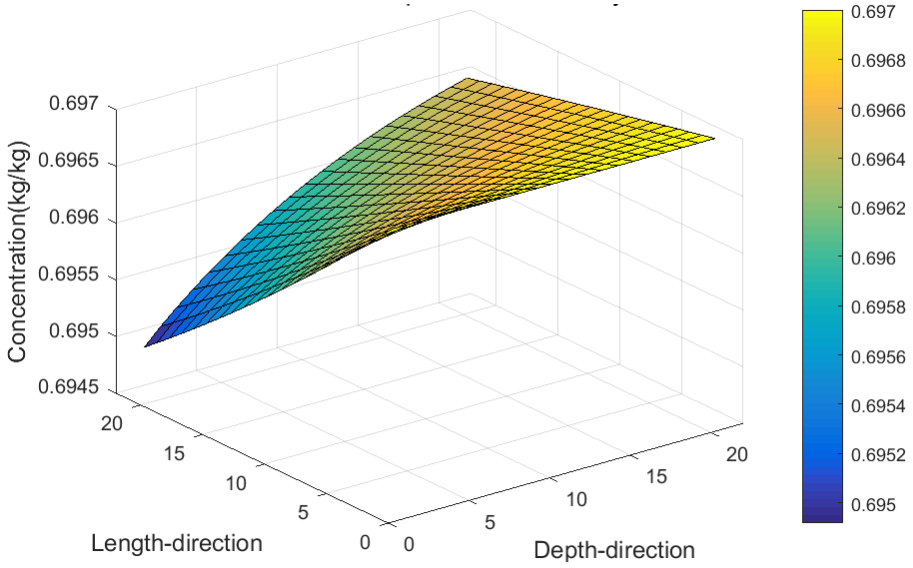

Figure 6.4 Concentration field of the solution layer.

6.2 Comparison between conventional liquid desiccants and ionic liquid desiccant

In this section, a performance comparison, including temperature fields for both air and solution, sensible and latent effectiveness, and MRR for a cross-flow MLDAD module using the conventional liquid desiccant (LiCl solution) and an ionic liquid desiccant ([EMIM][OAc] solution), based on the numerical model, are presented. In this case, an aqueous solution [EMIM][OAc] with a concentration of 69.7% and the 35% LiCl solution were used. All other conditions are identical with the baseline case.

The outlet results of the cross-flow MLDAD module using [EMIM][OAc] or LiCl are shown in Table 6.2. Different from the temperature profile using LiCl solution, the air outlet temperature in the case of [EMIM][OAc] is relatively higher. This is due to the larger heat of dilution released by the diluted [EMIM][OAc] solution. The heat of dilution for the [EMIM][OAc] and LiCl solutions at the baseline operating conditions are assumed to be 200 and 140 (kJ/kg vapor), respectively. Thus, more heat is conducted through the membrane to the air side to increase the air temperature while using ILD. Then the air is gradually cooled by the cold solution. The air outlet temperature for an MLDAD module using LiCl is 27.4°C. It is only 0.1°C lower than the baseline case. The solution outlet temperature is 28.2°C. It is 0.3°C higher than the baseline case. This is also due to the larger heat of dilution released to the bulk of the solution. Therefore, the sensible effectiveness increases from 49.71% to 51.64% if the LiCl solution is employed.

Table 6.2 Performance comparison between using different liquid desiccants.

Membrane material	[EMIM][OAc]	LiCl
Latent effectiveness	74.88%	75.57%
Sensible effectiveness	49.71%	51.64%
MRR [kg/s]	2.79E-06	2.82E-06

In the MLDAD module using LiCl solution, the air outlet humidity is about 8.7 g/kg. It is 0.1 g/kg lower than the baseline case. This is because the higher solution temperature leads to a higher EVP of the solution. The latent effectiveness is 75.57% in this case. The latent and sensible effectiveness and MRR for cross-flow MLDAD modules using LiCl and [EMIM][OAc] solutions with different air flow rates are plotted in Figure 6.5. It is found that the latent and sensible effectiveness decreases with the increase of air flow rate, while the MRR increases with the increase of air flow rate. The latent effectiveness and MRR of the module using [EMIM][OAc] solution only have slight reductions compared with the baseline performance. But the sensible effectiveness reduces more due to the effect of absorption heat. To sum up, the dehumidification performance for the MLDAD module using [EMIM][OAc] is comparable with that of the module using LiCl solution in this case, with only a slight reduction. Thus, it is feasible to replace conventional liquid desiccant LiCl solution with ILD.

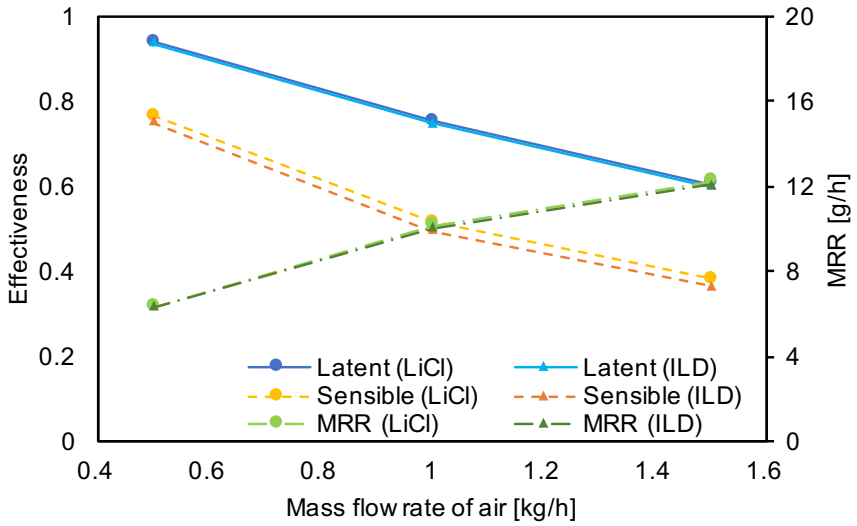

Figure 6.5 Performance comparison between using LiCl and [EMIM][OAc].

6.3 Comparison between porous membranes and non-porous/dense membranes

In this section, a performance comparison between a cross-flow MLDAD module using the porous membrane and a non-porous membrane based on the numerical model are presented.

The porous membrane used is the PVDF membrane with a thickness of 150 μm. Its mass transfer coefficient is calculated through equations. The nonporous membrane used in the model is a Nafion ionomer produced by DuPont™. Its mass transfer coefficient is obtained through the direct measurement conducted in ORNL, followed by the cup-method in ASTM E-96 standard. The detailed setup and results of the experiments are shown in Appendix B. For this case, the mass transfer coefficient (or the permeance) used for the nonporous membrane is assumed to be 2.3E-08 kg/(m^{2}sPa). The simulation results with the air temperature and humidity fields are shown in Figure 6.6-6.7. Since the non-porous membrane has smaller permeance compared with the porous membrane under the same conditions, the non-porous membrane has relatively larger vapor diffusion resistance. Therefore, the dehumidification performance for the non-porous membrane is worse. As illustrated in Figure 6.6, the air temperature changes more steeply when using non-porous membranes and the dark blue color dominates the color map. This is because the poor mass transfer results in less heat of absorption released, and thus, lead to a better heat transfer effectiveness. Due to the same reason, the solution temperature changes flatter. The air and solution outlet temperature using a nonporous membrane is 27.5°C and 26.5°C, respectively. They are 0.02°C and 2.0°C lower than the baseline case, respectively.

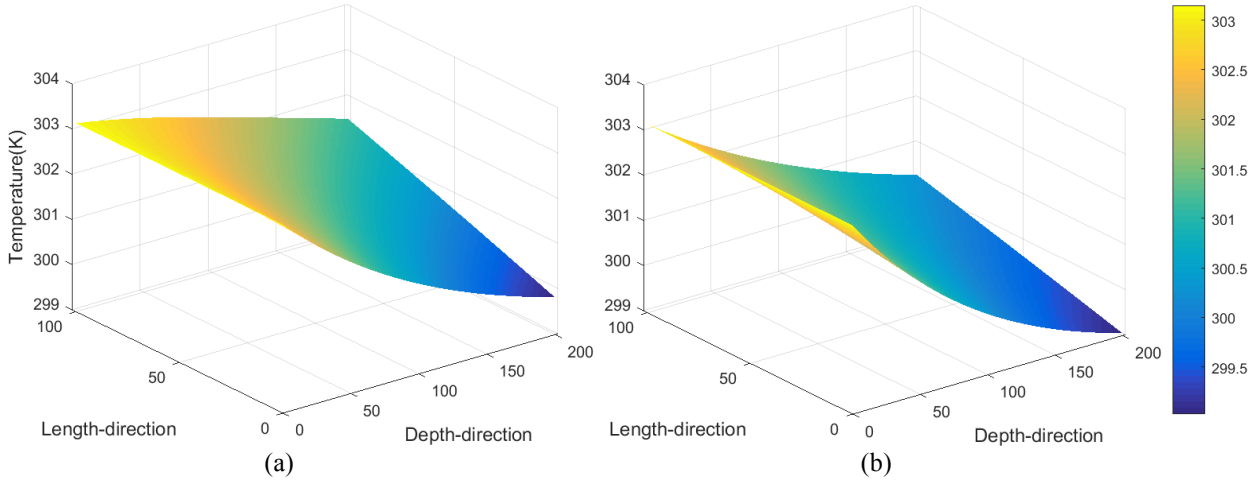

Figure 6.6 Temperature fields of air layer: (a) using porous and (b) non-porous membranes.

As plotted in Figure 6.7, the MLDAD module using porous membrane can dehumidify the air to the lower humidity, as shown in the blue region. But the use of the nonporous membrane cannot fully dehumidify the air, as the color map is dominated by yellow-green. In the latter case, the air outlet humidity and solution outlet concentration are 14.8 g/kg and 69.7%, which are 6.0

g/kg and 0.001% higher than the baseline case, respectively. Thus, for the nonporous MLDAD, a large membrane area is needed to achieve the same dehumidification performance as the porous membrane. The latent and sensible effectiveness and MRR performance are listed in Table 6.3. The use of a nonporous membrane, in this case, reduces the latent effectiveness and MRR by about 56%. But the sensible effectiveness increases a little. It is concluded that the membrane resistance has a significant influence on the dehumidification performance.

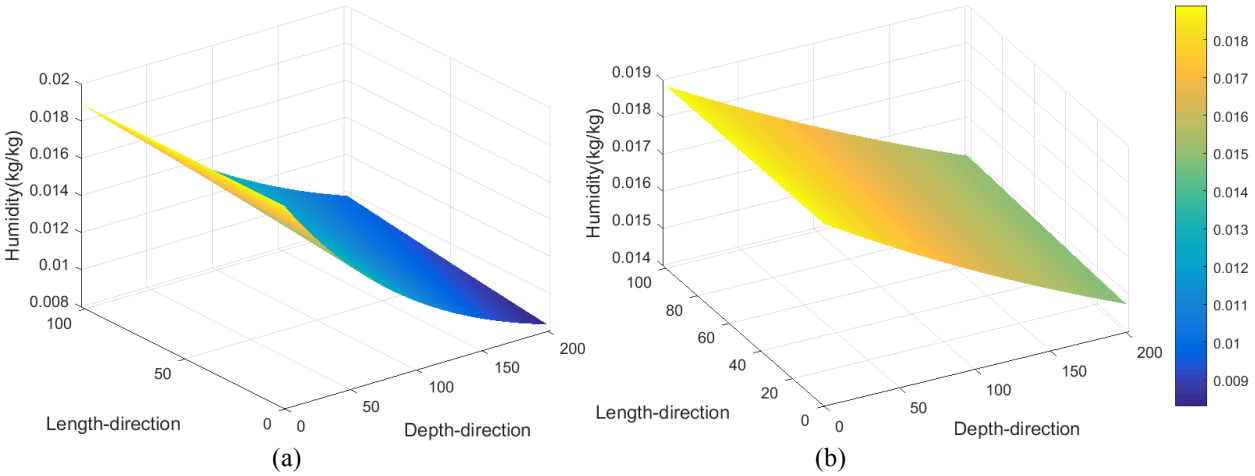

Figure 6.7 Humidity fields of air layer: (a) using porous and (b) non-porous membranes.

Table 6.3 Performance comparison between porous and nonporous membranes

Membrane material	Porous membrane	Nonporous membrane
Latent effectiveness	74.88%	30.22%
Sensible effectiveness	49.71%	50.17%
MRR [kg/s]	2.79E-06	1.13E-06

6.4 Comparison between cross-flow and counter-cross flow

In this section, a performance comparison between a cross-flow MLDAD module using the cross-flow and counter-flow configurations based on the numerical model are presented. For the counter-flow MLDAD module, as shown in Figure 6.8-6.9, the air flows from the right to the left side, and the solution flows in the opposite direction. In these figures, the upper region represents the air condition and the lower region represents the solution condition. As seen, the air/solution temperature and vapor pressure only change along the length direction. In this case, the air is cooled and dehumidified from 30°C to 27.3°C, and 18.9 g/kg to 8.7 g/kg, respectively. The air outlet temperature is 0.2°C lower, and the air outlet humidity is 0.1 g/kg lower than the baseline

case. The solution is heated and diluted from 25 °C to 28.6 °C, and 69.7% to 69.3%, respectively, which is 0.1°C higher and 0.003% lower than the baseline using crossflow configuration.

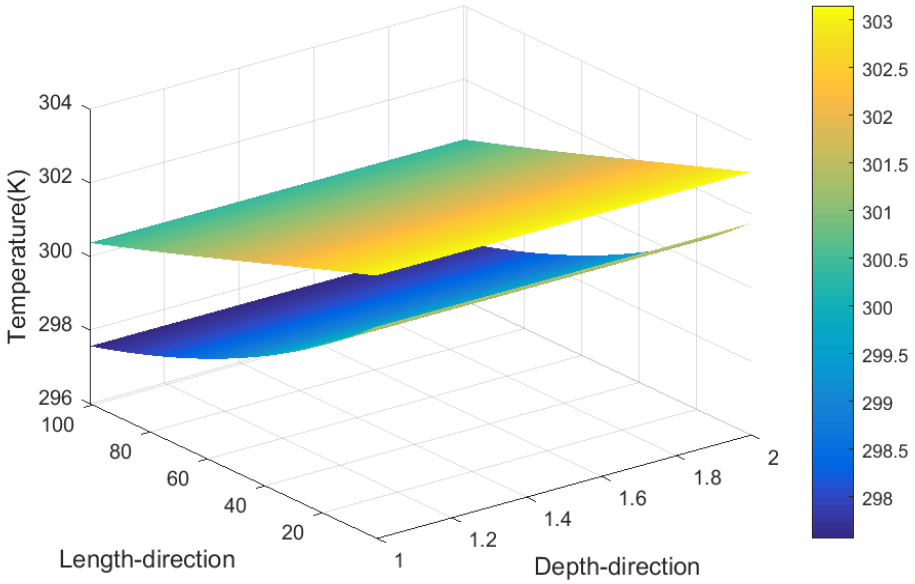

Figure 6.8 Temperature fields of air and solution in a counter-flow MLDAD module.

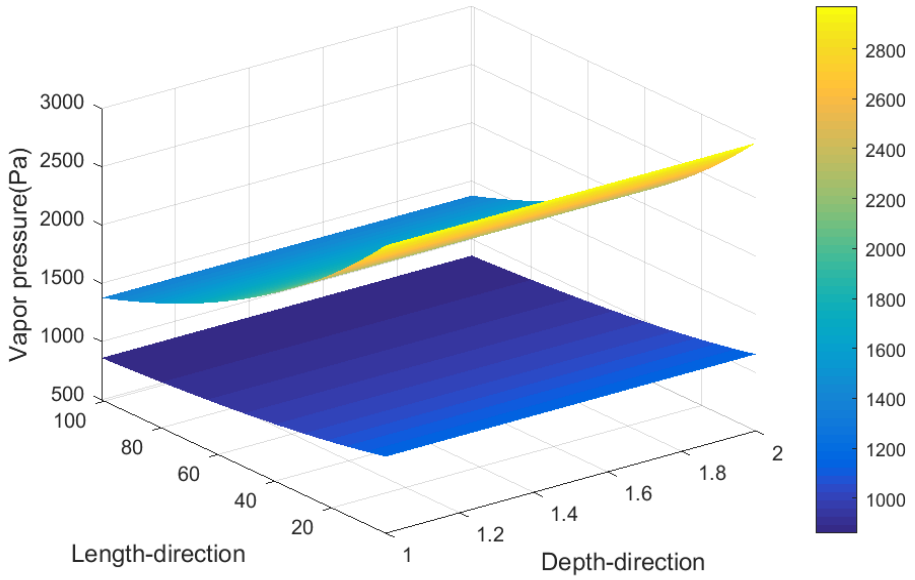

Figure 6.9 Vapor pressure fields of air and solution in a counter-flow MLDAD module.

The latent and sensible effectiveness and MRR for this case are 75.9%, 50.0%, and 2.79E-06 kg/s, respectively, with an inlet air temperature of 30 °C. Compared with the results of the baseline case, there is only a slight improvement of latent effectiveness and MRR when using

counter-flow configuration, but the sensible effectiveness is raised much more. Figure 6.10 illustrates the latent and sensible effectiveness and MRR for both cross-flow module and counter-flow module under different air flow rates. It indicates that the energy exchange performances for modules using these two flow patterns do not have a significant change even with various air flow rates.

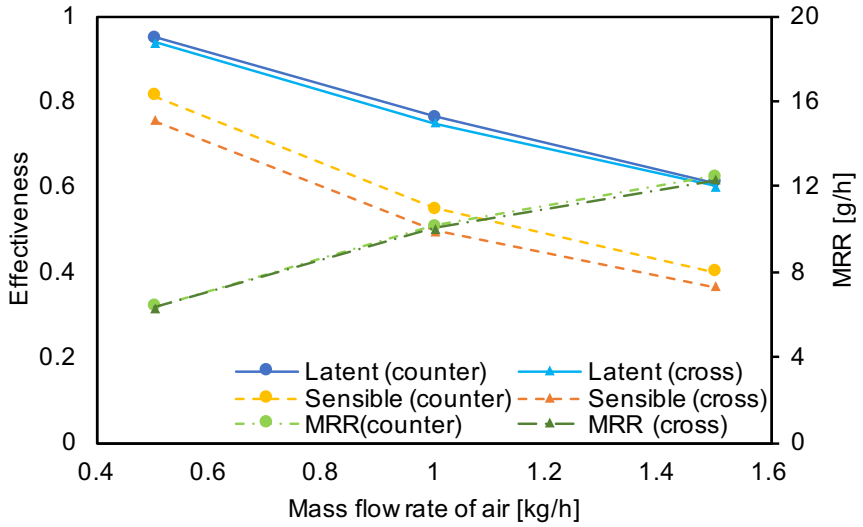

Figure 6.10 Performance comparison under crossflow or counterflow at various air temperatures.

6.5 Impacts of different dimensions for the module

In this section, a performance comparison of sensible and latent effectiveness, and MRR for a cross-flow MLDAD module with different dimensions are presented. The variables include the widths and heights of air and solution channels, and the membrane pore size, porosity, and thickness. The case studies aim to guide the module design and membrane selection or production. The default values in the baseline case and ranges of the variables in the studied cases are listed in Table 6.4.

Table 6.4 Design and operating conditions for cases studying the impact of design parameters.

Parameter	Unit	Base-line	Studied cases	Parameter	Unit	Base-line	Studied cases
Liquid desiccant	-	69.7% ILD		Membrane pore size	μm	0.24	0.1 – 1.1
Membrane type	-	Porous		Membrane porosity	%	35	10 – 90
Flow pattern	-	Crossflow		Membrane thickness	μm	150	50 – 400
Air channel length	m	0.1842	0.1 – 0.7	Air temperature	°C	30	
Solution channel length	m	0.1524	0.1 – 0.7	Solution temperature	°C	25	
Air channel Height	mm	13.6	1 – 25	Air relative humidity	%	70	
Solution channel Height	mm	13.6	1 – 25	Air flow rate	kg/h	1	
Membrane layer	-	1		Solution flow rate	kg/h	6	

6.5.1 Air channel length

In this case, the length of air channels in a cross-flow MLDAD module varies from 0.1 to 0.7 m. The solution flow rate is assumed to change with the air channel length (or solution channel width) linearly to keep a constant solution flow rate per membrane area. Figure 6.11 shows the performance of an MLDAD module with different air channel lengths. As the length of the air channel increases, the latent and sensible effectiveness, and the MRR increase at the same time. They rise rapidly when the air channel length increases from 0.1 to 0.3 m, and after that, the rates of growth slow down.

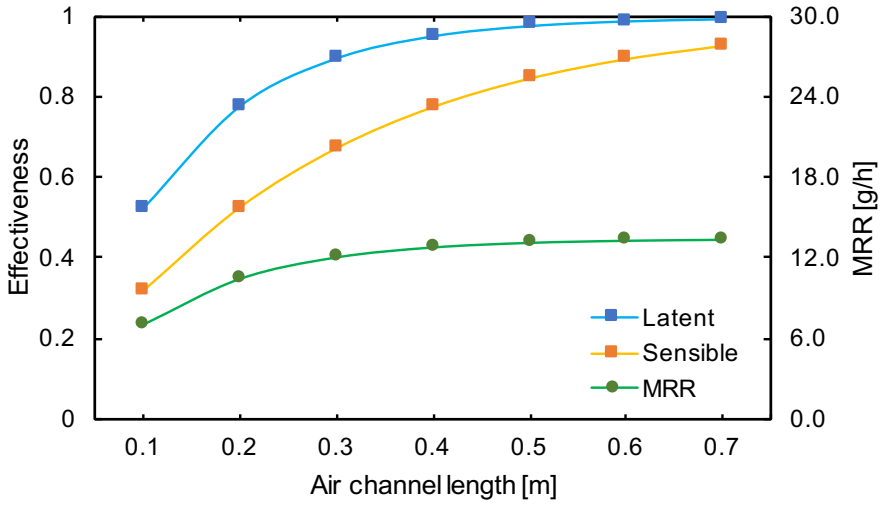

Figure 6.11 Performance of MLDAD under various air channel length.

6.5.2 Solution channel length

In this case, the length of solution channels in a cross-flow MLDAD module varies from 0.1 to 0.7 m. The air flow rate is assumed to change with the solution channel length (or the air channel width) linearly to keep a constant air flow rate per membrane area. Figure 6.12 shows the performance of an MLDAD module with different solution channel lengths. As the length of solution channel increases, the sensible effectiveness decreases a lot, but the latent effectiveness only has a slight reduction.

Therefore, a smaller length ratio of solution to air channels leads to a better cooling and dehumidification effectiveness. In order to have a smaller length ratio, a larger length of the air channel and a smaller length of solution channel are preferred. An air channel length larger than 0.3 m and a solution channel length smaller than 0.3 m, for this case, could be a reasonable choice

with the latent and sensible effectiveness larger than 70%. However, a too small air channel width may lead to an extremely lower MRR so that the total amount of air treated is less. To dehumidify a larger amount of air, more membrane layers can be applied to the module.

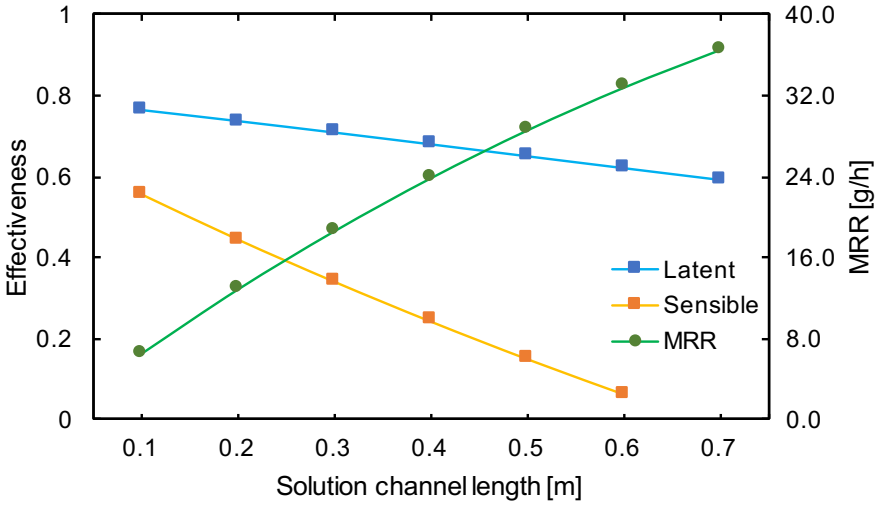

Figure 6.12 Performance of MLDAD under various solution channel length.

6.5.3 Air channel height

Figure 6.13 shows the performance of an MLDAD module with different air heights. In this case, the height of air channels varies from 1 to 25 mm, and the air flow rate is assumed to change with the height linearly to keep a constant air flow rate per membrane area.

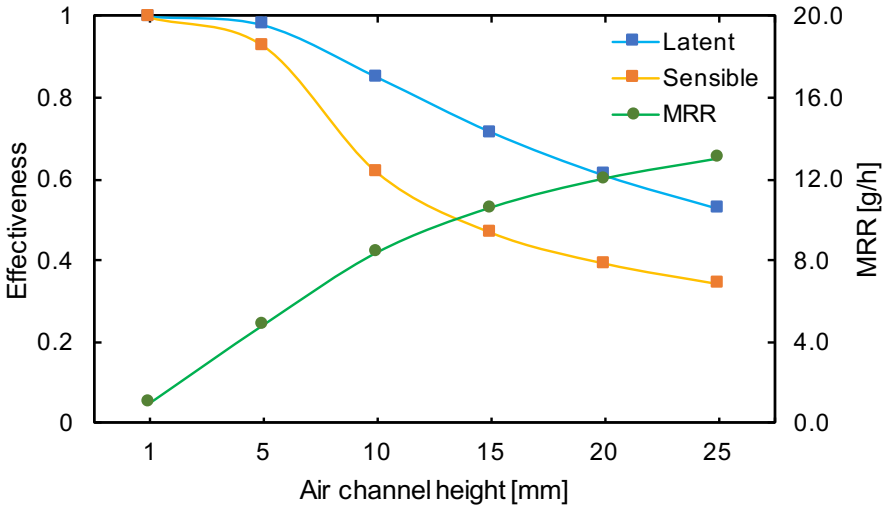

Figure 6.13 Performance of MLDAD under various air channel heights.

As the height of the air channel increases, the latent and sensible effectiveness decrease, but the MRR increases due to the increase of air flow rate. The reductions of latent and sensible effectiveness become more rapid when the air channel is larger than 5 mm.

6.5.4 Solution channel height

In this case, the height of solution channels varies from 1 to 25 mm, and the solution flow rate is assumed to change with the height linearly to keep a constant solution flow rate per membrane area. Figure 6.14 shows the performance of an MLDAD module with different solution channel heights. As the height of the solution channel increases, the latent and sensible effectiveness, and MRR increase at the same time. However, the growth of them becomes very limited when the solution channel height is larger than 5 mm.

To a conclusion, a smaller height ratio of air channel to the solution channel leads to a better cooling and dehumidification effectiveness. In order to have a smaller height ratio, a larger height of the solution channel or a smaller height of air channel is preferred. When the height ratio is fixed, the smaller the absolute value of each channel height, the better the performance will be.

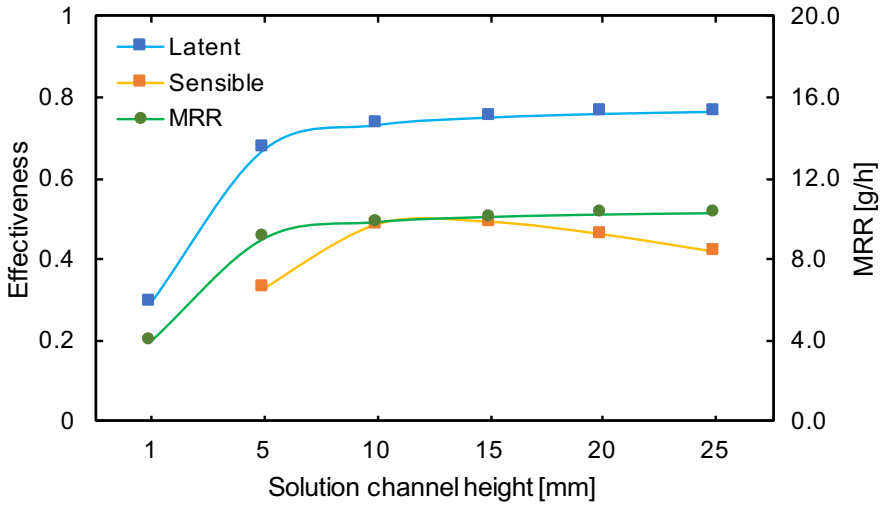

Figure 6.14 Performance of MLDAD under various solution channel heights.

6.5.5 Membrane pore size

Figure 6.15 shows the heat and mass transfer performance of a cross-flow MLDAD module using different membrane materials with pore size changing from 0.05 to 1.05 microns. The latent effectiveness and the MRR increase with larger pore size. They increase very rapidly when the

membrane pore size changes from 0.05 to 0.25 microns. The sensible effectiveness reduces slightly at the beginning and then raises. This is due to the conjugate effect of heat and mass transfer. A better mass transfer releasing more heat leads to a worse heat transfer. But with the even higher mass transfer, the heat of vapor in the air can be carried by the vapor movement to the solution side; then the sensible effectiveness starts to rise when the pore size is larger than 0.25 microns.

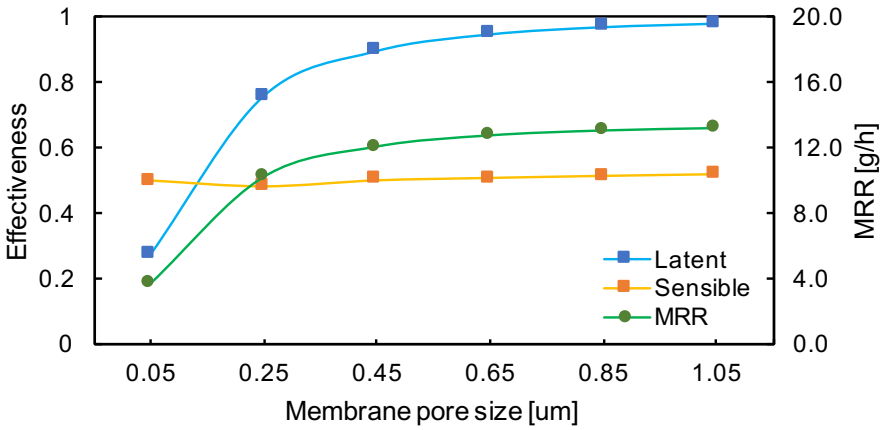

Figure 6.15 Performance of MLDAD under various membrane pore sizes.

6.5.6 Membrane porosity

Figure 6.16 shows the heat and mass transfer performance of a cross-flow MLDAD module using different membrane materials with porosity changing from 0.1 to 0.9. The latent effectiveness and the MRR increase with a larger porosity. However, they are almost unchanged when the porosity is more than 0.5. The sensible effectiveness reduces at the beginning and then grows when the porosity is larger than 0.5.

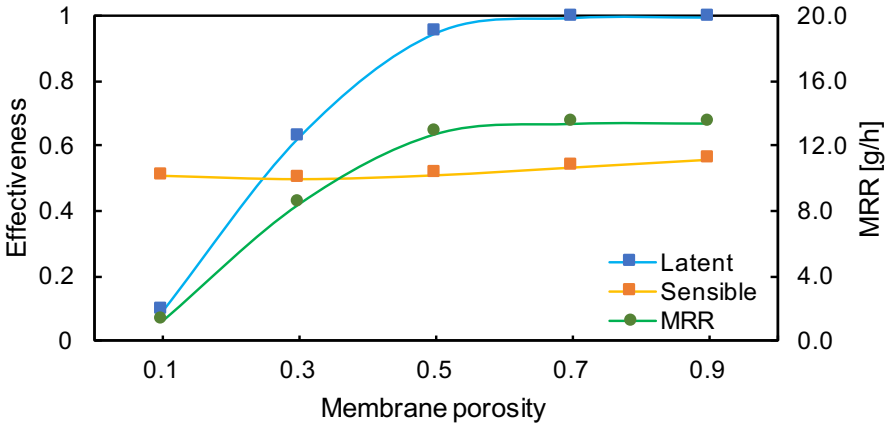

Figure 6.16 Performance of MLDAD under various membrane porosities.

6.5.7 Membrane thickness

Figure 6.17 shows the heat and mass transfer performance of a cross-flow MLDAD module using different membrane thickness varying from 50 to 450 microns. It proves that the increase in membrane thickness can decrease the dehumidification performance a lot.

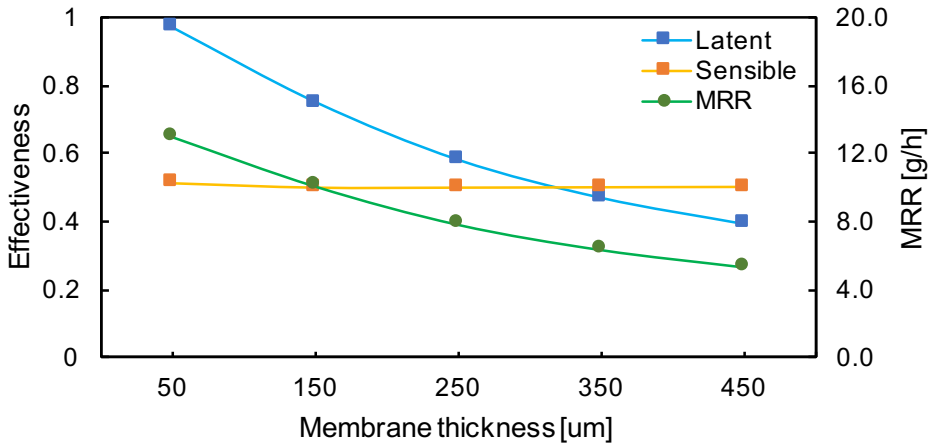

Figure 6.17 Performance of MLDAD under various membrane thicknesses.

6.6 Impacts of operating conditions

In this section, a performance comparison of sensible and latent effectiveness, and MRR for a cross-flow MLDAD module with different operating conditions are presented. The variables include the inlet temperature, the mass flow rates of air and solution, the air relative humidity, and solution concentration. The case studies aim to guide the experimental operation. The parameters in the baseline and ranges of the variables in the studied cases are listed in Table 6.5.

Table 6.5 Design and operating conditions for cases studying the impact of operating conditions.

Parameter	Unit	Base-line	Studied cases	Parameter	Unit	Base-line	Studied cases
Liquid desiccant	-	69.7%	60 – 100%	Membrane pore size	μm	0.24	
Membrane type	-	Porous		Membrane porosity	%	35	
Flow pattern	-	Crossflow		Membrane thickness	μm	150	
Air channel length	m	0.1842		Air temperature	°C	30	26 – 36
Solution channel width	m	0.1524		Solution temperature	°C	25	18 – 28
Air channel Height	mm	13.6		Air humidity	g/kg	18.9	14 – 24
Solution channel Height	mm	13.6		Air flow rate	kg/h	1	0.1 – 10
Membrane layer	-	1		Solution flow rate	kg/h	6	0.1 – 10

6.6.1 Air inlet temperature

Figure 6.18 shows the heat and mass transfer performance of a cross-flow MLDAD module under different air inlet temperatures varying from 26 to 36 °C. The temperature difference between air and solution changes from 1 to 11 °C. The sensible effectiveness and MRR increase and the latent effectiveness decreases slightly as air inlet temperature grows. This is because the larger the temperature difference, the larger the vapor pressure difference. Thus, increasing air inlet temperature improves MRR. Although the humidity difference of inlet and outlet air grows, the maximum potential of dehumidification has also increased. Therefore, the latent effectiveness reduces.

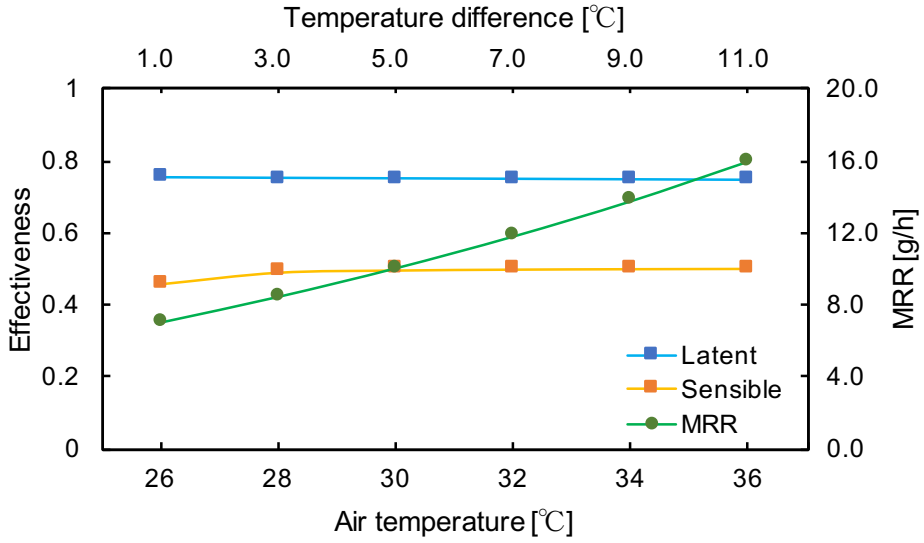

Figure 6.18 Performance of MLDAD under various air inlet temperatures.

6.6.2 Solution inlet temperature

Figure 6.19 shows the heat and mass transfer performance of a cross-flow MLDAD module under different solution inlet temperature varying from 18 to 28 °C. The temperature difference between air and solution changes from 12 to 2 °C. The sensible and latent effectiveness and MRR decrease slightly with a higher solution inlet temperature. In this case study, the smaller temperature difference between air and solution, the higher the air outlet temperature will be. And the decrease of the temperature difference between inlet air and outlet air is larger than the temperature difference between air and solution, therefore, the worse the sensible effectiveness is. Also, the vapor pressure difference of air and solution decreases, resulting in a decrease of MRR. Then, the latent effectiveness lessens slightly.

To a conclusion, the inlet temperatures of air and solution do not play a significant role in the latent and sensible effectiveness, especially when the temperature difference of air and solution are large enough. However, the MRR increases with the increase of temperature difference. Thus, enlarging the temperature difference of air and solution is able to raise the absolute amount of moisture to be removed from the air.

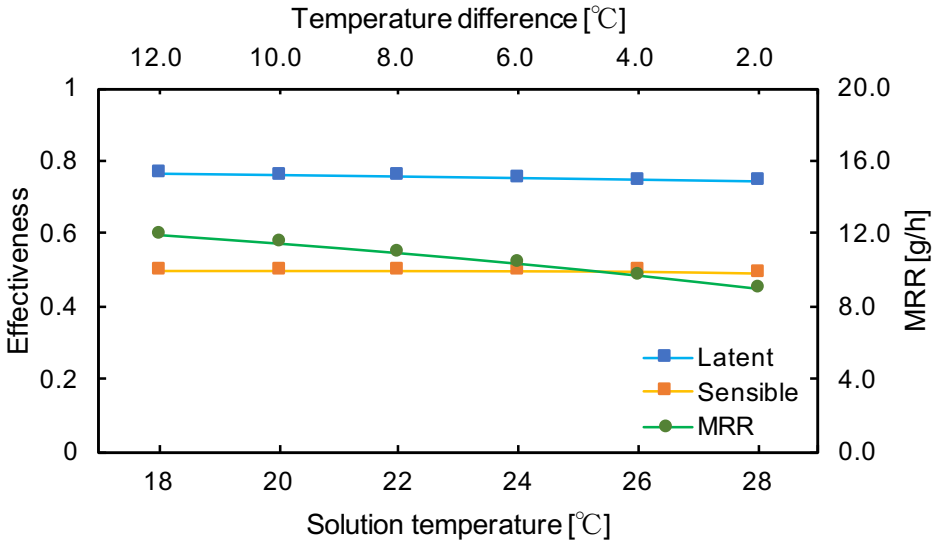

Figure 6.19 Performance of MLDAD under various solution inlet temperatures.

6.6.3 Air inlet humidity

Figure 6.20 shows the heat and mass transfer performance of a cross-flow MLDAD module under different air inlet humidity ratio varying from 12 to 20 g/kg. Due to the increase of air humidity, the vapor pressure difference becomes larger, and the water vapor removal rate per unit air can increase. Therefore, MRR is enlarged. But the better mass transfer performance released more heat of absorption, therefore, the sensible effectiveness is lower. Additionally, because the molecular, which is the actual MRR capacity, and the denominator, which is the maximum potential of MRR, increase simultaneously, the latent effectiveness remains almost unchanged with various air humidity.

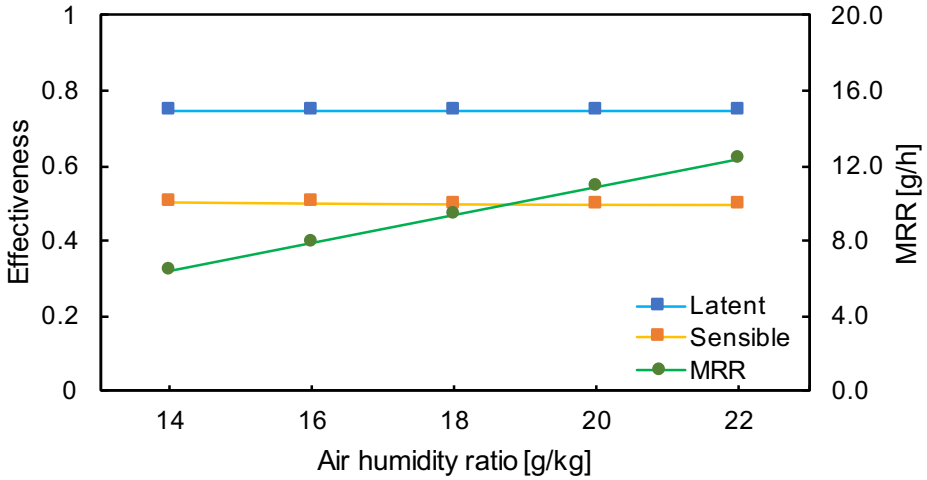

Figure 6.20 Performance of MLDAD under various air relative humidity.

6.6.4 Solution concentration

Figure 6.21 shows the heat and mass transfer performance of a cross-flow MLDAD module under different concentrations of [EMIM][OAc] solution varying from 70 to 95%. The latent effectiveness and MRR increase and the sensible effectiveness decreases when the solution concentration becomes stronger at this certain range. This is because the higher the concentration, the larger the vapor pressure difference, and the better the mass transfer performance is. But the larger water vapor flux also to leads to a growth of heat of dilution, therefore degrade the sensible effectiveness. However, for some liquid desiccant with an especially lower vapor pressure, the latent effectiveness may decrease with increasing the solution concentration, at extremely high concentrations.

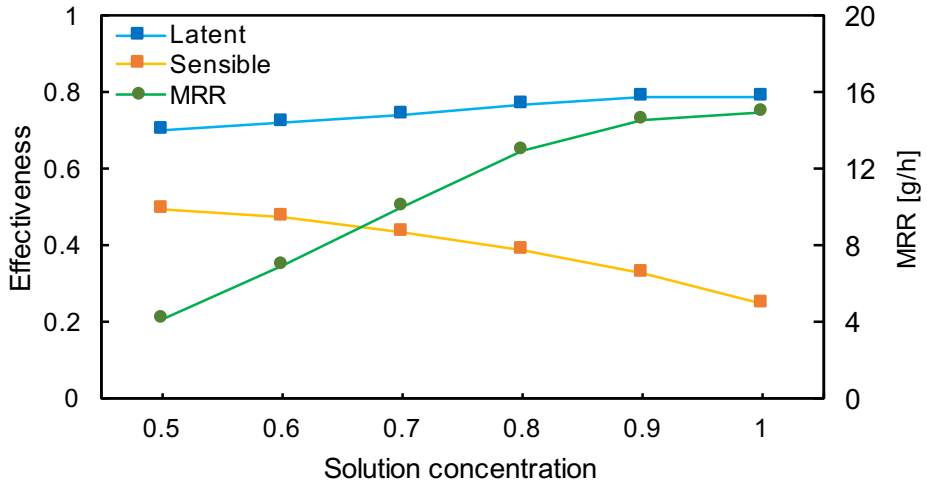

Figure 6.21 Performance of MLDAD under various solution concentrations.

6.6.5 Air mass flow rate

Figure 6.22 shows the heat and mass transfer performance of a cross-flow MLDAD module under different air mass flow rates varying from 0.1 to 10 kg/h. The latent and sensible effectiveness decreases a lot as the air flow rate increases and the mass flow rate ratio of solution to air decreases.

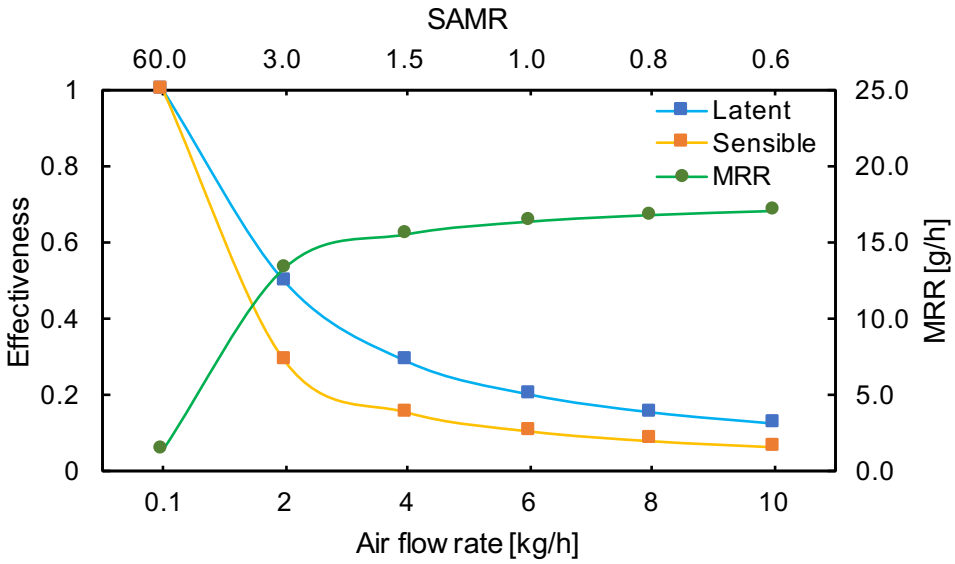

Figure 6.22 Performance of MLDAD under various air flow rates.

6.6.6 Solution mass flow rate

Figure 6.23 shows the heat and mass transfer performance of a cross-flow MLDAD module under different solution mass flow rates varying from 0.1 to 10 kg/h. The latent and sensible effectiveness increase as the air flow rate increases. After the solution rate reaches to 3 kg/h, the growth rate of effectiveness becomes slower.

To a conclusion, the flow rate plays a critical role in the performance of the MLDAD module. The change of air flow rate has great impacts on the effectiveness and MRR. The higher the air flow rate, the lower the effectiveness, and the larger the MRR. However, the solution flow rate has a relatively smaller influence on the performance. The greater the flow rate of the solution, the higher the effectiveness and MRR. Moreover, when the flow rate ratio of solution to air is fixed, the slower the flow rates of both streams, the higher the effectiveness is.

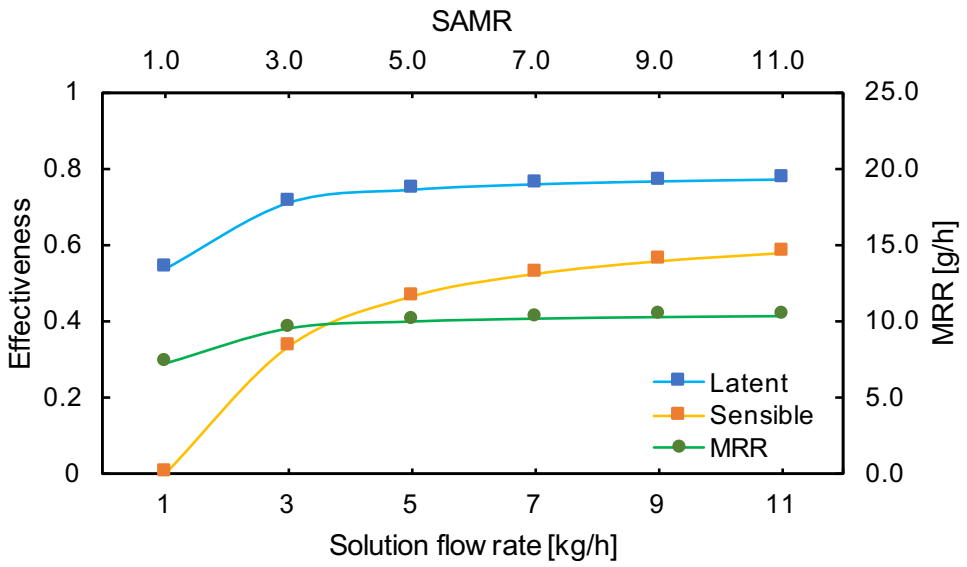

Figure 6.23 Performance of MLDAD under various solution flow rates.

6.7 Summary and module optimization

As discussed in Section 3.2, there are several indicators to evaluate the dehumidification performance of a MLDAD module. Among these indicators, the effectiveness is considered as the ratio between the actual performance and the maximum potential. They represent the extent of uses of the cooling capacity or the dehumidification capacity. For a dehumidifier, the latent effectiveness plays a more critical role than other effectiveness. The larger the latent effectiveness is, the larger proportion of the dehumidification capacity that is employed. The MR and MRR are all absolute values. However, MR cares more about the vapor be removed per unit amount of air. The larger the MR is, the drier the outlet air. And MRR cares more about the vapor be removed per unit time. Thus, the larger the MRR is, the more the amount of dry air we can have. For a dehumidifier, we seek for larger latent effectiveness, MR and MRR.

From the above parametric analysis studying the impacts of various parameters on the performance of MLDAD, with the aspects of liquid desiccants, membrane types, flow patterns, module designs, and operating conditions, several discussions and conclusions are made as follows.

- The performance of the MLDAD module using the conventional liquid desiccant such as the LiCl solution was compared to the one using one type of ionic liquids, [EMIN][OAc] solution. The results showed that the dehumidification performances of the MLDAD module, including the latent effectiveness and MRR, for two cases using LiCl and [EMIN][OAc] solutions, were very similar to each other. The big difference is reflected in the sensible effectiveness. This is

because the sensible effectiveness of MLDAD is affected by the heat of absorption released by the solution. However, the heat of absorption of [EMIN][OAc] is much larger than that of LiCl. Therefore, the cooling performance of air for the ILD module is worse than the LiCl module. But we still can use the ILD to replace the market of conventional liquid desiccants, since it has a comparable dehumidification ability, and it eliminates the danger caused by corrosion of pipelines and equipment. From an energy point of view, the use of ILD requires more cooling for the processing air, while the heating of the solution in the regeneration part can be slightly reduced. Its energy consumption is mainly reflected in its viscosity. The viscosity of ILD is much higher than that of conventional halide salt solutions so that ILD will increase the energy consumption of the solution pump.

- For different types of membranes, either porous membranes or nonporous membranes, their dehumidification abilities are both the combination of permeability and thickness of the material. The thinner the thickness and the greater the permeability lead to a larger mass transfer coefficient, and result in the significant increase of the dehumidification. Generally, the nonporous membrane has a thinner thickness but a smaller permeability per unit length. The porous membrane has a larger permeability per unit length but a thicker thickness. Therefore, the mass transfer coefficient, a comprehensive consideration of these two parameters, is hard to compare between a porous membrane and a nonporous membrane. In our case studies, we use the data of porous membranes in the literature and the coefficients of nonporous membranes we measured and brought them into models. The numerical results indicate that the dehumidification effectiveness of the porous membrane is much larger than that of the nonporous membrane we used. Therefore, it is recommended to apply the porous membranes to the MLDAD module.
- In our simulation, the performance of a cross-flow and a counter-flow MLDAD only had little difference on the dehumidification performance of MLDAD. However, due to the complexity of the sealing issues of the membrane module, and the difficulty to arrange a pure counter-flow dehumidifier in the HVAC system, it is suggested to use a cross-flow module.
- For module dimensions, reducing the thickness and width of air channels and increasing the thickness and width of solution channels can improve the sensible and latent effectiveness of the module. MRR can be increased by increasing the number of membrane layers. Table 6.6 summarized the results of a sensitivity analysis of module dimensions for an MLDAD module. For the baseline case with the same geometry of our initial prototype, it is recommended to

increase the air channel length above 0.3 m and to decrease the solution channel length at least below 0.3 m in order to have latent effectiveness larger than 70%. It is also suggested to decrease the air channel height below 5 mm, but to increase the solution channel height larger than 5 mm. The module geometry information for the existing experimental investigation on MLDAD is summarized in Table 1.4. In their studies, most of the lengths of the air channel are around 0.2-0.4 m, and the solution channel length is usually the half of the air channel length. Moreover, the heights (or the thickness) of a single solution channel and air channel are around 5 mm in some researches [53][59][64][65]. And the commonly used height is around 2-5 mm.

- The mass transfer coefficient is one of the most important parameters for the module performance. For porous membranes, the mass transfer coefficient can be calculated from equations. We studied the effects of the membrane pore size, porosity, and thickness on the dehumidification performance. The analysis shows that larger pore size and porosity with a smaller thickness can improve dehumidification effectiveness and MRR. But the increasing rates of the effectiveness and MRR decrease with the increasing pore size and porosity.
- The most important operating parameters affecting the module performance are the air flow rate and the solution to air flow rate ratio (SAMR). The decrease of air flow rate, or the increase of solution flow rate, which all lead to a larger SAMR number, can raise the dehumidification and cooling performance. And the impact of the air flow rate is more sensitive than that of the solution side. However, the inlet temperature and humidity of the air, and the inlet temperature and concentration of the solution only have little effect on the module effectiveness. Table 6.7 summarized the results of sensitivity analysis of operating conditions for an MLDAD module. They show great consistency with the results provided by Bai [145].

Table 6.6 The sensitive analysis of module dimensions for an MLDAD module.

Parameters	$width_{air}$ ↑	$width_{sol}$ ↑	$depth_{air}$ ↑	$depth_{sol}$ ↑	Pore size ↑	Porosity ↑	thickness↑
ε_{lat}	↓	↑	↓	↑	↑	↑	↓
ε_{sen}	↓	↑	↓	↑	↑	↑	↓
MRR	↑	↑	↑	↑	-	-	-

Table 6.7 The sensitive analysis of operating conditions for an MLDAD module.

Parameters	m_{air} ↑	m_{sol} ↑	m* ↑	T_{air} ↑	W_{air} ↑	T_{sol} ↑	C_{sol} ↑

ε_{lat}	↓↓	↑	↑↑	↑	↑	↓	↑
ε_{sen}	↓↓	↑	↑	↓	↓	↓	↓
MRR	↑	↑	↓	↑	↑	↓	↑

Through the above analysis, we made some adjustments to the geometry of the MLDAD module. In the optimization cases, the length of the air channel is increased from 0.1842 to 0.3 m, and the length of the solution channel is reduced from 0.1524 to 0.15m. The thickness of air and solution channels reduced from 13.6 to 5 mm. In the first optimization case, we maintain the constant air inlet velocity and then adjust the mass flow rates of two fluids accordingly. In the second optimization case, we keep the mass flow rate of the fluid unchanged and then adjust the air inlet velocity. The results for all cases are shown in Table 6.8. For case 1, the latent effectiveness is improved from 75% to 99%, and the sensible effectiveness enlarged from 50% to 93%. However, the MRR drops from 2.79E-06 to 1.35E-6 kg/s due to the decrease in the air flow rate. For case 2, the latent effectiveness is improved from 75% to 87%, and the sensible effectiveness enlarged from 50% to 75%. The effectiveness is not as high as that in case 1. However, the MRR increases from 2.79E-06 to 3.26E-6 kg/s. The performance of the module can also be improved by adding more layers of the membrane.

Table 6.8 The optimization cases for an MLDAD module.

Parameter	unit	Baseline	Optimized case 1	Optimized case 2
Membrane type	-	porous	porous	porous
Air inlet velocity	m/h	402.06	402.06	1111.11
m*	-	6	6	6
Air inlet temperature	C	25	25	25
Solution inlet temperature	C	30	30	30
Air relative humidity	-	0.7	0.7	0.7
Solution concentration	-	0.697	0.697	0.697
Air mass flow rate	kg/h	1	0.368	1.000
Solution flow rate	kg/h	6	2.206	6.000
Air channel length	m	0.1842	0.3	0.3
Solution channel length	m	0.1524	0.15	0.15
Air channel height	mm	13.6	5	5
Solution channel height	mm	13.6	5	5
Membrane layer	-	1	1	1
Membrane thickness	um	150	150	150

Membrane pore size	um	0.24	0.24	0.24
Membrane porosity	-	0.35	0.35	0.35
Latent effectiveness	-	0.7488	0.9847	0.8745
Sensible effectiveness	-	0.4971	0.9310	0.7486
MRR	kg/s	2.79E-06	1.35E-06	3.26E-06

7. CONCLUSION AND FUTURE WORK

7.1 Conclusion

The LDAD system has attracted increasing interests of researchers globally as an alternative to conventional vapor compression air conditioning-based dehumidification system. However, the carryover and corrosion problems limited its market share. Thus, there is a strong need to overcome these drawbacks of the conventional LDAD system. In this research, two new technologies are investigated. One is using semi-permeable membranes to separate the air and liquid desiccant so that the solution droplets cannot enter into the air stream to cause the corrosion of HVAC components and the quality deterioration of the supply air. Another new technology is using a non-corrosive ionic liquid desiccant to replace the conventional halide salt solutions. The hybrid of these two technologies in the LDAD module is named as the MLDAD module using ionic liquid.

In the study, the experimental researches and existing modeling methods on MLDAD were first extensively reviewed with the respects of the characteristics of liquid desiccants and membranes, the design of MLDAD modules, the performance assessment and comparison for MLDAD, and summary of modeling methods.

An initial MLDAD prototype was tested in ORNL by using ionic liquid desiccant. The prototype was able to dehumidify the humid air with an average mass transfer coefficient of 2.1E-14 for the dehumidification mode.

Two heat and mass transfer models of MLDAD modules have been developed for the uses of porous and dense or non-porous membranes, respectively. For the porous membrane, the mechanism of pore-flow diffusion is used to calculate the mass transfer coefficient by the microstructure parameters such as pore size, porosity, and tortuosity. For the nonporous membrane, the mechanism of solution-diffusion is dominated. The mass transfer coefficient can only be obtained by the measurement. A finite element method was applied to the two-dimensional heat and mass transfer modules, and the program was solved in MATLAB. Also, an operating interface based on the MATLAB GUI was developed.

The heat and mass heat transfer model for porous membranes was validated by the experimental data from Huang's group published in 2014. The model for nonporous membranes was validated by the experimental data from our preliminary performance test and the measurement of

the membrane properties. The results showed that the maximum discrepancy between numerical results and experimental data for $T_{air,out}$, $T_{sol,out}$, $W_{air,out}$, and ε_{sen} were 3%, 4%, 5%, and 6%, respectively. Both of the numerical results agreed very well with the experimental data obtained by ORNL and the available literature.

The validated models can provide the fields of temperature, humidity, and concentration of air and solution fluids. The parametric studies on the MLDAD module predict that ionic liquid desiccant [EMIM][OAc] can be used to as a substitute for the conventional liquid desiccant LiCl solutions, for they can achieve almost the same dehumidification ability. But the energy consumption of the ILD may be higher than the LiCl due to its higher viscosity. It is then found that the most important parameters for dehumidification performance are the mass transfer coefficient dominated by the pore size, porosity, and thickness of the membrane, as well as the mass flow rate ratio of solution to air. Thus, the membrane selection is important. Generally, the porous membrane has a larger mass transfer coefficient than the nonporous membrane. It is recommended to use the porous membrane in the MLDAD module. In addition, the impacts of flow patterns on the dehumidification performance is limited. Thus, an easier configuration of the flow pattern is preferred in the MLDAD system. These results can provide some design guidance for material selection, module design, operation, and control.

7.2 Future work

In order to achieve the ultimate goal of this research, future work will focus on the following aspects.

- Select better performance membrane materials for the MLDAD prototype, with high permeability and physical robustness.
- Design and optimize a complete MLDAD system, including dehumidification module, regeneration module, heat/cooling exchanger, solution reservoir and so on.
- Hybrid the MLDAD system with the conventional AC system, using the condensing heat to regenerate the solution for free.
- Analyze the energy consumption and life-cycle cost of the system.

APPENDIX A. PROPERTIES OF LIQUID DESICCANTS

A.1 Thermodynamic properties of [EMIM][OAc]

Equilibrium Vapor Pressures: The vapor pressure of the liquid desiccant can be calculated from Equation A.1. And the detailed parameters are defined in Equations A.2-A.11 [31].

$$P_{w,ILD} = P_{w,sat} \cdot x_1 \cdot \gamma_1 \tag{A.1}$$

where $P_{w,s}$ is the saturated vapor pressure, x_1 is the mole fraction of water in the aqueous solution, and γ_1 is the activity coefficient of water vapor. The equation for the weight fraction is defined in Equation A.2. Thus, the mole fraction of any substance is calculated by Equation A.3.

$$w_i = x_i \cdot \frac{M_i}{M} \tag{A.2}$$

$$x_i = w_i \cdot \frac{\sum x_i M_i}{M_i} \tag{A.3}$$

Evaluating such that i=2 corresponds to the liquid desiccant, and i=1 corresponds with water and recognizing that $x_2 = 1 - x_1$, Equation A.3 can be rewritten to give an expression for the mole fraction of the liquid desiccant in terms of the weight fraction of the desiccant and the molar mass of the desiccant and water.

$$x_1 = w_1 * \frac{x_1 M_1 + (1 - x_1) M_1}{M_1} = \frac{M_2}{\left(\frac{M_1}{w_1} - M_1 + M_2\right)} \tag{A.4}$$

The activity coefficient of water vapor is given by the Non-Random, Two-Liquid (NRTL) equation in Equation A.5. The parameters used in A.5 is identified in Equations A.6-A.11.

$$ln\,\gamma_1 = x_2^2 \left[\tau_{21}\left(\frac{G_{21}}{x_1 + x_2 G_{21}}\right) + \frac{G_{12}\tau_{12}}{(x_2 + x_1 G_{12})^2}\right] \tag{A.5}$$

$$G_{12} = exp(-\alpha_{12}\tau_{12}) \tag{A.6}$$

$$G_{21} = exp(-\alpha_{21}\tau_{21}) \tag{A.7}$$

$$\tau_{12} = \frac{\Delta g_{12}}{RT} \tag{A.8}$$

$$\tau_{21} = \frac{\Delta g_{21}}{RT} \tag{A.9}$$

$$\Delta g_{12} = 28938 \frac{J}{mol} \tag{A.10}$$

$$\Delta g_{21} = -25691 \frac{J}{mol} \tag{A.11}$$

Specific Heat Capacity: The specific heat capacity ($c_{p,ILD}$) of [EMIM][OAc] at different temperatures and concentrations can be solved by the equation below [31].

$$\begin{aligned} c_{p,ILD} = {} & 2.761077 + 0.008120T - 1.106151e(-5)T^2 \\ & -2.649514e(-8)C - 0.918307C^2 + 0.003580T \cdot C \end{aligned} \tag{A.12}$$

Density: The density (ρ_{ILD}) of [EMIM][OAc] at different temperatures and concentrations can be solved by the equation below [31].

$$\begin{aligned} \rho_{ILD} = {} & 1.012482e3 - 0.918013T + 6.25e(-5)T^2 \\ & +758.0905C - 497.846C^2 + 0.302582T \cdot C \end{aligned} \tag{A.13}$$

A.2 Thermodynamic properties of inorganic salt solutions

Equilibrium Vapor Pressures: In order to obtain the equilibrium vapor pressure related to different concentrations and temperatures of the inorganic solution, Cisternas and Lam used empirical data to find some correlations with the solution properties, and fitted the following formulas to solve the equilibrium value [141].

$$\log P_v = KI \left[A - \frac{B}{T - E_s} + C - \frac{D}{T - E_s} \right] \tag{A.14}$$

$$A = A_s + 3.60591 \times 10^{-4} \cdot I + \frac{M_s}{2303} \tag{A.15}$$

$$B = B_s + 1.382982 \cdot I - 0.031185 \cdot I^2 \tag{A.16}$$

$$C = C_s - 3.99334 \times 10^{-3} \cdot I - 1.11614 \times 10^{-4} \cdot I^2 + \frac{M_s \cdot I(1 - \chi)}{2303} \tag{A.17}$$

$$D = D_s - 0.138481 \cdot I - 0.027511 \cdot I^2 - 1.79277\times10^{-3} \cdot I^3 \qquad (A.18)$$

$$\chi = 2\frac{v_+ + v_-}{v_+ Z_+^2 + v_- Z_-^2} \qquad (A.19)$$

$$I = \frac{1}{2}\sum_i Z_i^2 m_i' \qquad (A.20)$$

where: K - electrolyte parameter;

I - ionic strength [mol/kg];

T - temperature of solution [K];

m - molar concentration of ionic species;

M_s - molecular weight of the solution [mol/kg];

v_+ - number of moles of cation;

v_- - number of moles of anion;

Z_+ - charge of cation;

Z_- - charge of anion;

A_s, B_s, C_s, D_s and E_s are constant coefficients which can be found in [141] for different solvents. The density, thermal conductivity, specific capacity of a salt-aqueous solution can also be calculated in [142][143].

The heat of Solution: The heat of dilution for ionic liquid and LiCl solutions at different temperature and concentrations are different. And the heat of dilution for several ionic liquids and LiCl can be found in Figure A.1.

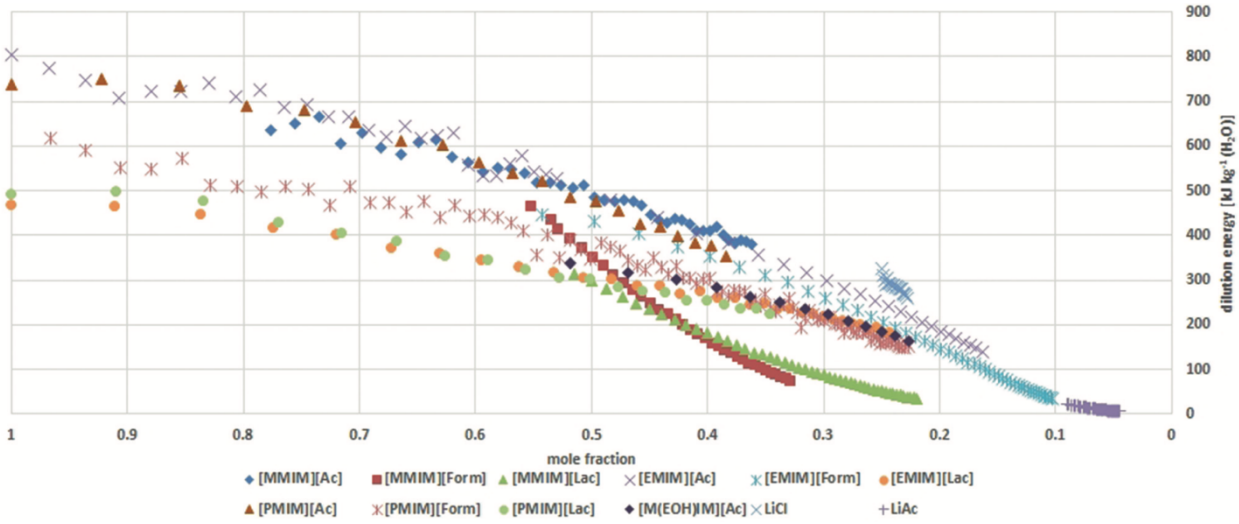

Figure A.1 The heat of dilution against the mole fraction of ILDs compared with LiCl [133].

APPENDIX B. MEASUREMENT OF MEMBRANE PERMEABILITY

The water vapor transportation processes discussed above follow the Fick's law – the rate of mass transfer is determined by the water vapor permeability of the membrane, the thickness of the membrane, and the difference of water vapor pressure across the membrane. As discussed in Chapter 4, the water vapor permeability of porous membranes can be calculated based on the characteristics of the porous membranes including pore size, porosity, tortuosity, thickness, as well as the operating conditions, which can be measured or obtained from the membrane manufacturers. However, for nonporous or dense membranes, their water vapor permeability can only be gained by measurement.

There are generally two methods to measure the mass transfer coefficient. One is using cup method, which is instructed by ASTM E96 standard, to measure the water vapor transmission rate and then to calculate the permeability; another is using the dynamic moisture permeation cell (DMPC) method to measure the water vapor diffusion resistance. All the coefficients tested are based on vapor-to-vapor mass transfer interface. However, in the MLDAD module, water vapor moves from the humid air side to the high-concentrated solution side, where the membrane is tightly bonded to the membrane without any air gaps. So, the mass transport occurs on the vapor-solution surface. Thus, how to accurately measure the coefficient of the water vapor permeability for the MLDAD system becomes a question.

To identify the most proper method for measuring the vapor-to-solution mass transfer coefficient for membranes used in MLDAD, different cup-methods have been applied. Comparisons between dry cup method and wet cup method, dry cup method and liquid desiccant cup method, wet cup method and reversed wet cup method, for both dense membranes and porous membranes have been conducted.

The following sections cover the experimental settings including materials, instruments along pictures and dimensions, and a detailed description of test programs including operating conditions. Then, results of the measurement including weight change with time and transmission rate change with time are addressed. The discussion and comparison of a different method, different membrane materials, and different operating conditions are presented. Finally, the conclusion and suggestion are drawn.

B.1 Method

B.1.1 Selection of membranes

Four PFSA (perfluorinated sulfonic-acid) non-porous membranes were provided by a manufacturer (Xergy). They are hydrophilic membranes. Their chemical composition and properties were documented by the literature [134]. Three porous membranes were provided by Tisch Scientific Company. They are all hydrophobic membranes. One of them is a laminated PTFE membrane (SF13867) with a pore size of 1.0 μm. Another two of them are unlaminated polypropylene membranes with the pore size of 0.2 μm (SF14555) and 1.0 μm (SF14837), respectively. The thickness, porosity, and wettability of the membrane are listed in Table. 1. Moreover, the micro-structures of the tested membrane are photographed using the transmission electron microcopy technology, as shown in Figure B.1 and B.2.

Table B.1 Properties of the membranes.

Index	1	2	3	4	5	6	7
Dense/Porous	Non-porous				Porous		
Wettability	Hydrophilic				Hydrophobic		
Pore size (um)	-	-	-	-	0.2	1.0	1.0

B.1.2 Test methods and conditions

The water vapor transmission rate (WVTR) of the membranes were measured with the wet cup and dry cup method described by ASTM E96, as well as some modified methods such as upright wet cup fulfilled with water, reversed wet cup, and an upright wet cup filled with liquid desiccant. The detailed description of the various methods is presented below.

Dry cup method – In the dry cup method, the test membrane is sealed at the opening of the permeability cup containing a certain amount of anhydrous calcium chloride ($CaCl_2$) as shown in Figure B.3(2). There is airspace existing between the membrane and the calcium chloride. The permeability cup then is placed on the top of a scale in an air-conditioned chamber with controlled air temperature and humidity. Periodic weighing is documented to determine the rate of water vapor movement through the membrane into the desiccant.

Wet cup method – In the wet cup method, the test membrane is sealed at the opening of the permeability cup containing a certain amount of distilled water as shown in Figure B.3(1). There is airspace existing between the membrane and distilled water. The permeability cup then is placed on the top of a scale in an air-conditioned chamber with controlled air temperature and humidity. Periodic weighing is documented to determine the rate of water vapor movement through the membrane from the vapor above the water to the controlled chamber.

Wet cup method with fulfilled water – This method is very similar to the wet cup method. The only difference is that the distilled water is fulfilled in the permeability cup and the membrane is fixed on the top of the cup so that there is no airspace between the water and the membrane as shown in Figure B.3(3). The membrane is bonded and contacted with the water tightly. The weighing is documented to determine the rate of vapor movement through the membrane from the membrane-water surface to the controlled chamber.

Reversed wet cup method – This method is also very similar to the wet cup method. The only difference is that the permeability cup is reversely placed in the chamber so that the distilled water inside the cup contacts with the membrane directly. Since the water in on the top of the membrane, no airspace occurs even when the water vapor is transferred to the chamber. The weighing is documented to determine the rate of vapor movement through the membrane from the membrane-water surface to the controlled chamber.

Liquid desiccant cup method – In the liquid desiccant cup method, the test membrane is sealed to the permeability cup containing aqueous calcium chloride solution ($CaCl_2$-water solution) with different concentration as shown in Figure B.3(4). The weighing is documented to determine the rate of vapor movement through the membrane from the chamber to the liquid desiccant.

The test conditions for both dense and porous membranes using a dry or wet cup with or without airspace are listed in Table B.2.

Table B.2. Summary of test conditions.

Cup method	Dry cup	Wet cup	Fulfilled wet cup	Reversed wet cup	Liquid desiccant cup
Test membrane	1234567	1234567	234	1234567	14567
Airspace	Yes	Yes	No	No	Yes
$T_{chamber}$ (C)	24.5				
$rh_{chamber}$ (-)	80.8%				
$Pv_{chamber}$ (pa)	2495				
Materials inside cup	$CaCl_2$	Distilled water	Distilled water	Distilled water	$CaCl_2$ solution
Pv_{cup} (pa)	0	3076			1300
Pv_{diff} (pa)	2495	581			1195

Figure B.3 (1) Wet cup, (b) dry cup, (c) fulfilled wet cup, and (d) liquid desiccant cup (photos credit to Xiaobing Liu, ORNL).

B.1.3 Measurement apparatus

The schematic of the measurement apparatus is shown in Figure 2. The measurement apparatus is comprised of a small cup made with stainless steel (Elcometer 5100/3), which has an opening area of 30 cm^2 and a volume of 75 cm^3; a high accuracy (0.01 g) electronic balance, and a data acquisition system. During the test, a membrane is placed over a gylon gasket on top of the permeability cup; and a metal ring is placed on top of the membrane and is secured by six screws retained clamps (Fig. 1) to ensure a tight seal. The gaps between the membrane and water surface were about 4 mm. The experiment was conducted in a climate chamber, where the indoor temperature and the relative humidity is maintained at set points (dry bulb temperature of 24.5°C and a relative humidity of 80.8%). The air inside the chamber is continuously circulated with a velocity sufficient to maintain uniform conditions at all test locations. The air velocity over the specimen shall be between 0.066 and 1 ft/s [0.02 and 0.3 m/s].

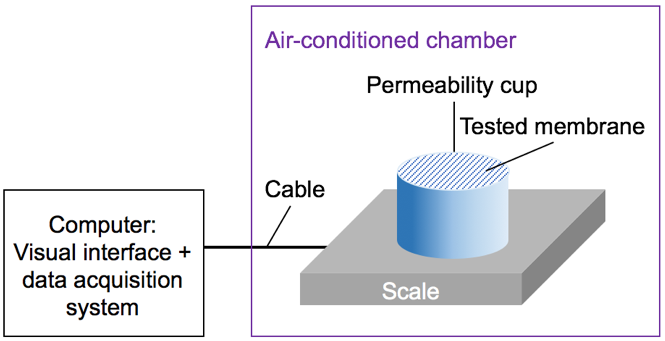

Figure B.4 The schematic of the measurement set up.

The mass of the cup assembly (including cup, water/desiccant, and the membrane) is measured with the electronic balance continuously during a test, which usually takes about 5~12 hours. The measured data was recorded by the data acquisition system. The water vapor transmission rate and other performance metrics of the tested membrane are calculated with following Eqs B.1-3.

B.1.4 Performance metrics

Water vapor transmission rate (WVTR*)* refers to the steady flow of water vapor through the unit area of a membrane in a unit time, perpendicular to a specific parallel surface, under specific temperature and humidity conditions on each surface. WVTR is calculated by Equation B.1, where G is the mass of water vapor permeated through the membrane, and t is the elapsed time, and A is the membrane area.

$$WVTR = \frac{G}{tA} \tag{B.1}$$

Water vapor permeance refers to the time rate at which water vapor passes through a flat membrane per unit area caused by the unit vapor pressure difference between two specific surfaces under specified temperature and humidity conditions. Permeance is an indicator of the overall water vapor transmission performance of the membrane under a given test condition. It is the reverse of the water vapor transmission resistance and can be called as the mass transfer coefficient. Permeance is defined as Equation B.2, where ΔP_v is the vapor pressure difference between two surfaces of the membrane.

$$Permeance = \frac{G}{tA\Delta P_v} = \frac{WVTR}{\Delta P_v} \tag{B.2}$$

Water vapor permeability (WVP) is the physical property of membrane materials, just like the thermal conductivity of materials. It is the time rate of water vapor transport per unit area of flat membrane with unit thickness caused by unit vapor pressure difference between two membrane surfaces under specific temperature and humidity conditions. Permeability can be calculated as the arithmetic product of the permeance and thickness of the membrane, as expressed by Equation B.3.

$$Permeability = Permeance \times thickness = \frac{G\delta}{tA\Delta P_v} \quad (B.3)$$

B.2 Results and discussions

B.2.1 Overall measurement results

Based on the test programs mentioned above, the water vapor transmission rate of seven membranes was tested at several different conditions, including a wet cup with airspace, wet cup without airspace, wet cup reversely placed and dry cup (using solid desiccant) with airspace. The weight change with time of the dense membrane (take Membrane 2, for example) under different test conditions is shown in Figure B.5. It can be seen that the weight of the test assembly decreased linearly with time under wet cup conditions and increased linearly with time under dry cup conditions. The R^2 value of the linear curve fit for the measured weight data in each test is higher than 0.99. The weight change rate, which is the slope of the linear curve fit, was used to determine water vapor permeance of the membranes. Because the membrane is very thin, and the mass transfer coefficient in governing equations can be simplified to the ratio of permeability to the thickness (which is the permeance), we only calculate permeance of membranes in this section. Table B.3 presents the overall results of water vapor permeance of the seven membranes. From the table, we can know that the permeance measured by the dry method without air layer is the highest among all tests in the wet cup condition, which is about 4.6E-08 kg/m^{2}sPa. However, the permeance obtained in the wet cup condition with airspace is about 0.8-1.1E-08 kg/m^{2}sPa, which is much lower. Moreover, in the dry cup method, when $CaCl_2$ solution is used as the liquid desiccant to absorb water vapor, the permeability can reach to about 2.3~3E-08 kg/m^{2}sPa.

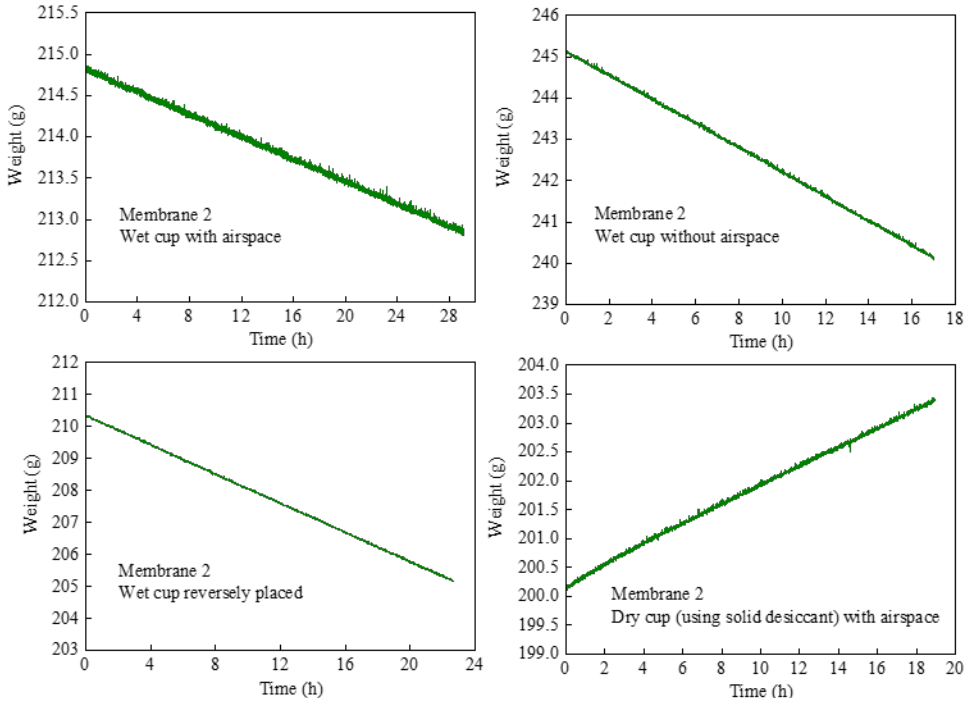

Figure B.5 Weight change with time for a dense membrane under various test conditions.

Table B.3 Measured water vapor permeance of the seven different membranes (E-08 kg/m^2-s-pa)

Method	Dense membrane				Porous membrane		
	1	2	3	4	5	6	7
Wet cup with airspace	0.8474	1.080	1.118	1.118	0.9810	1.010	0.9684
Wet cup without airspace	-	4.689	4.465	4.396	-	-	-
Wet cup reversely placed	3.150	3.638	3.482	3.654	3.155	3.168	3.133
Dry cup using solid desiccant with airspace	0.5796	0.6138	0.7546	0.6589	0.8110	0.6993	0.7773
Dry cup using LD without airspace	2.34	-	-	2.83	2.93	3.01	3.04

From the results, we can see that the existence of the airspace has a great influence on the mass transfer coefficient, and it can reduce the permeance or permeability largely. Therefore, in the experimental process, once there is incomplete contact between the solution and the membrane, the dehumidification effectiveness will decrease significantly. Since the LD solution is expected to be used and there is no airspace between the membrane and the solution in our models, it is suggested to use data from a dry method using liquid desiccant without airspace to verify the model.

By comparing the permeability of the same membrane in wet and dry cups, it was found that when water vapor was transferred from humid indoor air to dry cups, the permeance was much lower than the condition where water vapor transferred from wet cups to the dry chamber. This

may explain that when the first MLDAD prototype is used as a regenerator (water released from liquid desiccant enters the air stream, similar to wet cup test), it has a better potential effect than when it is used as a dehumidifier (water vapor in the air is absorbed by a liquid).

The test results indicate that the nonporous membranes do not have significantly higher permeance than the porous membranes (even with much lower permeance under the dry cup condition), but they are much more fragile than the porous membranes, which can endure with a higher flow rate of air and liquid desiccant without leakage. It is thus recommended to use porous membranes in the membrane-based dehumidifier instead of the dense membrane used in the 1st prototype of MLDAD.

The experimental results show that the permeance of nonporous membranes is not significantly higher than that of porous membranes, but they are more elastic than porous membranes. So, porous membranes can withstand higher air and liquid flow velocities without leakage. Therefore, it is suggested that porous membranes should be used in MLDAD systems.

APPENDIX C. MATLAB CODES

The MATLAB codes for the MLDAD module using LiCl solutions are shown as follows.

```
% Model of LiCL
%% allocate spaces
num_lsegment=100;
num_dsegment=200;
Temp_air=zeros(num_lsegment+2,num_dsegment+2);
Temp_sol=zeros(num_lsegment+2,num_dsegment+2);
rh_air=zeros(num_lsegment+1,num_dsegment+1);
P_air=zeros(num_lsegment+2,num_dsegment+2);
P_sol=zeros(num_lsegment+2,num_dsegment+2);
Temp_airmem=zeros(num_lsegment+2,num_dsegment+2);
Temp_solmem=zeros(num_lsegment+2,num_dsegment+2);
mflr_air=zeros(num_lsegment+1,num_dsegment+1);
mflr_sol=zeros(num_lsegment+1,num_dsegment+1);
mflwseg_air=zeros(num_lsegment+2,num_dsegment+2);
mflwseg_sol=zeros(num_lsegment+2,num_dsegment+2);
mflr_vap_air=zeros(num_lsegment+1,num_dsegment+1);
mflr_vap_sol=zeros(num_lsegment+1,num_dsegment+1);
mflwvapseg_air=zeros(num_lsegment+2,num_dsegment+2);
mflwvapseg_sol=zeros(num_lsegment+2,num_dsegment+2);
P_vap_air=zeros(num_lsegment+2,num_dsegment+2);
P_vap_sol=zeros(num_lsegment+2,num_dsegment+2);
humid_air=zeros(num_lsegment+2,num_dsegment+2);
Con_water_sol=zeros(num_lsegment+2,num_dsegment+2);
P_m_total=zeros(num_lsegment+1,num_dsegment+1);
P_m_air=zeros(num_lsegment+1,num_dsegment+1);
Temp_mem=zeros(num_lsegment+1,num_dsegment+1);
c_kd=zeros(num_lsegment+1,num_dsegment+1);
c_md=zeros(num_lsegment+1,num_dsegment+1);
c_pf=zeros(num_lsegment+1,num_dsegment+1);
Jvwat=zeros(num_lsegment+1,num_dsegment+1);
mflr_mem=zeros(num_lsegment+1,num_dsegment+1);
Cp_air=zeros(num_lsegment+1,num_dsegment+1);
Cp_sol=zeros(num_lsegment+1,num_dsegment+1);
mtdydx_air=zeros(num_lsegment+1,num_dsegment+1);
mtdydx_sol=zeros(num_lsegment+1,num_dsegment+1);
mflr_vap_mem_air=zeros(num_lsegment+1,num_dsegment+1);
mflr_vap_mem_sol=zeros(num_lsegment+1,num_dsegment+1);
htc_air=zeros(num_lsegment+1,num_dsegment+1);
htc_sol=zeros(num_lsegment+1,num_dsegment+1);
%% initial temperature [K]
Temp_air(1,1)=30+273.15; % air bulk temperature, [k]
Temp_sol(1,1)=25+273.15; % solution bulk temperature, [k]
%% initial relative humidity [-]
rh_air(1,1)=0.70458; % air relative humidity
pf_con_licl(1,1)=0.35; % solution initial concentration, [Kg/Kg]
Con_water_sol(1,1) = 1 - pf_con_licl(1,1); % water mass concentration,↙
[kg/kg]
%% initial pressure [Pa] The pressure is assume to be constant and the↙
same as the P_ATM
P_air(1,1)=1.01325e5; % air pressure, [pa]
P_sol(1,1)=1.01325e5; % solution pressure, [pa]
%% initial mass flow rate [kg/s]
mflr_air(1,1)=1*1.5/3600;  % mass flow rate of air, [kg/s]
mflr_sol(1,1)=6*3/3600; % mass flow rate of sol, [kg/s]
```

```
%% initial membrane temperature [C]
mm=0.5; %mf_fa(1,1)/(mf_fa(1,1)+mf_pf(1,1));
Temp_airmem(1,1) =mm*Temp_air(1,1)+(1-mm)*Temp_sol(1,1);  % air-mem↙
surface temp, [k]
Temp_solmem(1,1) = mm*Temp_air(1,1)+(1-mm)*Temp_sol(1,1);   % sol-mem↙
surface temp, [k]
%% Dimentions
length=10*1*0.01; % air channel width, [m]
depth=20*1*0.01; % solution channel width, [m]
lseg = length/(num_lsegment); % air channel width of each control↙
volume, [m]
dseg = depth/(num_dsegment); % sol channel width of each control volume,↙
[m]
num_layer=1; % number of membrane layer
numchannel_air = floor((num_layer+1)/2); % number of air channel
numchannel_sol = floor((num_layer+1)/2); % number of air channel
%% Membrane properties
delta_mem=150E-6; % thickness of the membrane, [m]
m_rp=0.12E-6; % membrane pore radius, [m]
m_ps=0.35; % membrane porosity, [-]
m_ts=(2-m_ps)^2/m_ps; % membrane turtuosity, [-]
k_mem=0.3; % membrane thermal conductivity, [kw/m/k]
%% air side coeff
Re_air=301.1;
Pr_air=0.7;
visco=1; % bulk/surface guess value
k_air=0.0263E-3;
r_air=3E-03; % thickness of air channel
dh_air=4*length*r_air/(length+r_air)/2; %
Nu_air=7.15+0.085*(Re_air*Pr_air*dh_air/depth)/(1+↙
(Re_air*Pr_air*dh_air/depth)^0.67)*(visco)^0.14;
h_air=Nu_air*k_air/dh_air;
%% sol side coeff
Nu_sol=8.24; % solution side Nusselt number
k_sol=0.5E-3;
r_sol=6E-03; % thickness of solution channel
dh_sol=4*depth*r_sol/(depth+r_sol)/2; % @
h_sol=Nu_sol*k_sol/dh_sol;
%% initial [segment] [mass] flow rate,[kg/s]
mflwseg_air(1,1) = mflr_air(1,1)/(num_lsegment*numchannel_air);
mflwseg_sol(1,1) = mflr_sol(1,1)/(num_dsegment*numchannel_sol);
%% initial [vapor/water] mass flow rate,[kg/s]
mflr_vap_air(1,1) = Airhumrat(Temp_air(1,1),rh_air(1,1))/(1+Airhumrat↙
(Temp_air(1,1),rh_air(1,1)))*mflr_air(1,1); % vapor in air
mflr_vap_sol(1,1) = mflr_sol(1,1) * Con_water_sol(1,1);   % water in↙
aqueous
%% initial [segment] [vapor] flow rate,[kg/s]
mflwvapseg_air(1,1) = mflr_vap_air(1,1)/(num_lsegment*numchannel_air);↙
% vapor in air
mflwvapseg_sol(1,1) = mflr_vap_sol(1,1)/(num_dsegment*numchannel_sol);↙
% water in aqueous
%% initial humidity ratio and vapor pressure
humid_air(1,1) = mflwvapseg_air(1,1)/(mflwseg_air(1,1)-mflwvapseg_air↙
(1,1));    % [kg Water /kg Air]
P_vap_air(1,1) = vapPstaturate(Temp_air(1,1))*Airrehum(Temp_air(1,1),↙
humid_air(1,1));    % [pa]
P_vap_sol(1,1)=Pi_licl(Temp_sol(1,1),pf_con_licl(1,1)); % equilibrium↙
vapor pressre of LiCl
W_sol(1,1)=0.622*P_vap_sol(1,1)/(101325-P_vap_sol(1,1)); % equilibrium↙
humidity ratio of LiCl
```

```
%% energy/mass analysis for all segments of a component device
for i = 1: num_lsegment+1
    for j = 1: num_dsegment+1
        if i==1
            Temp_sol(i,j)=Temp_sol(1,1);
            Temp_solmem(i,j)=Temp_solmem(1,1);
            mflr_vap_sol(i,j)=mflr_vap_sol(1,1);
            mflr_vap_mem_sol(i,j) =mflr_vap_mem_sol(1,1);
            mflwvapseg_sol(i,j)=mflwvapseg_sol(1,1);
            mflwseg_sol(i,j)=mflwseg_sol(1,1);
            Con_water_sol(i,j)=Con_water_sol(1,1);
            P_sol(i,j)=P_sol(1,1);
            P_vap_sol(i,j)=P_vap_sol(1,1);
            W_sol(i,j)=W_sol(1,1);
        end
        if j==1
            Temp_air(i,j)=Temp_air(1,1);
            Temp_airmem(i,j)=Temp_airmem(1,1);
            mflr_vap_air(i,j)=mflr_vap_air(1,1);
            mflr_vap_mem_air(i,j) =mflr_vap_mem_air(1,1);
            mflwvapseg_air(i,j)=mflwvapseg_air(1,1);
            mflwseg_air(i,j)=mflwseg_air(1,1);
            humid_air(i,j)=humid_air(1,1);
            P_air(i,j)=P_air(1,1);
            P_vap_air(i,j)=P_vap_air(1,1);
        end
          pf_con_licl(i,j)=1-Con_water_sol(i,j);
%% J_v, based on vapor pressure drive force [kg/m2-s]
        P_m_total(i,j) = (P_air(i,j)+P_sol(i,j))/2; % membrane vapor↙
pressure, [pa]
        Temp_mem(i,j) = (Temp_airmem(i,j) + Temp_solmem(i,j))/2; % mean↙
temp of membrane, [k]
        Mw=0.018;
        R=8.413;
        Gama=1.0; % coeff, the impact of silica gels
        Dk(i,j)=D_knudsen(m_rp,Temp_mem(i,j)); % knudsen, m2/s
        Dm(i,j)=D_molecular(Temp_mem(i,j), P_m_total(i,j)); % molecular
        Deff(i,j)=(1/Dk(i,j)+1/Dm(i,j))^-1;
        Deff_m(i,j)=Deff(i,j)*m_ps/m_ts;
        D_air=2.82e-5; %m2/s
%         delta_airboun=3e-4;
%         Rm_air(i,j)=delta_airboun/(D_air*Mw/R/t_mem(i,j));
        hm_air(i,j)=h_air/Vapcp(Temp_air(i,j))/0.564*0.7;
        rm_air(i,j)=1/hm_air(i,j);
        D_sol=3e-9;
%         delta_solboun=1e-8;
%         Rm_sol(i,j)=delta_solboun/(D_sol*Mw/R/t_mem(i,j));
        hm_sol(i,j)=h_sol/Vapcp(Temp_sol(i,j))/1390*28.36;
        rm_sol(i,j)=1/hm_sol(i,j);
        km(i,j)=Gama*Deff(i,j)*m_ps/delta_mem/m_ts*Mw/R/Temp_mem(i,j); %↙
permeance coeff, [kg/m2/s/pa]
        Rm_mem(i,j)=1/km(i,j);

        fv_kd_md(i,j)=km(i,j)*(P_vap_air(i,j) - P_vap_sol(i,j)); % vapor↙
flux, [kg/m2/s]
        if P_vap_air(i,j) >= P_vap_sol(i,j)
            Jvwat(i,j)= (P_vap_air(i,j) - P_vap_sol(i,j))/(rm_air(i,j)↙
+rm_sol(i,j)+Rm_mem(i,j));
        else
            Jvwat(i,j)=0;
        end
```

```
        dx = dseg;
        dy = lseg;
        % vapor mass flow rate/m2, kg/s
        mflr_mem(i,j) = Jvwat(i,j)*dx*dy;
       %% equation and matrix
        htc_correct=1; % correction of heat transfer
        enable_msf=1; % impact of membrane deflection
        htc_air(i,j)=h_air; %0.05;   %0.061;[kW/m^2-K]
        htc_sol(i,j)=h_sol; %0.35;   %[kW/m^2-K]
        Cp_air(i,j) = 1.005; % air cp [kj/kg-k]
        Cp_sol(i,j) = cp_licl(Temp_sol(i,j),pf_con_licl(i,j)); % pf_cp↙
of [LiCL] [kj/kg-k]
        % fa_coeff
        if ( num_layer == 1 || num_layer == 2 )
            fa_coeff = 1.0;
        else
            fa_coeff = 2.0;
        end
        % pf_coeff
        if ( num_layer == 1 )
            pf_coeff = 1.0;
        else
            pf_coeff = 2.0;
        end
        %% the govern equations
        ktdelta_mem=k_mem/delta_mem;
        H_hd(i,j)=pf_coeff*300*mflr_mem(i,j);
        H_hg(i,j)=pf_coeff*2450*mflr_mem(i,j);
       %% matrix
        mflwseg_dryair(i,j)=mflwseg_air(i,j)-mflwvapseg_air(i,j);
        mcpT_air(i,j)=mflwseg_dryair(i,j)*Cp_air(i,j);
        hAT_air(i,j)=fa_coeff*htc_air(i,j)*dx*dy*enable_msf;
        fvCpvT_air(i,j)=fa_coeff*mflr_mem(i,j)*Vapcp(Temp_air(i,j))↙
*enable_msf;
        fvCpvT_airmem(i,j)=fa_coeff*mflr_mem(i,j)*Vapcp(Temp_airmem(i,↙
j))*enable_msf;
        a=zeros(4,4);
        b=zeros(4,1);

        a(1,1) = mcpT_air(i,j)+ hAT_air(i,j)/2.0-fvCpvT_air(i,j)/2.↙
0+mflwvapseg_air(i,j)*Vapcp(Temp_air(i,j));
        a(1,2) = -hAT_air(i,j)/2.0+fvCpvT_airmem(i,j)/2.0;
        b(1,1) = (mcpT_air(i,j)-hAT_air(i,j)/2.0+mflwvapseg_air(i,j)↙
*Vapcp(Temp_air(i,j)))*Temp_air(i,j)-a(1,2)*Temp_airmem(i,j);

        a(2,1) = htc_air(i,j) + Jvwat(i,j)*Vapcp(Temp_air(i,j));
        a(2,2) = (-1)*(ktdelta_mem + htc_air(i,j) - Jvwat(i,j)*Vapcp↙
(Temp_airmem(i,j)));
        a(2,3) = ktdelta_mem;
        b(2,1) = 0;

        a(3,2) = ktdelta_mem + Jvwat(i,j)*Vapcp(Temp_airmem(i,j));
        a(3,3) = -ktdelta_mem - htc_sol(i,j) - Jvwat(i,j)*Vapcp↙
(Temp_solmem(i,j));
        a(3,4) =  htc_sol(i,j) ;
        b(3,1) = -(140+2450)*Jvwat(i,j);
```

```
        mcpT_sol(i,j)=mflwseg_sol(i,j)*Cp_sol(i,j);
        hAT_sol(i,j)=pf_coeff*htc_sol(i,j)*dx*dy*enable_msf;
        fvCpvT_sol(i,j)=pf_coeff*mflr_mem(i,j)*Vapcp(Temp_sol(i,j))↙
*enable_msf;
        fvCpvT_solmem(i,j)=pf_coeff*mflr_mem(i,j)*Vapcp(Temp_solmem(i,↙
j))*enable_msf;

        a(4,3)=-hAT_sol(i,j)/2.0+fvCpvT_solmem(i,j)/2;
        a(4,4)=mcpT_sol(i,j)+pf_coeff*mflr_mem(i,j)*enable_msf*Cp_sol(i,↙
j)+hAT_sol(i,j)/2.0-fvCpvT_sol(i,j)/2;
        b(4,1)= (mcpT_sol(i,j)-hAT_sol(i,j)/2.0+fvCpvT_sol(i,j)/2)↙
*Temp_sol(i,j)-a(4,3)*Temp_solmem(i,j)+pf_coeff*mflr_mem(i,j)↙
*enable_msf*(140+2450);
        %% solution
        % Scaled Gauss Elimination
        temp = a\b;
       %%
        %-------- next temperature ! outlet T(1,1) becomes inlet T(1,2)
        Temp_air(i,j+1) = temp(1);
        Temp_airmem(i,j+1) = temp(2);
        Temp_solmem(i+1,j) = temp(3);
        Temp_sol(i+1,j) = temp(4);
        %% mass transfer
        % segment permeate vapor mass flow rate
        mtdydx_air(i,j) = fa_coeff*mflr_mem(i,j)*enable_msf; %↙
fa_coeff*mfl_mem(i,j)*enable_msf;
        mtdydx_sol(i,j) = pf_coeff*mflr_mem(i,j)*enable_msf; %↙
pf_coeff*mfl_mem(i,j)*enable_msf;
        %-------- next vapor mass flow rate, kg/s
        mflwvapseg_air(i,j+1) = mflwvapseg_air(i,j)-mtdydx_air(i,j);
            % water in aqueous
        mflwvapseg_sol(i+1,j) = mflwvapseg_sol(i,j)+mtdydx_sol(i,j);
        % vapor mass flow rate through membrane
        mflwvapseg_air_mem(i,j) = mtdydx_air(i,j);
        mflwvapseg_sol_mem(i,j) = mtdydx_sol(i,j);
        %-------- next [humidity], kg/kg !
        % outlet vapor mass flow rate for this segment = inlet vapor↙
mass flow rate for next segment
        mflwseg_air(i,j+1) = mflwseg_air(i,j)-mtdydx_air(i,j);↙
%??????????????????
        humid_air(i,j+1) = mflwvapseg_air(i,j+1)/(mflwseg_air(i,j+1)-↙
mflwvapseg_air(i,j+1));    % mflwvapseg_fa, kg/s*per segment*per layer
        %mflwvapseg_pf(i+1,j) = mfvap_pf(i+1,j)/↙
(num_dsegment*numchannel_pf);
        mflwseg_sol(i+1,j) = mflwseg_sol(i,j)+mtdydx_sol(i,j);↙
%??????????????????
        Con_water_sol(i+1,j) = mflwvapseg_sol(i+1,j)/mflwseg_sol(i+1,j);
        %-------- next [vapor pressure]!
        P_vap_air(i,j+1) = vapPstaturate(Temp_air(i,j+1))*Airrehum↙
(Temp_air(i,j+1), humid_air(i,j+1));
        P_vap_sol(i+1,j)=Pi_licl(Temp_sol(i+1,j),(1-Con_water_sol(i+1,↙
j)));
        W_sol(i+1,j)=0.622*P_vap_sol(i+1,j)/(101325-P_vap_sol(i+1,j));
        P_air(i,j+1)=P_air(i,j);
```

```
        P_sol(i+1,j)=P_sol(i,j);
    end
end
%%
Temp_sol(num_lsegment+2,:)=[];
Temp_sol(:,num_dsegment+2)=[];
Temp_air(num_lsegment+2,:)=[];
Temp_air(:,num_dsegment+2)=[];
Con_water_sol(num_lsegment+2,:)=[];
Con_water_sol(:,num_dsegment+2)=[];
EMIM_concen=1-Con_water_sol;
humid_air(num_lsegment+2,:)=[];
humid_air(:,num_dsegment+2)=[];
P_vap_air(num_lsegment+2,:)=[];
P_vap_air(:,num_dsegment+2)=[];
Temp_airmem(num_lsegment+2,:)=[];
Temp_airmem(:,num_dsegment+2)=[];
Temp_solmem(num_lsegment+2,:)=[];
Temp_solmem(:,num_dsegment+2)=[];
%%
figure(1)
x=1:1:num_dsegment+1;
y=1:1:num_lsegment+1;%!!!
surf(x,y,Temp_air,'EdgeColor','none')
rotate3d on;
xlim([0, num_dsegment+2]);
ylim([0, num_lsegment+2]);
title('3D Temperature profile of air layer','FontSize',12);
xlabel('Depth-direction','FontSize',12); % Segment index of
ylabel('Length-direction','FontSize',12);
zlabel('Temperature(K)','FontSize',12);
figure(2)
x=1:1:num_dsegment+1;
y=1:1:num_lsegment+1;%!!!
surf(x,y,Temp_sol,'EdgeColor','none')
rotate3d on;
xlim([0, num_dsegment+2]);
ylim([0, num_lsegment+2]);
title('3D Temperature profile of solution layer','FontSize',12);
xlabel('Depth-direction','FontSize',12); % Segment index of
ylabel('Length-direction','FontSize',12);
zlabel('Temperature(K)','FontSize',12);
figure(3)
x=1:1:num_dsegment+1;
y=1:1:num_lsegment+1;%!!!
surf(x,y,humid_air,'EdgeColor','none')
rotate3d on;
xlim([0, num_dsegment+2]);
ylim([0, num_lsegment+2]);
title('3D Humidity profile of air layer','FontSize',12);
xlabel('Depth-direction','FontSize',12); % Segment index of
ylabel('Length-direction','FontSize',12);
zlabel('Humidity(kg/kg)','FontSize',12);
```

```
figure(4)
x=1:1:num_dsegment+1;
y=1:1:num_lsegment+1;%!!!
surf(x,y,EMIM_concen,'EdgeColor','none')
rotate3d on;
xlim([0, num_dsegment+2]);
ylim([0, num_lsegment+2]);
title('3D Concentration profile of solution layer','FontSize',12);
xlabel('Depth-direction','FontSize',12); % Segment index of
ylabel('Length-direction','FontSize',12);
zlabel('Concentration(kg/kg)','FontSize',12);
figure(5)
x=1:1:num_dsegment+1;
y=1:1:num_lsegment+1;%!!!
surf(x,y,Temp_airmem,'EdgeColor','none')
rotate3d on;
xlim([0, num_dsegment+2]);
ylim([0, num_lsegment+2]);
title('fam_tin','FontSize',8);
xlabel('D-direction','FontSize',8); % Segment index of
ylabel('L-direction','FontSize',8);
zlabel('T','FontSize',8);
%% output
Temp_air_out=mean(Temp_air(:,num_dsegment+1))-273.15;
Humid_air_out=mean(humid_air(:,num_dsegment+1));
Temp_mem_air_out=mean(Temp_airmem(:,num_dsegment+1))-273.15;
Temp_sol_out=mean(Temp_sol(num_lsegment+1,:))-273.15;
Con_sol_out=mean(EMIM_concen(num_lsegment+1,:));
Temp_mem_sol_out=mean(Temp_solmem(num_lsegment+1,:))-273.15;
Eff_lat=(humid_air(1,1)-Humid_air_out)/(humid_air(1,1)-W_sol(1,1));
Eff_sen=(Temp_air(1,1)-273.15-Temp_air_out)/(Temp_air(1,1)-Temp_sol↙
(1,1));
MRR=(-Humid_air_out+humid_air(1,1))*mflr_air(1,1); % water concentration↙
difference in air [kg/s]
HR_diff=-Humid_air_out+humid_air(1,1);    % humidity ratio↙
difference=water vapor removed [kg/kg]
```

REFERENCES

[1] U.S Energy Information Administration. Monthly Energy Review, Table 2.1, April 2018.

[2] U.S Energy Information Administration. Annual energy outlook 2018.

[3] U.S Energy Information Administration. 2015 Residential Energy Consumption Survey.

[4] U.S Energy Information Administration. 2012 Commercial Buildings Energy Consumption Survey: Energy Usage Summary.

[5] Abdel-Salam, M. R. H., Ge, G., Fauchoux, M., Besant, R. W., & Simonson, C. J. (2014). State-of-the-art in liquid-to-air membrane energy exchangers (LAMEEs): a comprehensive review. *Renewable & Sustainable Energy Reviews, 39*(6), 700-728.

[6] Rafique, M. M., Gandhidasan, P., & Bahaidarah, H. M. S. (2016). Liquid desiccant materials and dehumidifiers – a review. *Renewable & Sustainable Energy Reviews, 56*, 179-195.

[7] Woods, J. (2014). Membrane processes for heating, ventilation, and air conditioning. *Renewable & Sustainable Energy Reviews, 33*(33), 290-304.

[8] Klepeis, N. E., Nelson, W. C., Ott, W. R., Robinson, J. P., Tsang, A. M., & Switzer, P., et al. (2001). The national human activity pattern survey (nhaps): a resource for assessing exposure to environmental pollutants. *J Expo Anal Environ Epidemiol, 11*(3), 231-252.

[9] C. Bruce Wenger. (1948). The regulation of body temperature. *Medical Journal of Australia, 1*(8), 221.

[10] Dannemiller, K. C., Weschler, C. J., & Peccia, J. (2017). Fungal and bacterial growth in floor dust at elevated relative humidity levels. *Indoor Air, 27*(2), 354-363

[11] APAFrankel, M., Bekö, G., Timm, M., Gustavsen, S., Hansen, E. W., & Madsen, A. M. (2012). Seasonal variations of indoor microbial exposures and their relation to temperature, relative humidity, and air exchange rate. *Applied & Environmental Microbiology, 78*(23), 8289-8297.

[12] American Society of Heating, Refrigerating and Air-Conditioning Engineers. (2013). Thermal environmental conditions for human occupancy: ASHRAE standard 55-2013. Atlanta, GA: *American Society of Heating, Refrigerating and Air-Conditioning Engineers*

[13] American Society of Heating, Refrigerating and Air-Conditioning Engineers. (2016). Ventilation for acceptable indoor air quality: ASHRAE standard 62.1-2016. Atlanta, GA: *American Society of Heating, Refrigerating and Air-Conditioning Engineers*.

[14] Harriman, L. G., Plager, D., & Kosar, D. (1999). Dehumidification and cooling loads from ventilation air. *Energy Engineering, 96*(6), 31-45.

[15] Zhang, L. Z. (2006). Energy performance of independent air dehumidification systems with energy recovery measures. *Energy, 31*(8), 1228-1242.

[16] Fu, X., Ge, G., & Niu, X. (2011). Control performance of a dedicated outdoor air system adopting liquid desiccant dehumidification. *Applied Energy, 88*(1), 143-149.

[17] Ge, G., Xiao, F., & Xu, X. (2011). Model-based optimal control of a dedicated outdoor air-chilled ceiling system using liquid desiccant and membrane-based total heat recovery. *Applied Energy, 88*(11), 4180-4190.

[18] Qi R, Lu L, Yang H (2012). Investigation on air-conditioning load profile and energy consumption of desiccant cooling system for commercial buildings in Hong Kong. *Energy Build, 49*, 509-18.

[19] Giampieri, A., Ma, Z., Smallbone, A., & Roskilly, A. P. (2018). Thermodynamics and economics of liquid desiccants for heating, ventilation and air-conditioning – an overview. *Applied Energy, 220*, 455-479.

[20] Abdel-Salam, A. H., & Simonson, C. J. (2014). Annual evaluation of energy, environmental and economic performances of a membrane liquid desiccant air conditioning system with/without ERV. *Applied Energy, 116*, 134-148.

[21] Lin, L., Yu, H., & Ronghui, Q. (2015). Parameter analysis and optimization of the energy and economic performance of solar-assisted liquid desiccant cooling system under different climate conditions. *Energy Conversion & Management, 106*, 1387-1395.

[22] Rafique, M. M., Gandhidasan, P., & Bahaidarah, H. M. S. (2016). Liquid desiccant materials and dehumidifiers – a review. *Renewable & Sustainable Energy Reviews, 56*, 179-195.

[23] Lowenstein, A., Slayzak, S., & Kozubal, E. (2006). A Zero Carryover Liquid-Desiccant Air Conditioner for Solar Applications. *American Society of Mechanical Engineers 2006 International Solar Energy Conference*, 397-407.

[24] Qu, M., Abdelaziz, O., Gao, Z., & Yin, H. (2018). Isothermal membrane-based air dehumidification: a comprehensive review. *Renewable & Sustainable Energy Reviews, 82*(3), 4060-4069.

[25] Burns, P. R., Mitchell, R. B., & Bechman, W. A. (1985). Hybrid desiccant cooling systems in supermarket applications. *Intersolghty Five, 91*, 700-706.

[26] Jain, S., Tripathi, S., & Das, R. S. (2011). Experimental performance of a liquid desiccant dehumidification system under tropical climates. *Energy Conversion & Management, 52*(6), 2461-2466.

[27] Yang, B., Yuan, W., Gao, F., & Guo, B. (2013). A review of membrane-based air dehumidification. *Indoor & Built Environment, 24*(1), 11-26.

[28] Huang, S. M., & Zhang, L. Z. (2013). Researches and trends in membrane-based liquid desiccant air dehumidification. *Renewable & Sustainable Energy Reviews, 28*(8), 425-440.

[29] Mei, L., & Dai, Y. J. (2008). A technical review on use of liquid-desiccant dehumidification for air-conditioning application. *Renewable & Sustainable Energy Reviews, 12*(3), 662-689.

[30] Kudasheva, A., Kamiya, T., Hirota, Y., & Ito, A. (2016). Dehumidification of air using liquid membranes with ionic liquids. *Journal of Membrane Science, 499*, 379-385.

[31] Qu, M., Abdelaziz, O., Sun, X. G., & Yin, H. (2017). Aqueous solution of [EMIM][OAc]: property formulations for use in air conditioning equipment design. *Applied Thermal Engineering, 124*, 271-278.

[32] Sun J, Gong XL, Shi MH. (2004) Study on vapor pressure of liquid desiccants solution. *International Journal of Refrigeration, 25*(1), 28-30.

[33] McNelly L. (1979) Thermodynamic properties of aqueous solutions of lithium bromide. *ASHRAE Transactions, 85*(1), 412-434.

[34] Ertas, A., Anderson, E. E., & Kiris, I. (1992). Properties of a new liquid desiccant solution—lithium chloride and calcium chloride mixture. *Solar Energy*, 49(3), 205-212.

[35] Longo, G. A., & Gasparella, A. (2016). Experimental measurement of thermophysical properties of h 2 o/kcooh (potassium formate) desiccant. *International Journal of Refrigeration, 62*(4), 106-113.

[36] Fendu, E. M., & Oprea, F. (2013). Vapor pressure, density, viscosity, and surface tension of tetrapropylene glycol. *Journal of Chemical & Engineering Data, 58*(11), 2898-2903.

[37] Dow Chemical Company, Triethylene Glycol properties, 2007. Retrieved from http://msdssearch.dow.com/PublishedLiteratureDOW-COM/dh_0952/0901b80380952386.pdf

[38] Cisternas, L. A., & Lam, E. J. (1991). An analytic correlation for the vapor pressure of aqueous and non-aqueous solutions of single and mixed electrolytes. part ii. application and extension. *Fluid Phase Equilibria, 62*(s1-2), 11-27.

[39] Conde, M. R. (2004). Properties of aqueous solutions of lithium and calcium chlorides: formulations for use in air conditioning equipment design. *International Journal of Thermal Sciences, 43*(4), 367-382.

[40] Sahlot, M., & Riffat, S. B. (2016). Desiccant cooling systems: a review. *International Journal of Low-Carbon Technologies, 11,* 489-505.

[41] Qiu, G., Liu, H., & Riffat, S. B. (2013). Experimental investigation of a liquid desiccant cooling system driven by flue gas waste heat of a biomass boiler. *International Journal of Low-Carbon Technologies, 8*(3), 165-172.

[42] Tim, Dwyer. (2014). Module 71: Liquid desiccants for dehumidification in building air conditioning systems. Retrieved from https://www.cibsejournal.com/cpd/modules/2014-12/

[43] RASHA S., HASSAN A., RINKU T. (2012). Influence of pore structure on membrane wettability in membrane. *The Sixth Jordan International Chemical Engineering Conference*.

[44] OMEGA™, Equilibrium Relative Humidity Saturated Salt Solutions. Retrieved from https://www.omega.com/temperature/z/pdf/z103.pdf

[45] Rafique, M. M., Gandhidasan, P., & Bahaidarah, H. M. S. (2016). Liquid desiccant materials and dehumidifiers – a review. *Renewable & Sustainable Energy Reviews, 56*, 179-195.

[46] Afshin, M. (2010). Selection of the liquid desiccant in a run-around membrane energy exchanger (M.Sc. Thesis). University of Saskatchewan. Retrieved from https://harvest.usask.ca/handle/10388/etd-05262010-175310

[47] Al-Farayedhi, A. A., Gandhidasan, P., & Al-Mutairi, M. A. (2002). Evaluation of heat and mass transfer coefficients in a gauze-type structured packing air dehumidifier operating with liquid desiccant. *International Journal of Refrigeration, 25*(3), 330-339.

[48] Longo, G. A., & Gasparella, A. (2016). Experimental measurement of thermos-physical properties of H2O/KCOOH (potassium formate) desiccant. *International Journal of Refrigeration, 62*(4), 106-113.

[49] Elmer, T., Worall, M., Wu, S., & Riffat, S. (2017). Experimental evaluation of a liquid desiccant air conditioning system for tri-generation/waste-heat-driven applications. *International Journal of Low-Carbon Technologies, 12*(2), 1-16.

[50] Misha, S., Mat, S., Ruslan, M. H., & Sopian, K. (2012). Review of solid/liquid desiccant in the drying applications and its regeneration methods. *Renewable & Sustainable Energy Reviews, 16*(7), 4686-4707.

[51] Longo, G. A., & Gasparella, A. (2005). Experimental and theoretical analysis of heat and mass transfer in a packed column dehumidifier/regenerator with liquid desiccant. *International Journal of Heat and Mass Transfer, 48*(25), 5240-5254.

[52] Luo, Y., Shao, S., Qin, F., Tian, C, & Yang, H. (2012). Investigation on feasibility of ionic liquids used in solar liquid desiccant air conditioning system. *Solar Energy, 86*(9), 2718-2724.

[53] Isetti, C., Nannei, E., & Magrini, A. (1997). On the application of a membrane air—liquid contactor for air dehumidification. *Energy & Buildings, 25*(3), 185-193.

[54] Bergero, S., & Chiari, A. (2001). Experimental and theoretical analysis of air humidification/dehumidification processes using hydrophobic capillary contactors. *Applied Thermal Engineering, 21*(11), 1119-1135.

[55] Bergero, S., & Chiari, A. (2011). On the performances of a hybrid air-conditioning system in different climatic conditions. *Energy, 36*(8), 5261-5273.

[56] Moghaddam, D. G., Lepoudre, P., Ge, G., Besant, R. W., & Simonson, C. J. (2013). Small-scale single-panel liquid-to-air membrane energy exchanger (LAMEE) test facility development, commissioning and evaluating the steady-state performance. *Energy & Buildings, 66*(5), 424-436.

[57] Huang, S. M., Yang, M., & Yang, X. (2014). Performance analysis of a quasi-counter flow parallel-plate membrane contactor used for liquid desiccant air dehumidification. Applied *Thermal Engineering, 63*(1), 323-332.

[58] Zhang, L. Z., & Zhang, N. (2014). A heat pump driven and hollow fiber membrane-based liquid desiccant air dehumidification system: modeling and experimental validation. *Energy, 65*(65), 441-451.

[59] Abdel-Salam, M. R. H., Besant, R. W., & Simonson, C. J. (2016). Design and testing of a novel 3-fluid liquid-to-air membrane energy exchanger (3-fluid LAMEE*). International Journal of Heat & Mass Transfer, 92*, 312-329.

[60] Lin, J., Huang, S. M., Wang, R., & Chua, K. J. (2018). Thermodynamic analysis of a hybrid membrane liquid desiccant dehumidification and dew point evaporative cooling system. *Energy Conversion & Management, 156*, 440-458.

[61] Hongyu Bai, Jie Zhu, Ziwei Chen, Junze Chu. (2018). Parametric analysis of a cross-flow membrane-based parallel-plate liquid desiccant dehumidification system: Numerical and experimental data. *Energy and Buildings, 158*, 494-508.

[62] Annadurai, G., Tiwari, S., & Maiya, MP. (2018). Experimental performance comparison of adiabatic and internally-cooled membrane dehumidifiers. *International Journal of Low-Carbon Technologies, 13*(3), 240-249.

[63] Bettahalli, N. M. S., Lefers, R., Fedoroff, N., Leiknes, T. O., & Nunes, S. P. (2016). Triple-bore hollow fiber membrane contactor for liquid desiccant based air dehumidification. *Journal of Membrane Science, 514*, 135-142.

[64] Chen, Z., Bai, H., Ye, Z., & Zhu, J. (2016). Experimental study of a membrane-based dehumidification cooling system. *International Symposium of Heat Transfer and Heat Powered Cycles, 115*, 1315-1321.

[65] Bai, H., Zhu, J., Chen, Z., Ma, L., Wang, R., & Li, T. (2017). Performance testing of a cross-flow membrane-based liquid desiccant dehumidification system. *Applied Thermal Engineering, 119,* 119-131.

[66] Hout, M., Ghaddar, N., Ghali, K., Ismail, N., Simonetti, M., & Fracastoro, G. V., et al. (2017). Displacement ventilation with cooled liquid desiccant dehumidification membrane at ceiling; modeling and design charts. *Energy, 139*, 1003-1015.

[67] Erb, B., 2006. Run-Around Membrane Energy Exchanger Performance and Operational Control Strategies (M.Sc. Thesis), University of Saskatchewan. Retrieved from https://harvest.usask.ca/handle/10388/etd-12192009-145431

[68] Seyed-Ahmadi, M., Erb, B., Simonson, C. J., & Besant, R. W. (2009). Transient behavior of run-around heat and moisture exchanger system. part I: model formulation and verification. *International Journal of Heat & Mass Transfer, 52*(25), 6000-6011.

[69] Seyed-Ahmadi, M., Erb, B., Simonson, C. J., & Besant, R. W. (2009). Transient behavior of run-around heat and moisture exchanger system. part II: sensitivity studies for a range of initial conditions. *International Journal of Heat & Mass Transfer, 52*(25), 6012-6020.

[70] Mahmud, K. 2009. Design and testing of a laboratory RAMEE system with counter flow exchangers to transfer heat and water vapor between supply and exhaust air flows (M.Sc. Thesis). University of Saskatchewan. Retrieved from https://harvest.usask.ca/bitstream/handle/10388/etd-09092009-223833/Khizir_Mahmud_2009-Sep-28a.pdf?sequence=1&isAllowed=y

[71] Mahmud, K., Mahmood, G. I., Simonson, C. J., & Besant, R. W. (2010). Performance testing of a counter-cross-flow run-around membrane energy exchanger (RAMEE) system for HVAC applications. *Energy & Buildings, 42*(7), 1139-1147.

[72] Fakharnezhad, A., & Keshavarz, P. (2016). Experimental investigation of gas dehumidification by tri-ethylene glycol in hollow fiber membrane contactors. *Journal of Industrial & Engineering Chemistry, 34*, 390-396.

[73] Petukhov, Dmitrii., A. Eliseev, Ar., Poyarkov, A.A., Lukashin, A.V. & A. Eliseev, An. (2017). Porous polypropylene membrane contactors for dehumidification of gases. *Nanosystems: Physics, Chemistry, Mathematics, 8*(6), 798-803.

[74] Meggers, F., Teitelbaum, E., & Pantelic, J. (2017). Development of moisture absorber based on hydrophilic membrane mass exchanger and alkoxylated siloxane liquid desiccant. *Energy Procedia, 122*, 1117-1122.

[75] Pantelic, J., Teitelbaum, E., Bozlar, M., Kim, S., & Meggers, F. (2018) Development of moisture absorber based on hydrophilic nonporous membrane mass exchanger and alkoxylated siloxane liquid desiccant. *Energy and Buildings, 160*, 34-43.

[76] Chen, X., Su, Y., Aydin, D., Bai, H., Jarimi, H., & Zhang, X., et al. (2018). Experimental investigation of a polymer hollow fibre integrated liquid desiccant dehumidification system with aqueous potassium formate solution. Applied Thermal Engineering, 142, 632-643.

[77] Liu, X. B., Warner, J., Qu, M., Liu, X. L., Opadrishta, H., William, P. (2018). A Preliminary Experimental Study on the Performance of a Membrane-based Air Dehumidifier Using Ionic Liquid. *Purdue Herrick Conference*. Retrieved from https://www.conftool.com/Purdue2018/index.php?page=browseSessions&form_session=130

[78] Khayet, M., & Matsuura, T. (2001). Preparation and characterization of polyvinylidene fluoride membranes for membrane distillation. *Industrial & Engineering Chemistry Research, 40*(24), 5710-5718.

[79] Mackie, J. S., & Meares, P. (1955). The diffusion of electrolytes in a cation-exchange resin membrane. I. theoretical. *Proceedings of the Royal Society of London, 232*(1191), 498-509.

[80] Brandrup, J., & Immergut, EH. (1989). Polymer handbook. 3rd ed. New York: Wiley.

[81] Harper., CA. (1996). Handbook of Plastics, Elastomers and Composites. 3rd ed. New York: McGraw-Hill.

[82] Van Kreveleh, D.W. (1990). Properties of Polymers. 3rd ed. Amsterdam: Elsevier.

[83] Phattaranawik, J., Jiraratananon, R., & Fane, A. G. (2003). Heat transport and membrane distillation coefficients in direct contact membrane distillation. *Journal of Membrane Science, 212*(1), 177-193.

[84] Rao, L. J. M. (2010). Handbook of membrane separations: chemical, pharmaceutical, food, and biotechnological applications. *International Journal of Food Science & Technology, 44*(7), 1464-1466.

[85] Alkhudhiri, A., Darwish, N., & Hilal, N. (2012). Membrane distillation: a comprehensive review. *Desalination, 287*(8), 2-18.

[86] Concepts, R. (2014). E96-93 standard test methods for water-vapor transmission of materials. Annual Book of Astm Standards.

[87] Mondal, S., Hu, J. L., & Yong, Z. (2006). Free volume and water vapor permeability of dense segmented polyurethane membrane. *Journal of Membrane Science, 280*(1), 427-432.

[88] Phromphen, P., Mao, N., Russell, S. J., & Goswami, P. (2015). Liquid permeation and water vapour transmission properties of a temperature-sensitive pvdf-g-nipaam barrier membrane. Autex World Textile Conference.

[89] Lainioti, G., Bounos, G., Voyiatzis, G., & Kallitsis, J. (2016). Enhanced water vapor transmission through porous membranes based on melt blending of polystyrene sulfonate with polyethylene copolymers and their cnt nanocomposites. *Polymers, 8*(5), 190.

[90] Hu, Y., Topolkaraev, V., Hiltner, A., & Baer, E. (2010). Measurement of water vapor transmission rate in highly permeable film. *Journal of Applied Polymer Science, 81*(7), 1624-1633.

[91] Gibson, P., Kendrick, C., Rivin, D., Charmchii, M., & Sicuranza, L. (1997). An automated dynamic water vapor permeation test method. *Nasa Sti/recon Technical Report N, 96*.

[92] Yampolskii, Y., Pinnau, I., & Freeman, B. (2006). Solid-state facilitated transport membranes for separation of olefins/paraffins and oxygen/nitrogen. *Materials science of membranes for gas and vapor separation,10.1002/047002903X*, 391-410.

[93] Chung, T. S., Jiang, L. Y., Li, Y., & Kulprathipanja, S. (2007). Mixed matrix membranes (mmms) comprising organic polymers with dispersed inorganic fillers for gas separation. *Progress in Polymer Science, 32*(4), 483-507.

[94] Aroon, M. A., Ismail, A. F., Matsuura, T., & Montazer-Rahmati, M. M. (2010). Performance studies of mixed matrix membranes for gas separation: a review. *Separation & Purification Technology, 75*(3), 229-242.

[95] Sanchez C, Belleville P, Popall M, Nicole L. (2011). Applications of advanced hybrid organic inorganic nanomaterials: from laboratory to market. *Chemical Society Reviews, 40*(2), 696–753.

[96] Scovazzo, P. (2010). Testing and evaluation of room temperature ionic liquid (rtil) membranes for gas dehumidification. *Journal of Membrane Science, 355*(1), 7-17.

[97] Vandezande P. (2015). Next-generation pervaporation membranes: recent trends, challenges and perspectives. In: Woodhead publishing series in energy. *Oxford: Woodhead Publishing*, 107-141.

[98] Krull, F. F., Medved, M., & Melin, T. (2007). Novel supported ionic liquid membranes for simultaneous homogeneously catalyzed reaction and vapor separation. *Chemical Engineering Science, 62(*18), 5579-5585.

[99] Lozano, L. J., Godínez, C., Ríos, A. P. D. L., Hernández-Fernández, F. J., Sánchez-Segado, S., & Alguacil, F. J. (2011). Recent advances in supported ionic liquid membrane technology. *Journal of Membrane Science, 376*(1), 1-14.

[100] Malik, M. A., Hashim, M. A., & Nabi, F. (2011). Ionic liquids in supported liquid membrane technology. *Chemical Engineering Journal, 171*(1), 242-254.

[101] Grünauer, J., Shishatskiy, S., Abetz, C., Abetz, V., & Filiz, V. (2015). Ionic liquids supported by isoporous membranes for co 2 /n 2, gas separation applications. *Journal of Membrane Science, 494*, 224-233.

[102] Kudasheva, A., Kamiya, T., Hirota, Y., & Ito, A. (2016). Dehumidification of air using liquid membranes with ionic liquids. *Journal of Membrane Science, 499*, 379-385.

[103] Asfand, F., & Bourouis, M. (2015). A review of membrane contactors applied in absorption refrigeration systems. *Renewable & Sustainable Energy Reviews, 45*, 173-191.

[104] Zhang, L. Z., & Huang, S. M. (2011). Coupled heat and mass transfer in a counter flow hollow fiber membrane module for air humidification. *International Journal of Heat & Mass Transfer*, 54(5-6), 1055-1063.

[105] Zhang, L. Z. (2012). Coupled heat and mass transfer in an application-scale cross-flow hollow fiber membrane module for air humidification. *International Journal of Heat & Mass Transfer, 55*(21-22), 5861-5869.

[106] Larson, M. D., Simonson, C. J., Besant, R. W., & Gibson, P. W. (2007). The elastic and moisture transfer properties of polyethylene and polypropylene membranes for use in liquid-to-air energy exchangers. *Journal of Membrane Science, 302*(1-2), 136-149.

[107] Larson MD. (2006) The performance of membranes in a newly proposed runaround heat and moisture exchanger. (M.Sc. Thesis). University of Saskatchewan. Retrieved from https://www.collectionscanada.gc.ca/obj/s4/f2/dsk3/SSU/TC-SSU-12192006094159.pdf

[108] Li, W., & Yao, Y. (2018). Study on the method for testing the water vapor diffusion resistance of membranes. *Polymer Testing*, 69.

[109] Smolders, K., & Franken, A. C. M. (2017). Terminology for membrane distillation. *Desalination, 72*(3), 249-262.

[110] And, M. K., & Matsuura, T. (2001). Preparation and characterization of polyvinylidene fluoride membranes for membrane distillation. *Industrial & Engineering Chemistry Research, 40*(24), 5710-5718.

[111] Mansourizadeh, Ismail, A.F, & Matsuura. (2010). Effect of operating conditions on the physical and chemical co2 absorption through the PVDF hollow fiber membrane contactor. *Journal of Membrane Science, 353*(1), 192-200.

[112] Ismail, A.F, & Mansourizadeh. (2010). A comparative study on the structure and performance of porous polyvinylidene fluoride and polysulfone hollow fiber membranes for CO2 absorption. *Journal of Membrane Science, 365*(1), 319-328.

[113] Wickramasinghe, S. R., Semmens, M. J., & Cussler, E. L. (1991). Better hollow fiber contactors. *Journal of Membrane Science, 62*(3), 371-388.

[114] Zhang LZ. (2011). An analytical solution to heat and mass transfer in hollow fiber membrane contactors for liquid desiccant air dehumidification. *International Journal of Heat and Mass Transfer, 133*(9), 092001.1–8.

[115] Zhang, L. Z., Huang, S. M., & Pei, L. X. (2012). Conjugate heat and mass transfer in a cross-flow hollow fiber membrane contactor for liquid desiccant air dehumidification. *International Journal of Heat and Mass Transfer, 55*(25-26), 8061-8072.

[116] Moghaddam, D. G., Besant, R. W., & Simonson, C. J. (2014). Solution-side effectiveness for a liquid-to-air membrane energy exchanger used as a dehumidifier/regenerator. *Applied Energy, 113*(6), 872-882.

[117] Gommed, K., & Grossman, G. (2007). Experimental investigation of a liquid desiccant system for solar cooling and dehumidification. *Solar Energy, 81*(1), 131-138.

[118] Abdel-Salam, M. R. H., Besant, R. W., & Simonson, C. J. (2016). Design and testing of a novel 3-fluid liquid-to-air membrane energy exchanger (3-fluid lamee). *International Journal of Heat & Mass Transfer, 92*, 312-329.

[119] Huang, S. M., Yang, M., Hong, Y., & Ye, W. B. (2018). Performance correlations of an adjacently internally-cooled membrane contactor applied for liquid desiccant air dehumidification. *Applied Thermal Engineering, 129*, 1660-1669.

[120] Huang, S. M., Yang, M., Hu, B., Tao, S., Qin, F. G., Weng, W. L., Wang, W. H., & Liu, J. (2018). Performance analysis of an internally-cooled plate membrane liquid desiccant dehumidifier (IMLDD): An analytical solution approach. *International Journal of Heat and Mass Transfer, 119*, 577-585.

[121] Parmar, H., & Hindoliya, D. A. (2013). Performance of solid desiccant-based evaporative cooling system under the climatic zones of India. *International Journal of Low-Carbon Technologies, 8*(1), 52-57.

[122] Bai, H., Zhu, J., Chen, Z., Chu, J., & Liu, Y. (2018). Performance evaluation of a membrane-based flat-plate heat and mass exchanger used for liquid desiccant regeneration. *Applied Thermal Engineering, 139*, 569-584.

[123] Bergero, S., & Chiari, A. (2010). Performance analysis of a liquid desiccant and membrane contactor hybrid air-conditioning system. *Energy & Buildings, 42*(11), 1976-1986.

[124] Abdel-Salam, A. H., Ge, G., & Simonson, C. J. (2013). Performance analysis of a membrane liquid desiccant air-conditioning system. *Energy & Buildings, 62*(7), 559-569.

[125] Shah, R. K., & Sekuli, D. P. (2007). Basic Thermal Design Theory for Recuperators. Fundamentals of Heat Exchanger Design. *John Wiley & Sons, Inc.*

[126] Nasif, Mohammad & Morrison, Graham & Behnia, M. (2005). Heat and Mass Transfer in Air to Air Enthalpy Heat Exchangers. *6th International Conference on Heat Transfer, Fluid Mechanics and Thermodynamics*, Matsushima, Japan,

[127] Zhang, L. Z., & Niu, J. L. (2002). Effectiveness correlations for heat and moisture transfer processes in an enthalpy exchanger with membrane cores. *Journal of Heat Transfer, 124*(5), 922-929.

[128] Zhang, L. Z. (2011). An analytical solution to heat and mass transfer in hollow fiber membrane contactors for liquid desiccant air dehumidification. *Journal of Heat Transfer, 133*(9), 092001.

[129] Huang, S. M., Zhang, L. Z., Tang, K., & Pei, L. X. (2012). Fluid flow and heat mass transfer in membrane parallel-plates channels used for liquid desiccant air dehumidification. *International Journal of Heat & Mass Transfer, 55*(9-10), 2571-2580.

[130] Gao, Zhiming & Abdelaziz, Omar & Qu, Ming. (2017). Modeling and Simulation of Membrane-Based Dehumidification and Energy Recovery Process. *2017 ASHRAE Winter Conference*, At Las Vegas, NV.

[131] Zhang, L. Z. (2006). Mass diffusion in a hydrophobic membrane humidification/dehumidification process: the effects of membrane characteristics. *Separation Science, 41*(8), 18.

[132] Zhang, L. Z., & Jiang, Y. (1999). Heat and mass transfer in a membrane-based energy recovery ventilator. *Journal of Membrane Science, 163*(1), 29-38.

[133] Brünig, Thorge, Kreki, K., Bruhn, C., & Pietschnig, R. (2016). Calorimetric studies and structural aspects of ionic liquids in designing sorption materials for thermal energy storage. *Chemistry - A European Journal, 22*(45), 16200-16212.

[134] Kusoglu, A., & Weber, A. Z. (2017). New insights into perfluorinated sulfonic-acid ionomers. *Chemical Reviews, 117*(3), 987.

[135] Incropera, F.P., DeWitt, & D.P. (2007). Fundamentals of Heat and Mass Transfer (56h Ed.). Hoboken: Wiley, 490-515.

[136] Mazzotti, M., Gazzani, M., Milella, F., & Gabreilli, P. (2016). Membrane separations rate controlled separation processes. *ETH, Zurich*, 10.

[137] Leikens, O. (2000). Theory of transport in membranes: Ch. 2. PhD Thesis. Retrieved from http://netedu.xauat.edu.cn/jpkc/netedu/jpkc2009/szylyybh/content/wlzy/7/5/Theory%20of%20transport%20in%20membranes.pdf

[138] Seidel-Morgenstern, A. (2010). Membrane reactors: distributing reactants to improve selectivity and yield.

[139] Bai, H., Zhu, J., Chen, Z., & Chu, J. (2018). State-of-art in modelling methods of membrane-based liquid desiccant heat and mass exchanger: a comprehensive review. *International Journal of Heat and Mass Transfer, 125*, 445-470.

[140] Zhang, L.Z. (2011). An analytical solution to heat and mass transfer in hollow fiber membrane contactors for liquid desiccant air dehumidification. *J. Heat Transfer, 133*(9), 092001-092001-8.

[141] Cisternas, L. A., & Lam, E. J. (1991). An analytic correlation for the vapor-pressure of aqueous and nonaqueous solutions of single and mixed electrolytes. Part 2: application and extension. *Fluid Phase Equilibria, 62*(s1-2), 11-27.

[142] Andreas A. Zavitsas. (2001). Properties of water solutions of electrolytes and nonelectrolytes. *Journal of Physical Chemistry, 105* (32), 7805-7817

[143] Zavitsas, A.A., Aseyev, G.G. (1992). Properties of aqueous solutions of electrolytes and nonelectrolytes. *CRC Press, Boca Raton*.

[144] Baker, R. (2004). Membrane technology and applications, 2nd edition. *Metallurgical Transactions A*, 6.

[145] Bai, H.Y., Zhu, J., Chen, Z.W., & Chu, J.Z. (2018). Parametric analysis of a cross-flow membrane-based parallel-plate liquid desiccant dehumidification system: Numerical and experimental data. *Energy and Buildings, 158*, 494-508.